



UPPSALA
UNIVERSITET

*Digital Comprehensive Summaries of Uppsala Dissertations
from the Faculty of Science and Technology 2227*

Light-Induced Routes to Sustainable Biocrudes for Fuels and Lubricant Oils

LEANDRO CID GOMES



ACTA
UNIVERSITATIS
UPSALIENSIS
UPPSALA
2023

ISSN 1651-6214
ISBN 978-91-513-1682-6
URN urn:nbn:se:uu:diva-492631

Dissertation presented at Uppsala University to be publicly examined in Högssalen, 10132, Ångström, Lägerhyddsvägen 1, Uppsala, Friday, 24 February 2023 at 13:00 for the degree of Doctor of Philosophy. The examination will be conducted in English. Faculty examiner: Dr. Norbert Hoffmann (Director of Research at CNRS, Université de Reims, 51687 Reims, France).

Abstract

Cid Gomes, L. 2023. Light-Induced Routes to Sustainable Biocrudes for Fuels and Lubricant Oils. *Digital Comprehensive Summaries of Uppsala Dissertations from the Faculty of Science and Technology* 2227. 90 pp. Uppsala: Acta Universitatis Upsaliensis. ISBN 978-91-513-1682-6.

Fossil-based hydrocarbons are at present the ideal compounds for jet fuels and lubricant oils, so their replacement by novel technologies is not easy. Instead, sustainable routes to hydrocarbons, such as sunlight-driven processes, are desired to reduce the environmental impact by the transport sector. Photosynthetic microorganisms can convert water and CO₂ into small hydrocarbons, yet, a second step is needed to convert them into jet fuels and lubricant oils. The aim of this thesis is to investigate photochemical routes for this second step.

We first explore the triplet photosensitized dimerization of isoprene produced by cyanobacteria. We developed a combined photobiological-photochemical route from CO₂ to C₁₀ jet fuel via isoprene that has a climate change impact 80% lower than that of fossil jet fuel. The photosensitizer 1,1-dinaphthylmethanone absorbs in the near-UV light, so natural sunlight can be used with low photosensitizer loading (0.1 mol%). Later, other small conjugated dienes were investigated, providing a deeper understanding of the photodimerization. We concluded that isoprene is the ideal diene to be dimerized into jet fuel, as it has a suitable boiling point that facilitates its harvesting and as it dimerizes more efficiently than the other small volatile dienes.

The photodimerization is then expanded to larger substrates to produce lubricant oils and diesel-like fuels. We found that α -phellandrene dimerizes very efficiently (>90%, 12h), and we utilize it in a cross-dimerization with less reactive monoterpenes and with isoprene. We also investigated the influence of light intensity in the reaction of α -phellandrene and the rates of triplet quenching of the photosensitizer by different monoterpenes.

A final part of this thesis addresses the need of photochemical routes that can oligomerize unsaturated hydrocarbons other than conjugated dienes. The seminal idea is to use photoacids as catalysts. This journey started by designing a new photoacid based on the anilinium and dibenzotropylium cationic moieties. We found computationally a strong photoacidity, with pK_a = -12. We discovered that the photoacidity is operating by a novel mechanism involving a reorganization of charge distribution within the dibenzotropylium moiety upon excitation, which interacts electrostatically with the anilinium moiety and makes the acidic proton of the anilinium unit more acidic.

The work described in this thesis provides further understanding of the triplet photosensitized reactions first reported in the early 1960s, and it applies this important organic photoreaction in the context of renewable energy. Furthermore, the last part of this thesis contributes to new interpretations of photoacidity.

Keywords: Aviation fuels, triplet sensitization, photoacid, renewable energy, photochemistry

Leandro Cid Gomes, Department of Chemistry - Ångström, Synthetic Molecular Chemistry, 523, Uppsala University, SE-751 20 Uppsala, Sweden.

© Leandro Cid Gomes 2023

ISSN 1651-6214

ISBN 978-91-513-1682-6

URN urn:nbn:se:uu:diva-492631 (<http://urn.kb.se/resolve?urn=urn:nbn:se:uu:diva-492631>)

*To my parents
Antonio and Rute*

List of Papers

This thesis is based on the following papers, which are referred to in the text by their Roman numerals.

- I. Rana, A.; Cid Gomes, L.; Rodrigues, J. S.; Yacout, D. M. M.; Arrou-Vignod, H.; Sjölander, J.; Proos Vedin, N.; El Bakouri, O.; Stensjö, K.; Lindblad, P.; Andersson, L.; Sundberg, C.; Berglund, M.; Lindberg P.; Ottosson, H. A combined photobiological-photochemical route to C₁₀ cycloalkane jet fuels from carbon dioxide *via* isoprene. *Green Chem.*, **2022**, *24*, 9602 – 9619.
- II. Vajravel, S.;‡ Cid Gomes, L.;‡ Rana, A.; Ottosson, H. Towards a combined photobiological-photochemical route to kerosene-type fuels: Which small 1,3-diene photodimerizes most efficiently? *Manuscript*.
- III. Cid Gomes, L.; Rana, A.; Berglund, M.; Wiklund, P.; Ottosson, H. Light-driven (cross-)dimerization of terpenes as a route to renewable C₁₅ – C₃₀ crudes for fuel and lubricant oil applications. *Sustainable Energy and Fuels*, **2023** DOI: 10.1039/D2SE01370C.
- IV. Cid Gomes, L.; Pace, D. P.; Zubiria-Ulacia, M.; Casanova, D.; Nguyen, T. V.; Ottosson, H. Remote electrostatic repulsion triggered by excited state antiaromaticity relief as the origin of the photoacidity in an organic dye. *Manuscript*.

‡ These authors contributed equally to the investigation.

Reprints were made with permission from the publishers.

Papers I and III were previously discussed in the context of a licentiate thesis defense presented on 24 March 2021, entitled “*From terpenes to advanced biofuels: Light-induced routes to sustainable biocrudes for high energy density fuels*”. However, the content is revised extensively.

Contribution Report

- I. Performed the experiments in the photochemical part together with AR (*i.e.*, some of the dimerization reactions and most of the hydrogenations). Performed all the simulated and natural sunlight experiments, and the determination of quantum yields. Provided the data required for the LCA, together with AR. Contributed to the writing of all parts of the paper and supplementary information together with the other authors.
- II. Contributed to planning the project together with HO and AR. Guided and planned the experiments performed by SV. Performed all quantum chemical calculations and its data analysis. Wrote the manuscript together with SV and HO.
- III. Performed all the experiments and quantum chemical calculations, as well as its data analysis. Wrote and revised the manuscript and supplementary information with input and feedback from the other authors.
- IV. Planned the project together with HO and TVN. Performed all the experiments, except by the synthesis of the photoacid/conjugate base, their crystal structures determination and characterization by FTIR and HRMS. Performed all the quantum chemical calculations as well as its data analysis – except by the constrained DFT calculations. Wrote and revised the manuscript and supplementary information with input and feedback from the other authors.

Contents

1 Introduction.....	11
2 Background.....	13
2.1 Small Hydrocarbons as Renewable Substrates.....	13
2.2 Larger Hydrocarbons as Renewable Substrate.....	15
2.3 Key Aspects in Organic Photochemistry.....	16
2.4 Triplet Sensitized Reactions.....	19
2.5 Quantum Yields of Photochemical Reactions.....	21
2.6 Photoacids and Determination of Photoacidity.....	22
2.7 Topics in Computational Quantum Chemistry.....	24
2.8 Outline for Thesis.....	26
3 A Combined Photobiological-Photochemical Route to C ₁₀ Cycloalkane Jet Fuels From Carbon Dioxide <i>via</i> Isoprene (Paper I).....	29
3.1 Introduction.....	29
3.2 Bio-Isoprene Production.....	30
3.3 Isoprene Photosensitized Dimerization.....	31
3.4 Hydrogenated Isoprene Dimers as Jet Fuels.....	34
3.5 Computational Mechanistic Studies.....	36
3.6 Life Cycle Assessment.....	37
3.7 Conclusions.....	39
4 Towards a Combined Photobiological-Photochemical Route to Kerosene-Type Fuels: <i>Which Small 1,3-diene Photodimerizes Most Efficiently?</i> (Paper II).....	40
4.1 Introduction.....	40
4.2 Linear Conjugated Dienes.....	41
4.3 Cyclic Conjugated Dienes.....	45
4.4 Optimizing the Conditions of Dimerization for the Combined Photobiological-Photochemical Route.....	47
4.5 Conclusions.....	48
5 Light-Driven (Cross-)Dimerization of Terpenes as a Route to Renewable C ₁₅ – C ₃₀ Crudes for Fuel and Lubricant Oil Applications (Paper III).....	50
5.1 Introduction.....	50
5.2 Photodimerization of Monoterpenes.....	51
5.3 Myrcene and Ocimene Reactivities.....	55

5.4 Cross-Photodimerization and Beyond C ₂₀ Crudes	57
5.5 Physical Properties of Selected (Cross)Photodimers	59
5.6 Conclusions	61
6 Remote Electrostatic Repulsion Triggered by Excited State Antiaromaticity Relief as the Origin of the Photoacidity in an Organic Dye (Paper IV).....	62
6.1 Introduction	62
6.2 The Ground State of HDMAPAN-(BF ₄) ₂ and its Conjugate Base	64
6.3 The Excited State and Photoacidity of HDMAPAN-(BF ₄) ₂	66
6.4 Probing the Origins of the Photoacidity in HDMAPAN-(BF ₄) ₂	67
6.5 Conclusions	71
7 Conclusions and Outlook	72
Acknowledgements.....	74
Populärvetenskaplig Sammanfattning.....	76
Popular Science Summary	79
References.....	82

Abbreviations and Symbols

pK_a	Acid dissociation constant at logarithmic scale
pK_a^{hv}	Acid dissociation constant at logarithmic scale in the excited state
α	Alpha
β	Beta
ΔH	Enthalpy
ΔG	Gibbs free energy
I	Light intensity
R	Molar gas constant
P	Molar photon flux
n_x	Number of events
n_p	Number of photons absorbed
ϕ_x	Quantum yield
$k_{(x)}$	Rate constant
S_n	Singlet
T	Temperature
t	Time
E	Total electronic energy
T_n	Triplet
λ	Wavelength
DXS	1-Deoxy-D-xylulose-5-phosphate synthase
AP	Acidification potential
ASTM	American Society for Testing and Materials
CC	Climate change
DFT	Density functional theory
DCM	Dichloromethane
FLU	Fluctuation index
FTIR	Fourier-transform infrared spectroscopy
FEC	Fresh-water ecotoxicity
FE	Fresh-water eutrophication
GCMS	Gas chromatography – mass spectrometry
GHG	Greenhouse gas
HRMS	High-resolution mass spectrometry
HOMO	Highest occupied molecular orbital

CE	Human toxicity cancer effects
HTX	Human toxicity non-cancer effects
HGOD	Hydrogenated ginger oil dimers
HID	Hydrogenated isoprene dimers
HMD	Hydrogenated myrcene dimers
HAPID	Hydrogenated α -phellandrene and isoprene dimers
HAPD	Hydrogenated α -phellandrene dimers
IEF	Integral equation formalism variant
ISC	Intersystem-crossing
IDI	Isopentenyl-diphosphate isomerase
IspS	Isoprene synthase
LUMO	Lowest occupied molecular orbital
LBO	Lubricant base oil
ME	Marine eutrophication
MEP	Methylerythritol-4-phosphate
MCI	Multicenter index
NHOC	Net heat of combustion
NMR	Nuclear magnetic resonance
PM	Particulate matter
POF	Photochemical ozone formation
PCM	Polarizable continuum model
SOMO	Singly occupied molecular orbital
SASA	Solvent accessible surface area
SMD	Solvent model based on density
SOC	Spin-orbit coupling
TE	Terrestrial eutrophication
TD-DFT	Time dependent density functional theory
UV	Ultraviolet
UV-Vis	Ultraviolet-Visible

1 Introduction

“You put together two things that have not been put together before. And the world is changed. People may not notice at the time, but that doesn’t matter. The world has been changed nonetheless.”

-Julian Barnes, *Levels of Life*

A couple of years ago, the words of Julian Barnes had me thinking of the work described in this thesis. While Barnes was talking about combining ballooning and photography,¹ this thesis addresses the use of photochemical reactions to convert photobiologically produced compounds into fuels and lubricant oils – *i.e.* a combined photobiological-photochemical approach to reduce the environmental impact compared to traditional routes. As early as 1860s, CO₂ and other greenhouse gas (GHG) emissions have been correlated to climate change.^{2,3} Worldwide, the transport sector was responsible for releasing 22 % of the total CO₂ emissions in 2020.⁴ Renewable sources represent only 3 % of the final energy consumption by the transport sector, leaving crude oil as the main source for fuel production, which explains the high CO₂ and GHG emissions.⁵ Indeed, the oil industry poses several environmental issues: non-renewability of its source; high GHG emissions and release of hazardous chemicals during the extraction and refining processes; and often risk of water and land contamination. The unsustainable nature of crude oil also leads to environmental impacts from products other than fuels, such as lubricant oils and organic solvents.

A variety of approaches have been proposed to replace fossil fuels. Two of the cleanest alternatives are the use of electricity and hydrogen gas to power light vehicles.⁶⁻⁸ On the other hand, hydrocarbons are still the ideal compounds for high energy density fuel applications and lubricant oils.⁹⁻¹¹ Because the fuel combustion still produces CO₂, the focus to reduce environmental impacts is to find both sources and synthetic routes that are more sustainable. Therefore, several biological sources and chemical routes have been investigated in the past decades, giving rise to advanced liquid biofuels.⁷ They share similar chemical structure to fossil fuels, which allows for quicker transition without deep changes in the infrastructure of the fuel industry.¹¹

Advanced biofuels is a broad category that can be broken down into the sum of second-, third- and fourth-generation biofuels. The second-generation of biofuels are obtained from the conversion of non-edible biomass, mainly

hydrotreated vegetable oils, fermentation of waste or modification of byproducts from industrial processes, such as the hydrogenation of monoterpenes in turpentine from paper pulping process.¹² Third- and fourth-generation biofuels designate fuels derived from feedstock produced by microorganisms and bioengineered microorganisms, respectively, such as microalgae and cyanobacteria.¹³ The latter can utilize sunlight, water and CO₂ to produce a range of small hydrocarbons, such as ethylene, isobutene and isoprene, but also larger compounds, *e.g.*, α -phellandrene, myrcene and α -bisabolene, to name a few.^{14–23}

Depending on the targeted product, small hydrocarbons can be further oligomerized in longer chains, while larger compounds can be directly hydrogenated or further reacted to produce larger molecules. There are several routes to carry out these modifications, ranging from traditional methods utilized in the oil industry, to more recent developments with metal catalysis and photochemical reactions.^{12,24–29}

However, one may ask “*why to oligomerize e.g. isoprene produced by cyanobacteria into C₁₀ or C₁₅ compounds if the production of mono- and sesquiterpenes is also possible by cyanobacteria?*”. The answer relies on the increasing complexity and cost to remove the products from cell cultures as the size of the products increase.²³ Compounds as large as monoterpenes can also be toxic to the cyanobacteria strains,³⁰ therefore, compounds with lower molecular weight are more advantageous as they can escape from the cells more easily, saving the energy of harvesting the feedstock as well as sparing the cells for further cycles of production.

On the other hand, a price is paid when replacing some of the *work* done by cyanobacteria with chemical synthetic routes: the commercially available oligomerization methods do not utilize sunlight as driving force. Ideally, the further modifications of the photobiologically produced hydrocarbons should also make use of sunlight. Photosensitized and photoacid-catalyzed reactions are presented here as two such alternatives. The photochemical aspects of these routes and their implementation are the backbone of this thesis, accompanied by the investigation of which compounds can be sourced from photosynthetic microorganisms, and how some of them can be more efficiently oligomerized. At the same time, considering the present gap to achieve a commercial production of hydrocarbons by cyanobacteria, the work in this thesis was also written in the light of other renewable feedstocks that are more readily available at the present (second-generation of biofuels).

Similar to combining ballooning and photography, combining photobiology and photochemistry create challenges, yet, to a large extent, this thesis aims to address such challenges and present the development of solutions that will contribute to *change the world*.

2 Background

2.1 Small Hydrocarbons as Renewable Substrates

Several routes and feedstocks have been explored to address the need of advanced liquid biofuels. The “oil-to-fuel” route and the use of lignocellulosic biomass were earlier discussed in the context of a licentiate thesis, presented on 24 March 2021, entitled “*From terpenes to advanced biofuels: Light-induced routes to sustainable biocrudes for high energy density fuels*”. In the two first sections of the present thesis, focus is given to compounds that are possible to obtain from cyanobacteria (small hydrocarbons and terpenes), and other renewable sources available for these compounds.

Ethylene, isobutene and 1,3-butadiene (Fig. 2.1A) have industrial importance on the synthesis of fuels and polymers, so it is convenient that these building blocks – or their immediate precursors in case of 1,3-butadiene – can be photosynthetically produced by cyanobacteria.^{22,31–34} The photosynthetic production of ethylene *via* conversion of carbon dioxide was first reported in 1997,²¹ and since then, the overexpression of specific enzymes in the carbon fixation metabolism,³⁵ or immobilization of cyanobacteria in artificial biofilms,³⁶ represent some of the advances towards a future commercial and large-scale production of bio-ethylene.

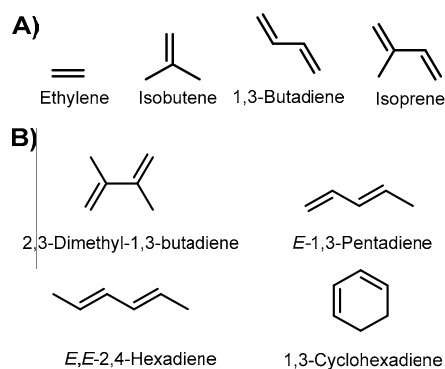


Fig. 2.1 A) Structures of small alkenes and conjugated dienes that can be produced by photosynthetic microorganisms. B) Structure of further small conjugated dienes from alternative renewable sources.

Though essential in the existing routes to fuels, ethylene, isobutene and 1,3-butadiene have boiling points below 0 °C, which requires the use of high pressure to perform further oligomerization reactions. Isoprene, on the other hand, is a liquid at room temperature, but volatile enough to rapidly escape from cell cultures.²³ Metabolically engineered cyanobacteria such as *Synechocystis* and *Synechococcus* can produce isoprene with titers up to 50 µg/g of dry cell weight/day.^{23,37}

The production of small hydrocarbons by cyanobacteria utilizes sunlight, CO₂ and water in the synthetic pathway, neutralizing CO₂ emissions and making the route possible to be carbon neutral. In Paper I, the production of bio-isoprene by cyanobacteria *Synechocystis sp.* was combined to its photochemical dimerization to yield a crude mixture of C₁₀-cycloalkenes. After mild thermal conversion and hydrogenation, the product has suitable properties to be used as jet fuel.

That study has directed our attention to the photochemical dimerization of other small conjugated dienes from bio-based sources (Fig 2.1B) in order to assess the effects of different chemical structures on the efficiency of the photochemical dimerization step, and to find out if another bio-based diene than isoprene could be ideal (Paper II).

In the broader set of small conjugated dienes, not all compounds are reported to be directly produced by photosynthetic organisms. The deoxydehydration of xylitol followed by deoxygenation can produce bio-based 1,3-pentadiene,³⁸ as well as the metal-catalyzed conversion of 1,4-pentanediol derived from levulinic acid obtained from lignocellulose.³⁹ Further conjugated dienes - 1,3-cyclohexadiene, 2,3-dimethyl-1,3-butadiene and 2,4-hexadiene – can be obtained from chemical transformations of compounds obtained from plant oils,⁴⁰⁻⁴² platform chemicals from lignocellulose biomass such as pinacol,⁴³ and photosynthetic microorganisms (in this case, the building block is bio-ethylene to produce 2,4-hexadiene).⁴⁴ Even though these several routes represent gains in renewability over the traditional fossil sources, our ultimate goal in Paper II was to evaluate if any of these conjugated dienes could serve as more efficient substrate in the photochemical dimerization step. If so, then it would be encouraged to seek photobiological routes to produce such conjugated dienes. Yet, the conclusion from Paper II was that isoprene is still the ideal substrate.

Besides the C₄ – C₆ conjugated dienes, longer conjugated dienes can be sourced from cyanobacteria or other alternative renewable sources. They are mainly derivatives of isoprene, forming the class of compounds named as terpenes. Utilizing the range from C₁₀ – C₁₅ as substrate enables the access to dimers in the range of diesel and lubricant oil applications (Paper III).

2.2 Larger Hydrocarbons as Renewable Substrate

Terpenes are both cyclic and open-chain hydrocarbons derived from isoprene and they can be grouped according to the n number of isoprene units, for example: $n = 2$, monoterpenes; $n = 3$, sesquiterpenes; $n = 4$, diterpenes, and so on (Fig. 2.2).⁴⁵ Two monoterpenes that are present in high amounts in turpentine are the bicyclic isomers α -pinene and β -pinene. The former can be photochemically converted to ocimene,⁴⁶ while the pyrolysis of β -pinene produces myrcene.⁴⁷ Another cyclic monoterpene, α -phellandrene, is present in substantial amounts in the leaf oil of pepper trees *Schinus mole* and also in eucalyptus oil (46 % and 31 %, respectively).^{48,49}

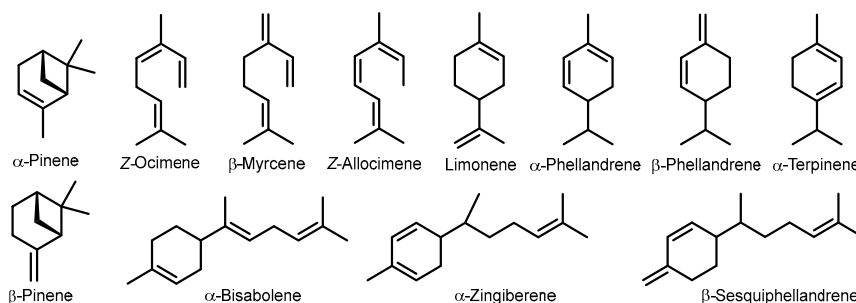


Fig. 2.2 Structures of several terpenes.

Despite the natural abundance of terpenes, their extraction is sometimes energetically costly, so alternative routes that use microorganisms in the production of terpenes should be more economically and environmentally beneficial, provided that better strategies to harvest them from cell cultures are also developed. Monoterpenes, such as limonene and myrcene, can be produced by aerobic fermentation of sugars by *Escherichia coli* strains,^{50,51} however, the supply of air required increases the costs of the production. A reported production of myrcene was improved by 34-fold as approaching to *in situ* extraction has minimized cell toxicity and myrcene evaporation.⁵¹ Microbial production of bisabolene by *E. coli* and *Saccharomyces cerevisiae* was also reported with high titers (900 mg L⁻¹).⁵² Furthermore, photosynthetic microorganisms that convert CO₂ directly into terpenes are even more advantageous. Several studies addressing metabolically engineered cyanobacteria from the genera *Synechocystis* and *Synechococcus* report the production of terpenes such as limonene,⁵³ β -phellandrene^{54,55} and bisabolene.²⁰

Owing to their multiple sources and the chemical structure similarities to fossil fuels, terpenes have been used as feedstock in a variety of biofuel synthetic routes. The most straightforward approach is the hydrogenation of mono- and sesquiterpenes, converting them into linear and cyclic alkanes. Blends of hydrogenated sabinene, limonene and α -pinene (sabinane, *p*-

menthane and pinane, respectively, catalyzed by PtO₂ or Pd/C) with synthetic paraffinic kerosene exhibit higher net heat of combustion (NHOC) compared to the conventional jet fuel Jet-A.¹² Hydrogenated bisabolene and farnesene were also shown to be candidates for diesel and jet fuel surrogates.^{52,56}

Some other routes involved more steps than just hydrogenation, yielding products with different applications. The thermal dimerization of myrcene, followed by the hydrogenation of the dimers afforded C₂₀ camphorane isomers with higher energy content compared to biodiesel from vegetable oil, and satisfactory cetane number and low temperature properties.²⁷ Yet, too high viscosity led the authors to test blends with diesel (50 %) which improved the viscosity. Further, an iron catalyzed cross-coupling between isoprene and myrcene was reported to yield C₁₅ – C₂₀ compounds suitable for jet fuel and diesel applications.²⁹ The acid catalyzed dimerization of pinenes, camphene and limonene has also been reported to generate renewable high-density fuels.^{57,58} Lastly, Major and co-workers developed a computational tool for the design of biofuels derived from terpenes and terpenoids, covering the estimation of cetane number and the calculation of heat of combustion (based on the enthalpies of combustion).⁵⁹

In light of the multiple renewable sources of terpenes, and especially the growing field of their production by photosynthetic organisms, we chose these compounds as the feedstock for production of high-density fuels and lubricant oils in Paper III *via* photosensitized (cross)dimerization of C₅ – C₁₅ substrates.

2.3 Key Aspects in Organic Photochemistry

Interaction between matter and light leads to photophysical and photochemical processes. In the former, no chemical modification occurs to the molecule, while in the latter the starting materials are changed into other compounds. The wavelength range from 290 to 820 nm corresponds to 35 and 100 kcal mol⁻¹, which is enough to break chemical bonds and promote photochemical reactions.⁶⁰ Photochemical reactions are useful routes to synthesize molecules that are not possible through thermal reactions. This is the case for many strained compounds such as cubanes and sterically hindered *Z*-isomers.^{61,62} It is also through interactions with light that aromatic compounds are turned into excited state anti-aromatic species, leading to reactivities that are opposed to those of the stable ground state aromatic compounds.⁶³ Photochemistry is also paramount to understand the formation of complex organic molecules in the outer space.⁶⁴ Back to Earth, the understanding of interactions between molecules and photons is essential to harvest and use sunlight: the most abundant energy source in renewable energy context, as seen in solar cells and in the synthesis of solar fuels.⁶⁵

Fundamental information of the electronically excited states of a compound is given by its corresponding UV-Vis absorption spectrum.⁶⁵ Though it is a

simple technique to perform in the laboratory, UV-Vis absorption spectroscopy reveals which wavelengths can promote a specific compound to its electronically excited states and, therefore, which light sources are suitable for promoting further photophysical or photochemical changes. It is also possible to rationalize ranges of light absorption based on the chemical structure and functional groups: for example, a purely saturated hydrocarbon will not absorb near-UV light (300 – 400 nm). In fact, alkanes absorb at wavelengths below 200 nm.⁶⁶ Ketones, on the other hand, have a redshifted absorption and when conjugated systems are added, *e.g.* aryl groups, their absorption can reach even the visible region, a feature of importance when developing reactions driven by sunlight.⁶⁷

In spectroscopy, the absorption frequencies match the energy differences between ground state and electronically excited levels, which are in general accessed *via* absorption of one photon.⁶⁵ Therefore, the relationship between functional groups and wavelengths that a compound absorbs is underlined by the energy levels of a molecule, especially its HOMO and LUMO energies, which are affected by different functional groups. For instance, π -conjugation lowers the energy gap between HOMO and LUMO, requiring less energy (*i.e.* longer wavelengths) to excite valence electrons.⁶⁰ Such reduced energy gaps can reflect on the energy gap between the electronic states of a molecule (S_0 , S_1 , S_2 , etc.). These states and the transitions between them are depicted in energy state diagrams (Fig. 2.3A), also known as Jablonski diagrams, named after the physicist Aleksander Jablonski, and they are an important representation when describing photophysical processes.

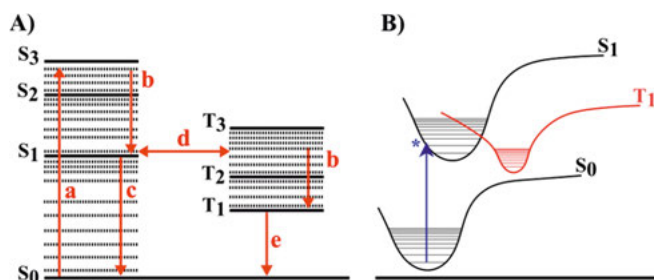


Fig. 2.3 A) Jablonski diagram with photophysical transitions. a) Electronic absorption, b) internal conversion/vibrational relaxation, c) fluorescence, d) intersystem crossing and e) phosphorescence. Dashed lines represent the vibrational levels. B) Representation of the Franck-Condon principle. The blue (*) represents the spectroscopic state originated from the vertical transition.

Jablonski diagrams display different electronic and vibrational levels of a molecule in a simplified way, in which it is possible to illustrate different transitions: in Fig. 2.3A, a) electronic absorption, b) internal conversion/vibrational relaxation, c) fluorescence/emission, d) intersystem crossing and e)

phosphorescence/emission.⁶⁸ For each of these transitions – as well as for photochemical reactions – a quantum yield (ϕ_x) can be determined, which measures the efficiency of the photophysical or photochemical process and it is equal to the number of events (n_x) divided by the number of photons absorbed (n_p) – see *Section 2.5*.⁶⁵

Relaxed ground state geometries can differ extensively from relaxed geometries in the excited state. On that account, according to Born-Oppenheimer approximation and the Franck-Condon principle, because electrons move much faster than nuclei, the electronic transitions take place at one single geometry of a molecule (Fig. 2.3B).⁶⁵ Therefore, they are also named as vertical transitions and the starting/ending points of such electronic transitions are called spectroscopic states. Any geometrical relaxation to a minimum occurs after the electronic transition.

Additionally, the singlet and triplet spin multiplicities are displayed in the Jablonski diagram. The electronic spin is a fundamental property of electrons,⁶⁹ and the spin of an electron can be assigned to either $+1/2$ or $-1/2$, or up and down. A singlet state is the case in which the electronic configuration of a molecule has all the electrons in different orbitals with paired spins ($\uparrow\downarrow$), *i.e.* spins with opposite signs (Fig 2.4). If two electrons in a system have unpaired spins ($\uparrow\uparrow$), the configuration is at a triplet state, *i.e.* the system has multiplicity $M = 3$.⁶⁵ The letters *S* and *T* are used to designate a singlet or triplet state, respectively, and a subscript number indicates in which level the state related to the ground state of the molecule (S_0). Although excited states higher than S_1 and T_1 exist, the internal conversion from the higher states to S_1 or T_1 often occurs very rapidly, with radiative processes being unable to compete with them.⁶⁰ Consequently, processes other than internal conversion, such as emission (fluorescence or phosphorescence), intersystem crossing and photochemical reactions, are mostly considered to happen from S_1 or T_1 states - the so-called Kasha's rule.

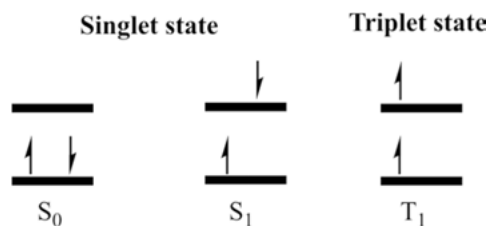


Fig. 2.4 Qualitative and simplified representation of singlet and triplet states. The arrows represent electrons and their direction represents the sign of the spin.

Singlet excited states have short lifetimes due to the competition with other allowed transitions (*i.e.* fluorescence), while triplet states have longer lifetimes and hence they are easier to control and more likely to partake in

chemical reactions, giving rise to varying reactivity and products according to which spin multiplicity is involved.⁷⁰ The transition from singlet to triplet is called intersystem crossing (ISC) and it requires an electron spin flip induced by magnetic interactions,^{60,65} which allows for the mix of spin states and provides conservation of the total angular momentum. The rate constants for ISC are usually very low because of the general weak magnetic coupling of electron spin to another source of angular momentum.^{60,65} However, in the case of a transition of which the magnetic moment of the electron spin flip can be strongly coupled to the magnetic moment of the orbital motion - spin-orbit coupling (SOC) - the rates of ISC are higher and, indeed, molecules that exhibit this feature have quantum yields of ISC up to unit.

A strong SOC occurs when the energy gap between the states involved is small (energy gap law), or/and when a heavy atom is near the electron that has its spin flipped.^{60,68} As the energy gap between S_1 and T_1 become smaller, spin-vibronic coupling and mixing of T_n states can boost the ISC – if symmetry allowance can be borrowed from the other T_n states.⁶⁸ On the other hand, the heavy atom effect is a consequence of the higher orbital magnetic moment originated by the higher acceleration of the electron when it approaches the nucleus, which is a higher acceleration because of the higher nuclear charge in heavy atoms compared to lighter atoms.⁶⁰ The same heavy atom effect can be triggered by an external heavy atom, as in a solvent.⁶⁸ The resulting interpretation of SOC factors is translated into the El Sayed's rule,^{65,71,72} which states that faster rates of ISC are observed when there is a change in the orbital type during the transition. Therefore, transitions of the type $^1n,\pi^* \rightarrow ^3\pi,\pi^*$ or $^1\pi,\pi^* \rightarrow ^3n,\pi^*$ are allowed, whilst transitions are forbidden when only the spin state is changed (*e.g.* $^1n,\pi^* \rightarrow ^3n,\pi^*$). Noteworthy, ketones often satisfy these criteria.

In view of such selection rules, it is expected that several compounds display inefficient intersystem crossing by direct excitation – *i.e.* compounds that do not meet the selection rules requirements. However, triplet states in these compounds are still accessible through sensitization.

2.4 Triplet Sensitized Reactions

A molecule absorbing light at certain wavelength can be excited and then transfer that energy to another molecule that does not absorb light of the same wavelength. This process is called sensitization or photosensitization, and it is based on the occurrence of energy transfer from a singlet or triplet excited donor (D^*) to an acceptor (A), resulting in the excitation of A to its singlet or triplet excited state.⁶⁵ The mechanisms considered for energy transfer between D^* and A are either *via* dipole-dipole interaction (also designated as Coulombic, Förster or resonance mechanism, Fig 2.5A), or *via* electron exchange, which were theorized by Förster⁷³ and by Dexter,⁷⁴ respectively (Fig. 2.5B).⁶⁰

In the former mechanism, D^* has an oscillating dipole field induced by the oscillation of its excited electron.⁶⁰ When the oscillation frequency matches a natural frequency of A, both species can resonate and, as a result, A^* is populated by excitation of its electron under the influence of the oscillating dipole field generated. An overlap of the orbitals of D^* and A is not required and the interaction occurs through space.

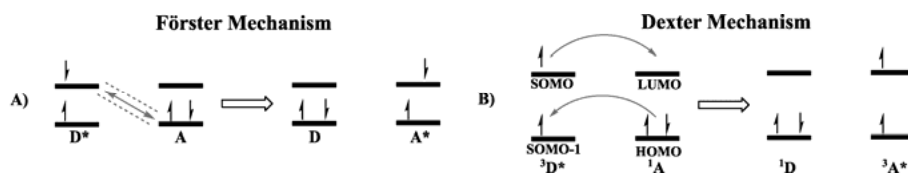


Fig. 2.5 Energy transfer mechanisms.

On the other hand, the Dexter mechanism requires orbital overlap (between SOMO of D^* with LUMO of A and between SOMO-1 of D^* with HOMO of A, see Fig. 2.5B) and van der Waals contact between D^* and A. Consequently, dilution can affect the rates of energy transfer operating *via* the Dexter mechanism to a larger extent.⁶⁵ The amount of electronic states that can resonate once D^* and A is coupled by orbital overlapping also affects the efficiency of the energy transfer.⁶⁰ For the particular case of triplet-triplet energy transfer, though it is overall a spin allowed transition (the spins are conserved), it cannot occur *via* dipole-dipole interaction mechanism since A has a zero transition dipole moment in the singlet-triplet absorption.⁶⁵ Hence, triplet-triplet energy transfer are plausible to occur *via* the Dexter mechanism.

In photosensitized reactions, the species D is called photosensitizer (later designated as **PS** in this thesis). Certainly, a triplet photosensitizer must have a high ϕ_{ISC} for efficient sensitization, as well as a triplet energy higher than the triplet energy of the sensitized molecule A.⁶⁵ Arylketones and their derivatives (*e.g.* xanthone and thioxanthone) are common examples to possess high ϕ_{ISC} and triplet energies between 60 – 70 kcal mol⁻¹, thereby they can sensitize molecules that have triplet energies below those values. In fact, triplet photosensitization is also observed when the sensitized molecule has a triplet energy higher than that of the photosensitizer, however, in this case the transition in the sensitized molecule is believed to start from a vibrational excited level, *i.e.* it needs to be thermally excited.⁶⁵

Arylketones such as benzophenone absorb light in the near-UV range and it has been observed that extending the π -conjugation enables redshifted absorptions and efficient ISC. This is due to the reduction of energy gap between HOMO and LUMO, which leads to better mixing of states and spin-vibronic coupling, and allowed transitions such as $S_1 \rightarrow T_4 \rightarrow T_1$.^{67,68} UV-vis absorptions and triplet energies can also be tuned by electron donor and electron acceptor substituents, such as reported for thioxanthone derivatives.⁷⁰

Ketones, arylketones and other aromatic compounds have been used extensively on the photosensitized dimerization of conjugated dienes in the early 1960s.⁷⁵ In most cases, the products were cyclic compounds whose cycloaddition is thermally forbidden.⁷⁶ Isoprene – among other small conjugated dienes – was dimerized under benzophenone photosensitization to afford [2+2], [4+2] and [4+4] photocycloaddition products.^{77,78} Interestingly, a study with several photosensitizers and isoprene revealed the dependence of the dimer distribution upon the triplet energy of the photosensitizer.⁷⁹ This observation is explained by the fact that some dimers resulted from *s*-cis isoprene (six-member rings), and others resulted from *s*-trans (four- and eight-member rings). Since the *s*-cis and *s*-trans isoprene triplets have different energies (the triplet energy is 6 kcal mol⁻¹ smaller for *s*-cis), a photosensitizer with lower triplet energy will preferably excite *s*-cis isoprene.

Previously, monoterpenes were also subject to photosensitized reactions, such as α -phellandrene, ocimene and myrcene.^{76,77,80} Ocimene was studied for its *E/Z* photosensitized isomerization and α -phellandrene was reported to dimerize when naphthalene was used as photosensitizer. Myrcene was reported to both dimerize and also to produce a byproduct from the internal diene addition to its isolated double bond.

2.5 Quantum Yields of Photochemical Reactions

As stated earlier, quantum yield is defined as the number n_x of events x divided by the amount n_p of photons absorbed by the reactant (Equation 2.1).⁶⁵ It is paramount to strictly define what is the process x when comparing different quantum yields, e.g. if it is the disappearance of a reactant or if it is the product formation.

$$\phi_x(\lambda) = \frac{n_x}{n_p} \quad \text{Equation 2.1}$$

The number of incident photons n_p per unit of time is the molar photon flux P (Equation 2.2).

$$P = \frac{n_p}{t} \quad \text{Equation 2.2}$$

When replacing n_p by P in Equation 2.1, it is possible to use the rate constant $k(x)$ for the formation of products in process x :

$$\phi_x(\lambda) = \frac{k(x)}{P} \quad \text{Equation 2.3}$$

The Equation 2.3 provides the basis to actinometry, *i.e.* the use of a photochemical reaction with well-known quantum yield to determine the n_p via photon flux P .⁸¹ The actinometer is a compound that undergoes a known photochemical reaction with an accurately known quantum yield.⁶⁵ In this case, the photon flux that reaches a sample is calculated based on the measured rate constant for the reaction of the actinometer, and later that value is used to calculate the quantum yield of the studied photochemical reaction by running it under the same conditions.

Potassium ferrioxalate is a widely used actinometer, yet, its quantum yield is wavelength dependent.^{81,82} If a non-monochromatic light source is used, a full spectra analysis is needed in this case.^{81,83} Taking a photosensitized reaction as example, the full spectra analysis embodies: a) the determination of the actual light intensity absorbed by the actinometer, done by multiplying the emission intensity of the light source by the transmittance of the actinometer at each wavelength (and the same is done for the photosensitizer); and b) the integration of spectra obtained in (a) to determine the total light intensity absorbed by the actinometer and by the photosensitizer. The final equation to determine the quantum yield ϕ_x should include the total intensities determined in (b):

$$\phi_x = \frac{k(\text{product formation})}{P} \times \frac{I(\text{actinometer,total})}{I(\text{photosensitizer,total})} \quad \text{Equation 2.4}$$

This method was used to determine the quantum yield of the photosensitized dimerization described in Paper I.

2.6 Photoacids and Determination of Photoacidity

Despite being a very useful route, the triplet photosensitized dimerization methodology under visible light is energetically restricted to conjugated dienes. Other bio-based building blocks such as ethylene, isobutene, limonene and pinenes are not possible to be sensitized, as their triplet state energies lie too high above the triplet state energy of the photosensitizers absorbing in the visible light range. Traditionally, pure alkenes are industrially dimerized or oligomerized in acid catalyzed processes.²⁸ It is then possible to envision that a photochemical route to the oligomerization of alkenes could be found on the realm of photoacids. We start this journey in Paper IV, by computationally investigating the strong photoacidity of a new photoacid and its mechanism of photoacidity.

Photoacids are neutral or charged organic compounds that become more acidic upon excitation.⁸⁴ Such changes in acidity are reflected in the changes of values of pK_a in the ground state and in the excited state (pK_a^{hv}). In the most traditional example of photoacid, 2-naphthol has a basic pK_a in the

ground state ($pK_a = 9.5$), but in the S_1 state it has a low and acidic pK_a^{hv} of 2.8.⁸⁵ 2-Naphthol is among the photoacids earlier studied by Förster and Weller.⁸⁵⁻⁸⁸ The former was the first to describe a thermodynamic cycle to illustrate the relative energies of a photoacid and its conjugate base, and as a consequence, the cycle is known as “Förster cycle” (Fig 2.6).

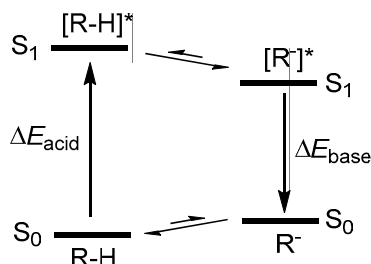


Fig. 2.6 The Förster cycle showing the relative energies of a photoacid and its conjugate base in the ground and first excited state.

From the Förster cycle one can roughly estimate the pK_a^{hv} from the known pK_a by using the differences in the excitation energies of the transition $S_0 \rightarrow S_1$ in both acid and base.

$$pK_a^{hv} = pK_a + \frac{\Delta\Delta E}{RT \ln 10} \quad \text{Equation 2.5}$$

Where $\Delta\Delta E = \Delta E_{base} - \Delta E_{acid}$. The excitation energies ΔE_{acid} and ΔE_{base} can be obtained from experimental UV/Vis absorption spectroscopy or from the emission spectra of the acid and base. Alternatively, the energies can be calculated by computational methods such as time-dependent density functional theory, TD-DFT.⁸⁹ The Förster cycle is useful for estimating the pK_a^{hv} , and, even though it does not always give accurate results as it does not consider changes in molecular conformations or solvation relaxation,^{90,91} it still gives a good estimation and is much easier to perform than time resolved techniques.

Nevertheless, the use of the Förster cycle requires previous knowledge of the ground state pK_a . Experimentally, the pK_a of a compound can be measured by quantifying the amount of acid and conjugate base in equilibrated solutions of different pH, using traditional analytical techniques such as UV/Vis absorption spectroscopy.⁹² An alternative and more robust method to determine the pK_a of a compound is through the Born-Haber thermodynamic cycle (Fig. 2.7).

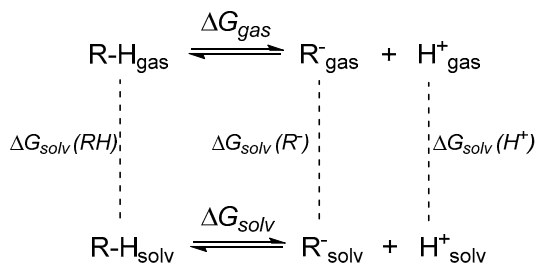


Fig. 2.7 Born-Haber thermodynamic cycle.

The Born-Haber cycle is used to find the reaction free energy ΔG° for the deprotonation of the acid. To determine ΔG° , the solvation free energy is calculated by considering the free energies of the equilibrium between the acid and the conjugate base in both gas phase and solvent phase.^{89,93} Note that the Born-Haber cycle can be used to determine both pK_a and pK_a^{hv} , provided that one computes the geometries in the ground and excited states, respectively. We utilized both the Born-Haber and the Förster cycles, as well as experimental methods to determine the pK_a and pK_a^{hv} of a new photoacid in Paper IV, and further discussed the origins of the photoacidity on that compound based on computational analyses.

2.7 Topics in Computational Quantum Chemistry

Throughout this thesis the experimental work is accompanied by quantum chemical calculations. In general, density functional theory (DFT) methods were used to investigate in detail the reaction mechanisms and reactivities of different substrates in the triplet photosensitized dimerization reactions (Papers I, II and III), and to compute the enthalpy of combustion of some hydrogenated dimers (Papers I and III). In Paper IV, DFT and TD-DFT methods were used to support experimental data on the conformational characterization of the photoacid in solution, to investigate its electronic structure, to determine the pK_a and pK_a^{hv} of the photoacid and to test the hypothesis of the origin of its photoacidity.

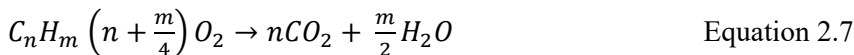
In this section, I would like to comment briefly on some of the computational topics that are more specific to the work presented in this thesis – *i.e.* the quantum chemical protocol to compute fuel properties developed by Major and co-workers,⁵⁹ the choice of the Solvation Model Based on Density (SMD) as the solvent model used in our studies; and the computational indices Multicenter Index (MCI) and Fluctuation Index (FLU) to quantify (anti)aromaticity. The reader is referred to textbooks^{94,95} and to a tutorial review⁹⁶ for general discussions of DFT and TD-DFT methods and the use of different basis sets.

Major and co-workers have recently developed a protocol to compute several physical properties of compounds used as biofuels,⁵⁹ such as the cetane number, boiling point and enthalpies of vaporization and combustion. We applied their method to compute the enthalpies of combustion of selected hydrogenated dimers in Papers I and III. The enthalpies of vaporization (ΔH_{vap}) of water and of the hydrogenated dimers are needed to compute the enthalpy of combustion $\Delta H_{combustion}$ according to the Eq. 2.6:

$$\Delta H_{combustion} = n \cdot (E^{corr})_{CO_2(g)} + \frac{m}{2} \cdot [(E^{corr})_{H_2O(g)} - \Delta H_{vap,H_2O}] - [(E^{corr})_{C_nH_m(g)} - \Delta H_{vap,C_nH_m} + (n + \frac{m}{4}) \cdot (E^{corr})_{O_2(g)}]$$

Equation 2.6

where E^{corr} is the electronic energy plus the enthalpy correction at 298 K, which are computed by a hybrid DFT method in the gas phase, and the factors n , $\frac{m}{2}$, and $n + (\frac{m}{4})$ are related to the stoichiometry of the combustion reaction and will depend upon the chemical formula of the hydrogenated dimer, Eq. 2.7:



The correction to the liquid phase is done by adding the enthalpies of vaporization of water and of the hydrogenated dimer in Eq. 2.6. The enthalpy of vaporization for the dimer is obtained from the conversion of the computed free energy of solvation, ΔG_{solv} with Equation 2.8:

$$\Delta H_{vap} = a \cdot (-\Delta G_{solv}) + b \cdot T \cdot SASA + c$$

Equation 2.8

where SASA is the solvent accessible surface area⁹⁷⁻⁹⁹ (172.863 Å² for toluene, the solvent modeled in our calculations in Paper I and III), and T is the temperature (298 K). Using multiple linear regression for a set of terpenes, Major and co-workers determined the factors a , b and c as $a = 1.170093$, $b = 0.000084$ and $c = 0.059668$.

The solvent modeled to compute the free energy of solvation (toluene) was modeled by the implicit solvation model SMD.¹⁰⁰ The same solvent model was used in Paper IV to compute the NMR spectra and the free energies of solvation of the photoacid. The main descriptors utilized in the SMD model are dielectric constant, refractive index, bulk surface tension, and acidity and basicity parameters.¹⁰⁰ The SMD model is a Polarizable Continuum Model (PCM) and uses solutions of the integral equation formalism variant (IEF),¹⁰¹⁻¹⁰⁴ thus being part of the IEF-PCM methods. The main difference is that in the SMD method the solute is described by its total continuum charge density, in

opposition to the representation of the solute as the sum of its partial atomic charges.¹⁰⁰ At the present, the SMD is the recommended model for computing free energy of solvation,¹⁰⁵ and it has been the solvent model chosen in computations of pK_a and pK_a^{hv} of (photo)acids,^{89,106} as it is done in Paper IV.

A final topic to be discussed in this section is the computational assessment of (anti)aromaticity. Aromaticity in the excited state is described by the rules derived by Baird in 1972.¹⁰⁷ They are the reversal of Hückel's rule in the S_0 state, *i.e.* systems with $4n+2$ π -electrons are antiaromatic in their lowest $\pi\pi^*$ triplet and singlet excited states.¹⁰⁸ Excited-state aromaticity and antiaromaticity have been used to explain several photophysical and photochemical processes.¹⁰⁹⁻¹¹⁵ (Anti)aromaticity can be computationally assessed by geometric, energetic, magnetic and electronic indices. The multicenter index (MCI)^{116,117} and aromatic fluctuation index (FLU)¹¹⁸ are examples of electronic indices and they were utilized in Paper IV.

In electronic indices, the extent of electron delocalization is the source of the (anti)aromaticity assessment. In the FLU index, the electron delocalization of the molecule of interest is compared to a known aromatic compound as reference. The FLU index returns values close to zero for aromatic compounds, and larger positive values for non-aromatic and antiaromatic compounds. On the other hand, MCI values close to zero designate antiaromatic/nonaromatic systems and larger values are found for aromatic systems.

2.8 Outline for Thesis

The more sustainable production of biofuels and lubricant oils is needed to reduce the GHG emissions and their effects on climate change. We have proposed as ideal the approach of combining photobiological production of volatile substrates to their photochemical conversion into fuels and lubricant oils. Photosynthetic microorganisms such as cyanobacteria have been shown to be good candidates for the photobiological part. On the other hand, despite the historical close interaction that photochemistry and renewable energy had over the years, there is no example of a photochemical route coupled to the photobiological production of substrates, therefore, the photochemical pathway to be used in that approach requires more studies within that context. On the photochemical part, we chose the photosensitized dimerization of conjugated dienes as the manifold to oligomerize the bio-substrates produced by cyanobacteria. The first three papers of this thesis is devoted to study the photosensitized dimerization of conjugated dienes in the context of the photobiological-photochemical production of fuels and lubricants. Therefore, a direct focus is to find conditions with a higher efficiency in the use of sunlight for the reaction, shorter reaction times, understanding of different reactivities among substrates and the effects of diluted conditions. Finding the most

suitable substrates is also required. Furthermore, this thesis also initiated a search for alternative photochemical steps where the photosensitized dimerization could not be used – *i.e.* a photoacid catalyzed oligomerization of alkenes. In this context, deeper understanding of photoacidity phenomenon and its mechanisms might guide us towards a successful route.

In Chapter 3 (Paper I), the proof-of-principle of the combined photobiological-photochemical production of bio-jet fuels is presented utilizing the photosensitized dimerization of isoprene in the photochemical step. The first challenges on the photochemical step, along to its solutions, are discussed. We highlight how the choice of the photosensitizer 1,1-dinaphthylmethanone could allow the use of wavelengths available in the emission spectrum of the sun. The quantum yield of the reaction shows an efficiency twice higher for 1,1-dinaphthylmethanone when compared to the traditional photosensitizer benzophenone. Further design of reactors to increase surface area exposure to light was used to increase the yields of dimers. In the context of jet fuel, the initial hydrogenated dimers were not yet fully within the specifications, so we performed mild thermal isomerization of the [2+2] dimers in order to adequate the fuel properties. Finally, an LCA corroborates that our approach contributes to a reduction of the climate impact in the production of fuels when compared to fossil fuels.

In Chapters 4 and 5 (Papers II and III) we deepened the understanding of the varying reactivities of different substrates in the photosensitized dimerization. In Chapter 4, we addressed the need of finding the most suitable substrate. Our study revealed that isoprene is the ideal substrate in the photochemical step. Moreover, we identified how its structure favors the dimerization by having a reduced substitution of methyl groups, which decreases the steric hindrance, but still makes the triplet state energetically accessible. 1,3-Cyclohexadiene was found to be extremely efficient for the photochemical step, due to the endocyclic nature of the conjugated diene unit and, consequently, the longer lifetime of its triplet state. However, 1,3-cyclohexadiene is not as volatile as isoprene, which imparts the harvesting from the cells in the photobiological step. We further put the reaction in the present context of photobiological production of conjugated dienes, *i.e.* very diluted conditions, and we explored how to optimize the reaction.

In Chapter 5, more information is gained on the different reactivities of larger substrates (monoterpenes), which are more complex than the small substrates studied in the preceding chapters. The reaction is then affected by intramolecular byproducts that can be formed and trap the reactants, sterically hinderance of the radical sites, the triplet lifetimes of the substrates (as studied in Chapter 4), and also how they quench the photosensitizer. The chapter also contributes to understand the light intensity dependency of the reaction. Finally, we show that the photosensitized dimerization can be used to produce diesel-like fuels and lubricant oils.

In Chapter 6 (Paper IV), we study a new photoacid and propose a novel mechanism of photoacidity. The chapter is an ensemble of mainly computational, but also experimental investigations, which lead us to conclude that the new compound has photoacidic properties that could be useful to the oligomerization of alkenes. Yet, the short lifetimes of singlet excited states can be an issue for the observation of reaction and lack of thereof. Nonetheless, this is a seed-work that contributes to further development in the study of photoacids and the development of photochemical oligomerization reactions of small alkenes.

In the final outlook of this thesis (Chapter 7), a general summary is given, highlighting the importance of understanding the photosensitized dimerization of conjugated dienes as an important contribution to climate change mitigation. The final chapter also addresses the further development required to bring the photosensitized dimerization to a large-scale level, and to develop the photoacid-catalyzed oligomerization.

3 A Combined Photobiological-Photochemical Route to C₁₀ Cycloalkane Jet Fuels From Carbon Dioxide *via* Isoprene (Paper I)

In this chapter, the combined photobiological-photochemical production of C₁₀ hydrocarbons *via* isoprene is described at a laboratory scale. Several aspects of this novel and interdisciplinary approach are addressed: 1) the photobiological production of isoprene by cyanobacteria, and the strategies of trapping the photobiologically produced bio-isoprene; 2) The photochemical tools and optimization of conditions required for the photosensitized dimerization of isoprene under natural and simulated sunlight; 3) Computational investigation of the mechanism in the photochemical step; 4) Further chemical transformations of the isoprene dimers to provide a mixture of alkanes suitable as jet fuel; 5) The sustainability metrics of the combined photobiological-photochemical approach using Life Cycle Assessment tool.

3.1 Introduction

In order to obtain a drop-in sustainable fuel, renewable sources should be combined with sustainable routes to produce biofuels that resemble the existing fossil fuels – *i.e.* hydrocarbons. Both photobiological and photochemical routes enable the use of sunlight as the main energy source. While photosynthetic microorganisms can produce small hydrocarbons that can escape easily from the cultures,^{22,23} these compounds are too short for being used as jet fuels. On the other hand, photobiological production of longer hydrocarbons (*e.g.* monoterpenes) poses toxicity to the cells and demands more costly methods of harvesting.^{30,119} Therefore, it should be beneficial to have a subsequent step that can oligomerize the photobiologically produced small hydrocarbons, and be driven by sunlight. The work presented in this chapter tests the approach of combining a photobiological step to a photochemical step to produce C₁₀ hydrocarbons to be used as jet fuel, and the work has been developed in collaboration to microbial chemistry groups of Pia Lindberg, Karin Stensjö, and Peter Lindblad.

The small hydrocarbon utilized as substrate is isoprene, which can be produced by metabolically engineered cyanobacteria *Synechocystis sp.* We highlight the possibility of using sunlight in the two main steps, namely the CO₂ and water

conversion into isoprene and its further photosensitized dimerization into C₁₀ cycloalkenes (products of [2+2], [4+2] and [4+4] cycloaddition).

C₁₀ cycloalkanes showing excellent jet fuel properties were provided after small thermal modifications of some of the dimers, followed by their hydrogenation. The mechanism of reaction was studied by computational methods (density functional theory, DFT) in order to understand the near absence of larger oligomers formation. Finally, the system was modelled to a larger scale and evaluated by a Life Cycle Assessment (LCA) tool, which showed the potential of the technology to reduce environmental impact when compared to traditional fossil fuels.

3.2 Bio-Isoprene Production

The work in this section has been performed by the microbial chemistry groups and has also been discussed in the Doctoral Thesis of Dr. João Rodrigues. Isoprene is not naturally produced by cyanobacteria and, therefore, metabolic engineering is required. The modifications in the methylerythritol-4-phosphate (MEP) pathway were performed by introducing genes encoding three different enzymes that catalyze three different steps (see Fig. 3.1): A) conversion of pyruvate and glyceraldehyde-3-phosphate into methylerythritol-4-phosphate; B) isomerization of isopentenyl diphosphate to dimethylallyl diphosphate; C) and conversion of dimethylallyl diphosphate into isoprene. The cultures of metabolically engineered *Synechocystis* were exposed to constant illumination during four days, and then the headspace of the cultures was flushed with air in order to drag the isoprene vapors into a collector tube containing cold heptane (kept at -40 °C). The bio-isoprene trapped in heptane was later used in photochemical dimerization experiments. The titer achieved was up to 1.60 mg L⁻¹ and the trapping efficiency reached up to 89 %.

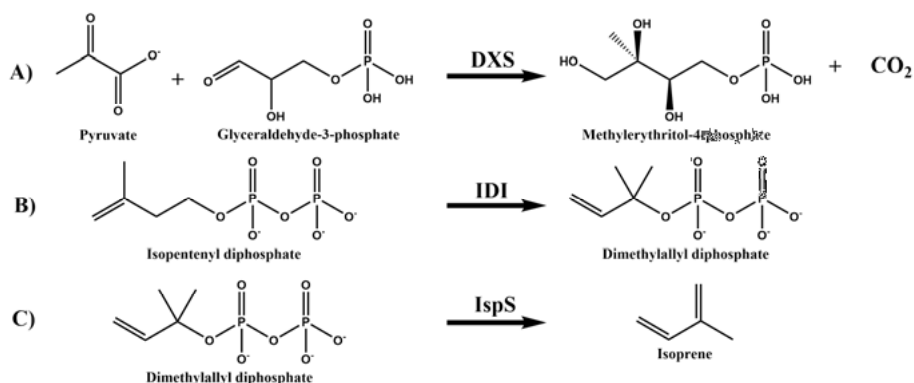


Fig. 3.1 Reactions catalyzed by the three enzymes introduced in the metabolically engineered *Synechocystis*. **A)** conversion of pyruvate and glyceraldehyde-3-phosphate into methylerythritol-4-phosphate, catalyzed by DXS (1-deoxy-D-xylulose-5-phosphate synthase); **B)** isomerization of isopentenyl diphosphate to dimethylallyl diphosphate, catalyzed by IDI (isopentenyl-diphosphate isomerase); and **C)** conversion of dimethylallyl diphosphate into isoprene, catalyzed by IspS (isoprene synthase).

In addition, two problematic aspects of the production of bio-isoprene were investigated: genetic instability of the *Synechocystis* strains, which caused variable production of isoprene; and inhibition of cell growth and productivity caused by accumulation of isoprene and oxygen. The genetic instability was addressed by expressing the genetic constructors from the cyanobacterial chromosome instead of expressing them from a plasmid. The new strains were superior in stability (evaluated over several weeks of cultivation). Improvements on the growth and productivity were achieved by incorporating frequent vent cycles during the cultivation, collecting the gas phase containing isoprene. All experiments with frequent vent cycles showed higher cumulative amounts of isoprene compared to experiments without vent cycles. This was an important finding to pave the development of efficient bio-isoprene production in larger scale.

3.3 Isoprene Photosensitized Dimerization

Isoprene has an experimental triplet energy of 59.6 kcal mol⁻¹ for the *s*-trans conformer and 53.5 kcal mol⁻¹ for the *s*-cis.⁷⁸ Therefore, we tested various suitable arylketones to promote the isoprene triplet photosensitized dimerization under 365 nm, 44 h (Fig. 3.2).

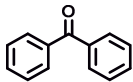
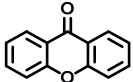
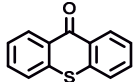
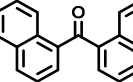
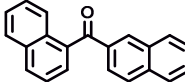
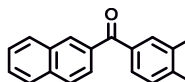
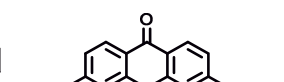
				
ID ($E(T_1)$) kcal mol ⁻¹	3.1 (62.7, 68.6)	3.2 (67.4, 74.1)	3.3 (61.1, 63.3)	3.4 (54.0, 56.5)
Dimers yield (%)	22	12	32	42
				
ID ($E(T_1)$) kcal mol ⁻¹	3.5 (54.7, 57.8)	3.6 (54.6, 59.2)	3.7 (70.0, n/a)	
Dimers yield (%)	28	28	5	

Fig. 3.2 Photosensitizers tested and their respective triplet energies in parenthesis (blue is the adiabatic triplet energies in kcal mol⁻¹ computed at (U)B3LYP-D3/6-311+G(d,p) level; red is the experimental value).^{79,120–123} It also shows the isolated yields of isoprene dimers obtained for each photosensitizer tested (loading of 0.1 mol%), in quartz test tube under irradiation at 365 nm for 44 h.

After the screening of photosensitizers and performing optimization of the setup (*vide infra*), 1,1-dinaphthylmethanone **3.4** was found to give the best results (91% yield, 0.1 mol% loading, 44 h), exceeding the performance of the conventional photosensitizer benzophenone **3.1**. The compound **3.4** has, indeed, a higher molar extinction coefficient at 365 nm and a smaller singlet-triplet energy gap, favoring the ISC.⁶⁷ Even though the isomers of **3.4** (**3.5** and **3.6**) have a higher absorption extinction coefficient at 365 nm, they performed worse. The compounds **3.2** and **3.3** have poor solubility in isoprene and much higher triplet energies. Additionally, we determined the quantum yield of the photosensitized dimerization of isoprene for benzophenone ($\phi_{BP} = 0.43$), and for 1,1-dinaphthylmethanone ($\phi_{DNM} = 0.91$), which is almost twice higher. Potassium ferrioxalate was used as the actinometer, since it is a standard compound used in actinometry and it absorbs at the near-UV light range.

Besides the beneficial spectroscopic properties that **3.4** exhibit, the more efficient dimerization also resulted from using a reaction setup with higher surface area compared to a regular quartz test tube. The setup was composed of a TeflonTM tubing (O.D. \times I.D.: 3.18 mm \times 2.1 mm) coiled around a water condenser (Fig. 3.3A). A similar approach is employed in further experiments using simulated and natural sunlight, albeit a redesign into a flat spiral was required to fit the setup according to the light source (sun or solar simulator, Fig. 3.3B).

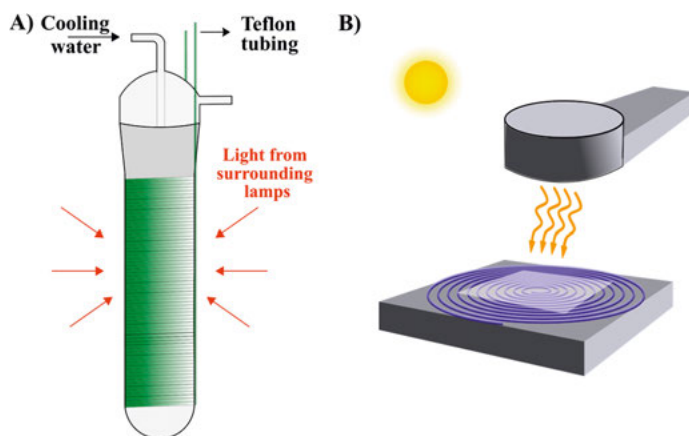


Fig. 3.3 Illustrative representation of the reaction setups designed for higher surface area to be exposed to light. **A)** Teflon tubing (O.D. \times I.D.: 3.18 mm \times 2.1 mm) coiled on a water condenser, allowing for cooling and irradiation from surrounding lamps - as using a Rayonet photoreactor. **B)** Same Teflon tubing in a flat spiral reaction setup designed for natural and simulated sunlight experiments.

The extended π -conjugation in **3.4** allows a redshifted absorption compared to benzophenone.⁶⁷ Indeed, the band absorption tail stretches up till approximately 400 nm (Fig. 3.4). This feature is extremely important in order to carry out the photosensitized dimerization under sunlight. Using the flat spiral setup, 4 mL scale, the isoprene dimerization was tested both under simulated sunlight (one sun equivalent, AM 1.5G, 44 h, 61% yield) and natural sunlight (20 h, 17 % yield, Uppsala, Sweden 59°51'09.5"N 17°39'19.9"E, approximately 30 m above sea level on May 30 - 31, 2020). These results were important to highlight the feasibility of this reaction to be performed under solar irradiation. Regarding the natural sunlight experiment, it is important to clarify its qualitative nature, considering the relative low sunlight intensity in Sweden and the intermittence of sunlight during the day. Under the same conditions, using benzophenone in 2 mol% loading and 24h of irradiation, the yield of dimers was only 10 %.

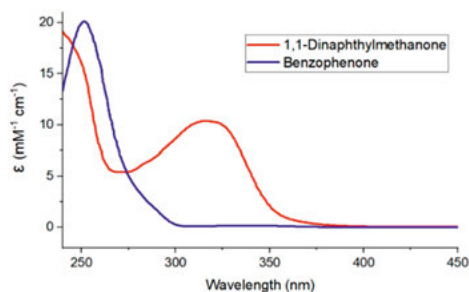


Fig. 3.4 UV-Vis absorption spectra of 1,1-dinaphthylmethanone and benzophenone in DCM.

At last, we combined the photochemical dimerization under simulated sunlight with the photobiological production of bio-isoprene by the *Synechocystis* cells. The heptane solution, earlier used to trap bio-isoprene from the cyanobacteria cultures, was mixed with **3.4** (0.02 M) and irradiated under simulated sunlight (24 h, 1 sun, AM 1.5 G). The reaction produced bio-isoprene dimers that could be identified by GCMS analysis, proving the viability of a photobiological-photochemical route from CO₂ and water to C₁₀ hydrocarbons *via* isoprene.

Apart from demonstrating the use of sunlight in both isoprene production and photodimerization, it is noteworthy to mention additional advantages regarding the usage of the photosensitizer **3.4**: its separation from the products are readily possible by distillation, silica column or recrystallization, and the reactions can be carried out under ambient conditions (92 % yield when degassing was not applied). Furthermore, the recovered photosensitizer can be reused and its synthesis is on one-pot basis, from inexpensive starting materials.

3.4 Hydrogenated Isoprene Dimers as Jet Fuels

The different isomers of isoprene dimers were further hydrogenated to produce **HID-1** (hydrogenated isoprene dimers) and some key fuel properties were measured (Table 3.1, column **HID-1**). The heats of combustion were also computed using calculated enthalpies of combustion.⁵⁹ Despite having both volumetric net heat of combustion (NHOC) and kinematic viscosity within the specifications for jet fuel (Jet-A, ASTM D1665),²⁶ the density of **HID-1** and its flash point were below the corresponding values required in the jet fuel specification.

Table 3.1 Fuel properties of different hydrogenated dimers.

Fuel property	HID-1	HID-2	HID-3	Jet-A²⁶
Density (15 °C) g mL⁻¹	0.770	0.809	0.808	>0.775
Volumetric NHOOC, MJ L⁻¹	34.05	35.25	35.22	>33.17
Kinematic viscosity (-20 °C), mm² s⁻¹	1.71	3.16	2.92	<8.00
Flash point, °C	33.5	38.5	38.5	>38
Freezing point, °C	<-78	<-78	<-78	<-40
Flash point, °C	33.5	38.5	38.5	>38

Therefore, further modifications in the isoprene dimers were needed. Since the flash point can be roughly correlated to the boiling point, the lower boiling point cyclobutane-containing dimers were thermally converted into six- and eight-member ring isomers (Fig. 3.5). The thermal rearrangements were performed at two different temperatures, 135 °C and 160 °C, producing two different mixtures to be hydrogenated separately to form **HID-2** and **HID-3**, respectively. Noteworthy, the conversion into eight-member ring isomers is *via* the Cope-rearrangement.¹²⁴ The fuel properties were measured once more for the new **HID** mixtures, revealing that **HID-2** and **HID-3** were in accordance to the specifications to jet fuels (Table 3.1, columns **HID-2** and **HID-3**).

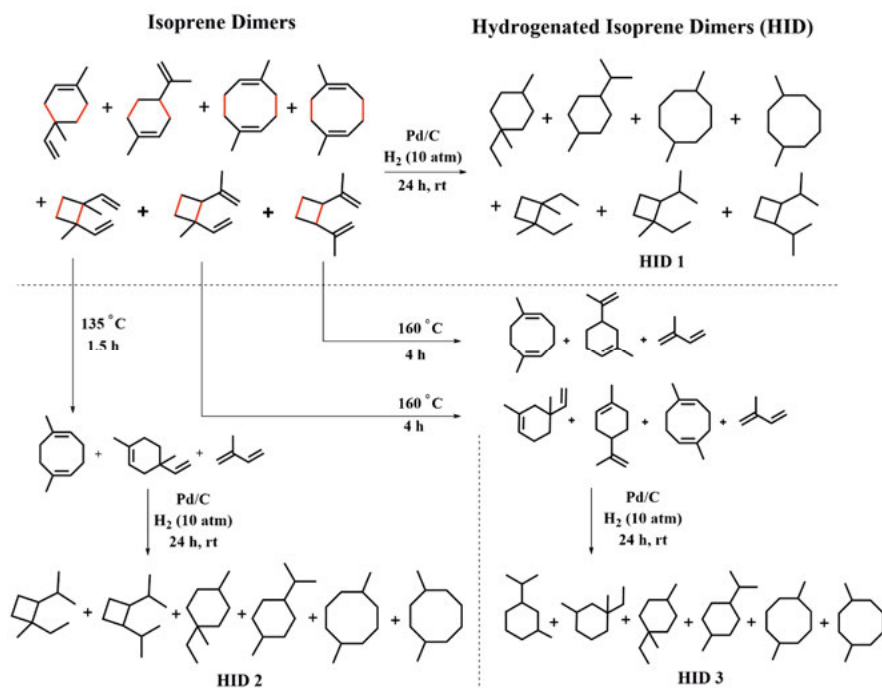


Fig. 3.5 Syntheses of hydrogenated isoprene dimers, including the thermal rearrangements of four-member rings into six- and eight-member rings. Bonds in red are the bonds formed in the dimerization.

3.5 Computational Mechanistic Studies

According to the DFT calculations at (U)B3LYP/6-311G(d,p) level, the isoprene dimerization occurs through five downhill steps (Fig. 3.6): 1 – excitation of the photosensitizer followed by ISC; 2 – triplet energy transfer to isoprene; 3 – alkyl or allyl radical addition to another ground state isoprene, forming a *bis*(allyl) radical pair; 4 – ISC to the singlet diradical and 5 – ring closure from the radical pair combination. Further evidence was also found to explain why trimers and other oligomers were formed in very small amounts: while step 3 has the lowest energy barrier of 13.4 kcal mol⁻¹, the lowest energy barrier for the addition of the *bis*(allyl) radical pair to another isoprene molecule was calculated to be higher (19.8 kcal mol⁻¹). Moreover, the ring closure in step 5 is more kinetically favored than a bimolecular reaction (addition of *bis*(allyl) radical pair to another isoprene in its S₀ state). Additionally, the possible pathway to trimers from the addition of T₁ isoprene to one of the dimers formed had an energy barrier of at least 18.9 kcal mol⁻¹ – a step that renders a single carbon-centered radical, which is less stable than a *bis*(allyl) radical pair (step 3).

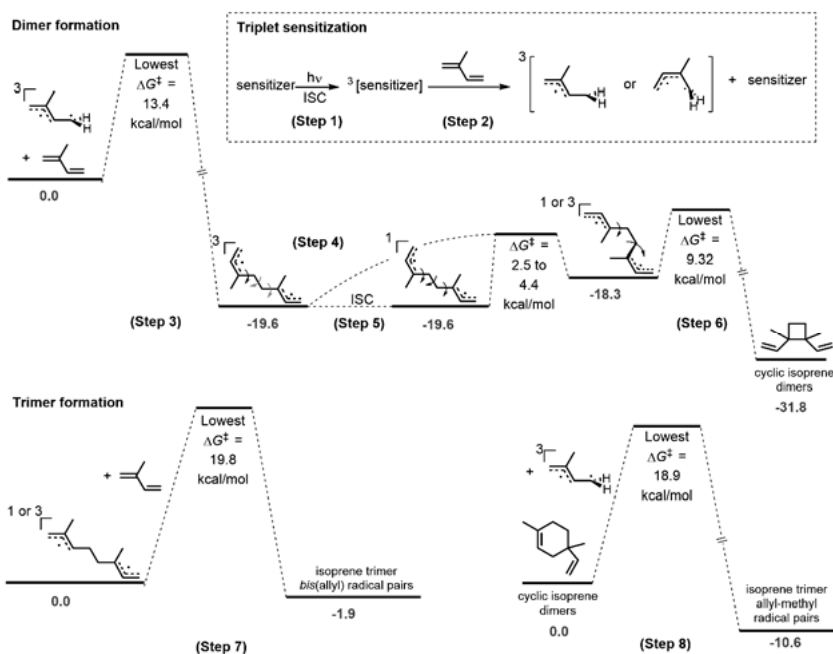


Fig. 3.6 Reaction mechanism and energy barriers in the formation of the cyclic isoprene dimers and trimers. Energies were calculated at (U)B3LYP/6-311G(d,p) level. ISC = intersystem crossing.

3.6 Life Cycle Assessment

A life cycle assessment was performed to evaluate the environmental sustainability metrics of our present system in a large scale, as well as to identify what improvements are required. The functional unit was set as one tonne of fuel (1000 kg). The input data for the photobiological step was based on the model used for cyanobacterial production of butanol recently reported by Nilsson *et al.*⁹⁸ The photobioreactor was set to have 750 m³ and to cover 1 ha of land (1 ha = 10000 m²), and further assumptions were made: carbon fixation at 1.2 g L⁻¹ day⁻¹; 80 % of water is recycled; and the Swedish energy mix is used as the model for electricity supply.^{125,126}

Based on the laboratory scale experiments, the time required for the sunlight-driven dimerization of isoprene to reach 51 % yield was set to 60 h (extrapolation of the experiment giving 17 % yield in 20 h). The high recovery percentage of the photosensitizer (95 %) associated with the low loading (0.1 mol%) supported the decision to exclude it from the LCA. Further input data for the downstream processes was based on reported literature of consolidated industrial processes (*e.g.* distillation, hydrogenation of alkenes and production of N₂).

The LCA evaluated the process in ten different categories of environmental impact: Climate change (CC), human toxicity non-cancer effects (HTX), human toxicity cancer effects (CE), particulate matter (PM), photochemical ozone formation (POF), acidification potential (AP), terrestrial eutrophication (TE), freshwater eutrophication (FE), marine eutrophication (ME) and freshwater ecotoxicity (FEC). The climate change impact was found to be 0.7 tonne CO₂ eq./tonne fuel, which is 80 % lower than the conventional Jet A. It is also a value lower or comparable to other recently reported biofuels.^{98,99}

The percentage contribution of different processes to the different categories of environmental impact are shown on Fig. 3.7. The use of sodium nitrate (*i.e.* its production) is the major contributor in all categories (from 78 % in HTX to 97.1 % in TE), representing the bottleneck of the system in terms of sustainability. Sodium nitrate is an essential macronutrient for the cultivation of cyanobacteria, and therefore more environmentally friendly alternatives must be found, such as waste streams sources or the efficient recycling of the utilized sodium nitrate.¹²⁷⁻¹²⁹ Following the sodium nitrate, the electricity is the second major contributor on the climate change category, while the production of ZnSO₄ heptahydrate and tap water use represents the second major contributors in the HTX and CE categories, respectively. Other processes not mentioned had contributions lower than 5 % in the different categories.

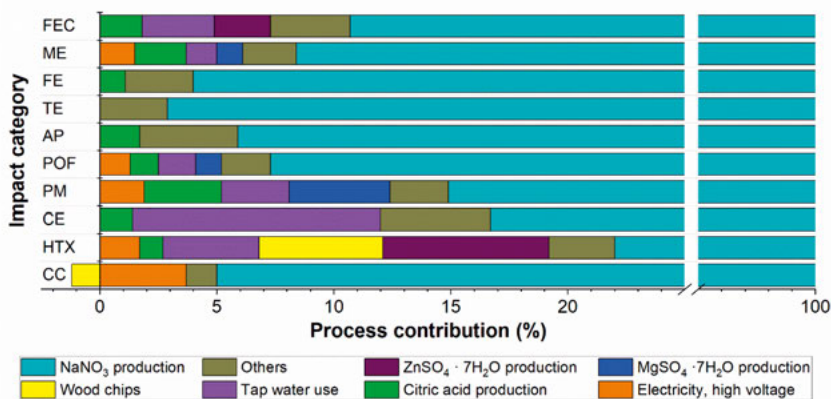


Fig. 3.7 Contribution analysis showing percent of impacts originating from the different processes in the different environmental impact categories. Climate change (CC), human toxicity non-cancer effects (HTX), human toxicity cancer effects (CE), particulate matter (PM), photochemical ozone formation (POF), acidification potential (AP), terrestrial eutrophication (TE), freshwater eutrophication (FE), marine eutrophication (ME) and freshwater ecotoxicity (FEC).

3.7 Conclusions

We showed for the first time, as a proof-of-concept, the possible coupling between the photobiological production of isoprene and its photochemical dimerization using sunlight irradiation to afford C₁₀ hydrocarbons. On the photochemical part, it is valuable that the reaction can run under ambient conditions with a reusable photosensitizer in very low concentration. The accomplishment of high yield dimerization by modifications in the reaction setup exemplifies that further adjustments could provide even better results in industrial scale. The final product - the thermally modified dimers - revealed a jet fuel composition that entirely fulfils and even excel the Jet-A specifications. Noteworthy, even **HID-1** is already nearly ideal product to be used as jet fuel.

The present work faces several challenges regarding enhancement for industrial scale. The production of bio-isoprene needs to achieve higher titers, while the photodimerization step should ideally be optimized to shorter reaction times or photosensitizers that can utilize longer wavelengths of the solar spectrum. Nevertheless, the LCA indicates that the reported route is an exciting alternative for a drop-in bio-jet fuel generated primarily from CO₂, water and sunlight, as it allows the mitigation of CO₂ emissions compared to existing fossil fuels.

Lastly, we conclude that further small conjugated dienes should be investigated to gain more mechanistic information and to find out the ideal substrate for the photochemical step.

4 Towards a Combined Photobiological-Photochemical Route to Kerosene-Type Fuels: *Which Small 1,3-diene Photodimerizes Most Efficiently?* (Paper II)

In this chapter, we investigate a broader set of conjugated dienes as substrates in the photosensitized dimerization route introduced in Paper I. These dienes are also available from renewable sources, mainly indirectly through the conversion of platform chemicals from lignin or photosynthetically produced bio-precursors. This work addresses the following three questions: How do different structures of conjugated dienes affect the efficiency of the triplet photosensitized dimerization reaction? What are the main factors driving such different reactivities? And lastly, is isoprene the most suitable diene for the combined photobiological-photochemical production of jet fuel hydrocarbons, or are there other small dienes that are more attractive based on their chemical properties, the sustainability of their sources and their efficiency in the photo-dimerization step?

4.1 Introduction

Small conjugated dienes are traditional substrates in the production of fuels and polymers. However, the non-renewability of the sources associated to the traditional methods for the oligomerization of these substrates cause the existing routes to be unsustainable. While efforts to develop more environmentally friendly methods of oligomerization have been proposed, *e.g.* using thermal or metal catalyzed cyclodimerization that operates at lower temperatures,²⁴⁻²⁶ our sunlight-driven dimerization of isoprene strategy from Paper I can also be applied to different conjugated dienes, affording lower CO₂ emissions when compared to the existing routes.

On the other hand, despite that several conjugated dienes other than isoprene have already been reported to dimerize under triplet photosensitized conditions, it is expected that different structural and electronic features might affect the dimerization efficiencies, which is crucial to the development of cleaner routes to fuels that are also economically viable. Conveniently, the mechanistic investigation of structural effects can be coupled to a selection of

conjugated dienes that can be produced by renewable sources, especially photosynthetic microorganisms (Fig. 4.1), rendering a study that not only addresses the differences in reactivity of different conjugated dienes, but also shines light onto the most desirable combined photobiological-photochemical route to biofuels.

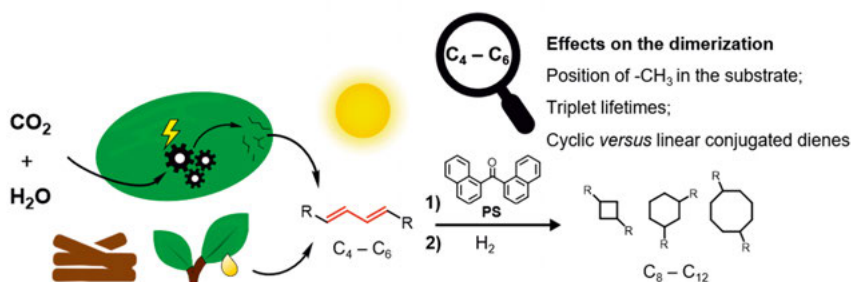


Fig. 4.1 The combined photobiological and photochemical production of $C_8 - C_{12}$ hydrocarbons from CO_2 , together with the aspects investigated in this chapter. Sources represented: photosynthetic microorganisms, lignocellulose (for fermentation), and plant oils. See the main text for further details. PS = photosensitizer, 1,1-dinaphthylmethanone.

In addition, the routes to produce and harvest small conjugated dienes *via* photosynthetic microorganisms have, at the moment, intrinsic conditions that affect the overall efficiency of the photochemical-photobiological route. One example is the current diluted amounts of photobiologically produced small dienes that are trapped in solvents. From this perspective, we also study the effects of such conditions and ways to optimize the photosensitized dimerization step.

4.2 Linear Conjugated Dienes

A set of small conjugated dienes was selected to assess how structural differences can affect the rates of the triplet photosensitized dimerization (Figure 4.2, compounds **4.1** – **4.7**). As described in Chapter 2, these compounds can be obtained directly or indirectly from photosynthetic organisms or other renewable sources. However, we stress that the production by photosynthetic organisms (cyanobacteria) should be the preferred one. The compounds **4.8** and **4.9** were later added in order to assess the particular reactivity found for cyclic conjugated dienes (*vide infra*).

Going from **4.1** – **4.3** and **4.4** – **4.5**, the effects of increasing the number of methyl substituents can be assessed. Comparing the sub-sets **4.2/4.4** and **4.3/4.5/4.6**, gives information regarding the effects of the methyl substituent

position. Finally, the comparison of **4.5** and **4.7** gives information about the influence of a cyclic structure *versus* a linear structure on the reactivity.

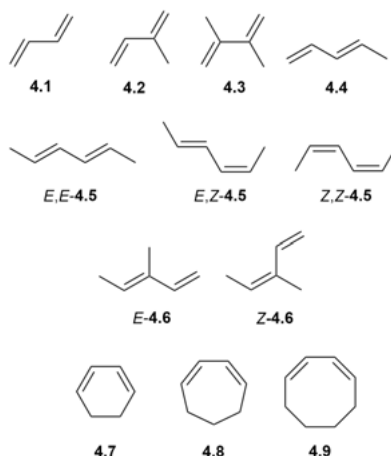


Fig. 4.2 Structure of the selected small conjugated dienes: 1,3-butadiene **4.1**, isoprene **4.2**, 2,3-dimethyl-1,3-butadiene **4.3**, *E*-1,3-pentadiene **4.4**, 2,4-hexadiene **4.5** (mixture of isomers), 3-methyl-1,3-pentadiene **4.6** (mixture of isomers), 1,3-cyclohexadiene **4.7**, 1,3-cycloheptadiene **4.8**, *Z,Z*-1,3-cyclooctadiene **4.9**.

Neat conjugated dienes were mixed with 0.1 mol% of 1,1-dinaphthylmethanone as the photosensitizer and irradiated using the same coiled setup as in Paper I. The irradiation was limited to 24 h and the isolated yields are reported in Table 4.1. Only 1,3-butadiene **4.1** was initially irradiated in dilute solution (15 wt% in hexane) as it is commercially available. Later, isoprene **4.2** and 2,4-hexadiene **4.5** were also irradiated diluted in hexane in order to compare the results with the reaction of **4.1** (foot note “a” in Table 4.1).

Table 4.1: Yields of photosensitized dimerization of different small conjugated dienes (0.1 mol% 1,1-dinaphthylmethanone) and triplet energy $E(T_1)$ of conjugated dienes.

Entry	Diene	Dimer yield (wt%)	$E(T_1)$ (kcal mol ⁻¹)
1	1,3-Butadiene	6.5 ^a	50.4
2	Isoprene	66	49.8
3	2,3-Dimethyl-1,3-butadiene	18 ^a	50.1
4	<i>E</i> -1,3-Pentadiene	29	49.7

5	2,4-Hexadiene	9	46.4 ^b / 47.3 ^c / 49.4 ^d
		1.0 ^a	
6	3-Methyl-1,3-pentadiene	8.7	46.7 ^e / 47.2 ^f
7	1,3-Cyclohexadiene	93	46.4
8	1,3-Cycloheptadiene	45	47.3
9	Z,Z-1,3-Cyclooctadiene	7	45.1

^a Yield when using diluted diene samples (15 wt% in hexane). ^b Z,Z-isomer. ^c E,Z-isomer. ^d E,E-isomer. ^e Z-isomer. ^f E-isomer. Energies calculated at (U)B3LYP-D3/6-311+G(d,p) level of theory with thermal free energy corrections at 298 K.

The results with neat linear conjugated dienes reveal that the dimerization of isoprene **4.2** is the most efficient, and that the least reactive substrates are 2,4-hexadiene **4.5** and 3-methyl-1,3-pentadiene **4.6**. The set of diluted dienes confirms the dimerization of isoprene having the highest yield (higher than the one for 1,3-butadiene **4.1**) and that 2,4-hexadiene **4.5** is the least reactive (less reactive than **4.1**). In the set of neat conjugated dienes, isoprene is followed by 2,3-dimethyl-1,3-butadiene **4.3**, which has half of the yield of dimers compared to isoprene, and then E-1,3-pentadiene.

We initially observed that the addition of one methyl group (**4.1** versus **4.2**) can benefit the photosensitized dimerization, while adding a second methyl substituent (**4.2** versus **4.3**) reduces the efficiency of the photodimerization. The addition of one methyl group reduces the triplet energy of the conjugated diene (Table 4.1), which makes it more energetically accessible in the triplet energy transfer step.¹³⁰ The triplet biradicals formed when the triplet energy is transferred to the conjugated diene are twisted structures with one allyl radical and one alkyl radical (Fig. 4.3). The decrease in energy is due to the stabilization of the triplet radical through hyperconjugation with the methyl group.

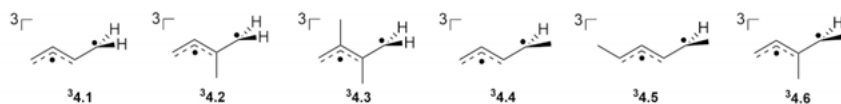


Fig. 4.3 Most stable biradical structures of conjugated dienes **4.1** – **4.6** in their T_1 state ($^3\mathbf{4.1}$ – $^3\mathbf{4.6}$), based on the optimized geometries at (U)B3LYP-D3/6-311+G(d,p) level.

On the other hand, the addition of a second methyl group (**4.2** versus **4.3**) does not further stabilize the triplet biradical since the second methyl group will be attached to the central atom of the allyl radical moiety, which has no orbital coefficients of SOMO, and therefore, no hyperconjugation adds up to the stabilization. Instead, the steric hindrance effect of a more congested transition state dominates as seen in the calculated structure for the transition of the

addition of one triplet conjugated diene to a ground state diene (Fig. 4.4). Comparing the transition state for the reaction of **4.2** and **4.3**, one can see that the bond forming distance in **4.3** is shorter, which forces a longer distance between the neighboring hydrogens of the different units, when compared to **4.2**.

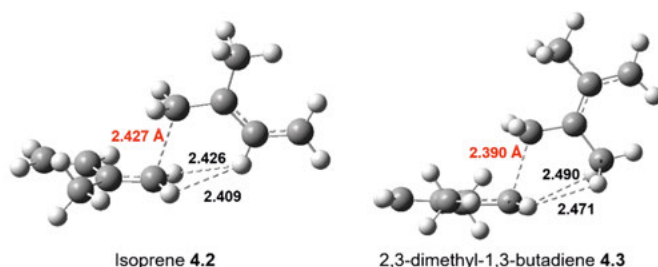


Fig. 4.4 Transition state geometries calculated for isoprene **4.2** and 2,3-dimethyl-1,3-butadiene **4.3**. Values in red are the bond forming distances in the transition states, and the values in black are the distances between the neighboring hydrogen atoms. All distances are in Å. Structures calculated at (U)B3LYP/6-311+G(d,p) level.

The higher steric hindrance in the transition state of the addition step in the dimerization of **4.3** is also reflected in the energy barriers calculated for that step (Fig. 4.5), in which **4.3** shows an energy barrier that is 2.6 kcal mol⁻¹ higher than the one of **4.2**.

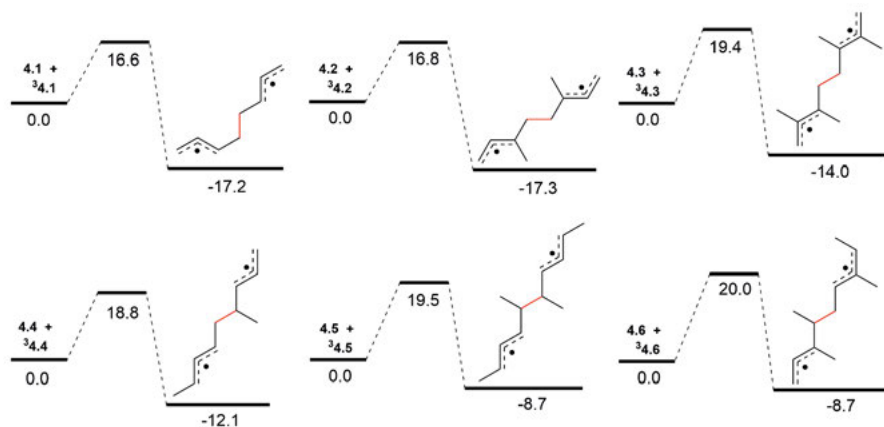


Fig. 4.5 Activation barriers for the addition of a T₁ state diene biradical to an S₀ state diene. The energy barriers were calculated at (U)B3LYP/6-311+G(d,p) level as Gibbs free energies at 298 K. The energy barriers and energies of intermediates formed are in kcal mol⁻¹ and they are relative to the energies of the corresponding reactants.

The next trend observed in our results is related to the position of the methyl substituents. In the linear dienes there is a decrease in the yield of dimers when the methyl group is attached to the terminal carbons of the conjugated diene units, compared to being attached to the central atoms – see results for **4.2** versus **4.4** and **4.3** versus **4.5**. A similar explanation involving the steric hindrance of these sites could be used, as the substitution in the terminal sites yields to alkyl radicals in internal carbons. However, the energy barriers of **4.4** and **4.5** do not exceed the values calculated for **4.3**. In this case, we believe the dominant effect is the local stabilization of the alkyl radical in the compounds with terminal methyl substituents – *i.e.* the alkyl radical in **4.3** is more reactive than the alkyl radical in **4.5** because the alkyl radical in **4.5** is stabilized by hyperconjugation.

In addition, *E*-1,3-pentadiene **4.4** shows higher yield than **4.5** because it has the possibility of forming a triplet biradical in which the alkyl radical is in a terminal carbon – even though this is not the lowest triplet biradical option for **4.4**. Yet, why should **4.4** exhibit a higher yield than **4.6**, since both have the terminal/primary alkyl radical as a possibility? The answer relies on the energy difference between the two possible biradicals in the two compounds (Fig. 4.6): while the two twisted structures are separated by 0.7 kcal mol⁻¹ in the case of **4.4**, that energy difference is of 2.8 kcal mol⁻¹ for **4.6**. Therefore, the structure with the secondary alkyl radical is more favored in the compound **4.6**.

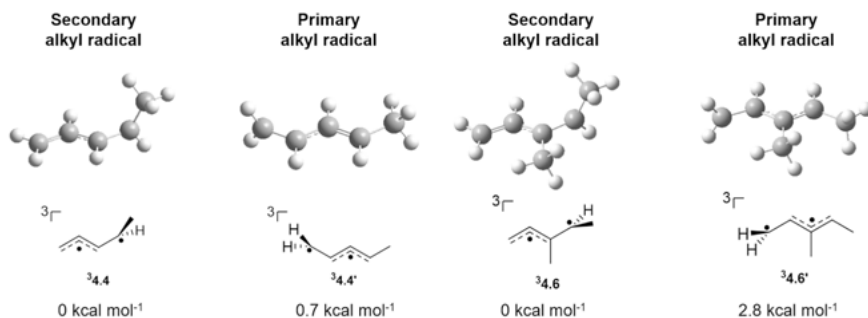


Fig. 4.6 Different twisted triplet biradicals of compounds **4.4** and **4.6**. Relative energies calculated at (U)B3LYP/6-311+G(d,p) level.

4.3 Cyclic Conjugated Dienes

Conversely, the two alkyl radicals in the triplet biradical of 1,3-cyclohexadiene **4.7** are also secondary radicals. Yet, **4.7** has the highest yield in the photosensitized dimerization, exceeding that of isoprene. Even after only 12 h of irradiation, the yield of dimers of **4.7** was already at 80 wt%. Unlike the acyclic dienes, 1,3-cyclohexadiene triplet biradical is not twisted, therefore, the

alkyl radicals are much more reactive due to the Pauli repulsion between the two same-spin π -electrons (Fig. 4.7). For being confined in a small ring, ${}^3\mathbf{4.7}$ has restricted mobility that also yields to a longer triplet lifetime. In fact, the triplet lifetime of ${}^3\mathbf{4.7}$ is two orders of magnitude higher than the values of acyclic conjugated dienes (1300 ns).¹³¹

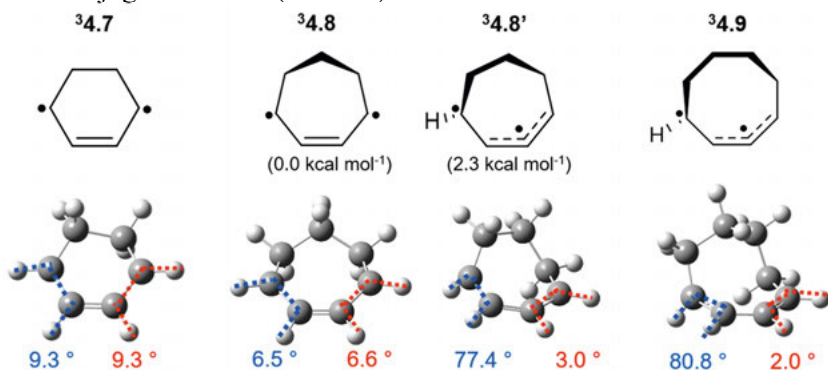


Fig. 4.7 Geometries of the cyclic conjugated dienes $\mathbf{4.7} - \mathbf{4.9}$ in their T_1 states, calculated at (U)B3LYP-D3/6-311+G(d,p) level. The dihedral angles are written in red and blue. For 1,3-cycloheptadiene two minima were found, and their relative Free energies are shown in parentheses.

The larger cycloalkadienes, 1,3-cycloheptadiene $\mathbf{4.8}$ and *Z,Z*-1,3-cyclooctadiene $\mathbf{4.9}$, have gradually decreasing triplet lifetimes (550 ns and 120 ns, respectively).^{132,133} As expected, these compounds have also a higher flexibility due to their larger rings and, therefore, twisted biradicals (less reactive biradicals) are formed in their triplet states (Fig. 4.7). We found two possible triplet biradical structures for $\mathbf{4.8}$, one is planar as in 1,3-cyclohexadiene while the other is twisted. Further testing the dienes $\mathbf{4.8}$ and $\mathbf{4.9}$ in the photosensitized dimerization reaction (same conditions as 1,3-cyclohexadiene) has shown a decrease in the yields as the size of the ring increases (Table 4.1). The results of *Z,Z*-1,3-cyclooctadiene $\mathbf{4.9}$ are comparable to the low reactive 2,4-hexadiene. It allows us to conclude that the main factors responsible for the efficient dimerization of 1,3-cyclohexadiene are: (a) its two highly reactive alkyl radicals in the triplet state biradical (*i.e.* more reactive due to the non-twisted structure); and (b) its longer triplet state lifetime, which increases the concentration of triplet excited state 1,3-cyclohexadiene in the solution, favoring the attack to another 1,3-cyclohexadiene molecule.

Up to this point, isoprene shows advantages from the photobiological point of view, as it can be produced directly from CO₂, water and sunlight by cyanobacteria, plus advantages from the photochemical aspect, as it is the best performing acyclic diene in the photosensitized dimerization reaction. Despite being even more efficient in the photochemical step, 1,3-cyclohexadiene has not yet been directly produced by cyanobacteria. Furthermore, 1,3-

cyclohexadiene is much less volatile than isoprene (their boiling points are respectively 80 °C and 34 °C), and therefore, the eventual escape of 1,3-cyclohexadiene from cyanobacteria cultures would be less rapid than that of isoprene. We then proceed with optimizing the conditions of the dimerization of isoprene in conditions related to its photobiological production.

4.4 Optimizing the Conditions of Dimerization for the Combined Photobiological-Photochemical Route

Comparing the results with neat and diluted isoprene in Table 4.1 and in Chapter 3 we see that, as expected, the dilution reduces the efficiency of the photosensitized dimerization. We then performed a few experiments to assess to what extent it affects the dimerization efficiency and how one can improve it. First, we tested different concentrations of isoprene in hexane solutions, mixed with 0.1 mol% of 1,1-dinaphthylmethanone (PS, load related to the amount of isoprene). We could see a linear dependence between the yield of dimers after 24 h of irradiation and the concentration of isoprene (Fig. 4.8A), with yields below 10% when approaching a concentration of isoprene of 10 wt%. Since present titers of bio-isoprene production would render even lower concentration in trapping solvents, we checked how much the yield can be improved if increasing the amount of photosensitizer, using a solution of isoprene 15 wt% in hexane (Fig. 4.8B).

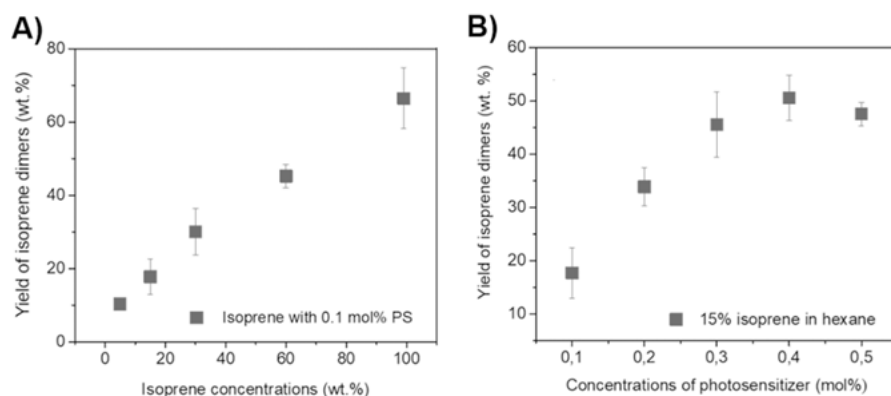


Fig. 4.8 Effect of different concentrations of isoprene and 1,1-dinaphthylmethanone on the photochemical dimerization. (A) The total yield of dimers (wt%) from the photodimerization of various concentrations of isoprene (5-99 wt% in hexane) with 1,1-dinaphthylmethanone 0.1 mol% (related to the isoprene amount); (B) the total yield of dimers from the photodimerization of 15% isoprene in hexane with different concentrations of 1,1-dinaphthylmethanone (0.1-0.5 mol%).

Increasing the amount of photosensitizer has improved the conversions of isoprene into dimers and an optimal value was found for the solution of isoprene 15 wt% (0.4 mol% of photosensitizer). Interestingly, our experiments also show that this approach cannot be used to enhance the yields of neat conditions, as the yields start to decrease when using higher amounts of sensitizer. This effect is due to self-quenching by photosensitizer molecules or back transfer from triplet isoprene to a photosensitizer molecule, given that their triplet energies are close.¹³⁰

Lastly, we assessed the influence of solvents with different viscosities as the medium for the photosensitized dimerization. We selected four different solvents: hexane (0.3 cP), cyclohexane (0.1 cP), tetradecane (2.3 cP), and hexadecane (3.4 cP), and irradiated solutions of 15 mol% of isoprene mixed with 0.1 mol% of photosensitizer. In contrast to what has been observed by Liu *et al.*,⁷⁹ our results show a higher yield of isoprene dimers when utilizing solvents with lower viscosity. Therefore, among the solvents investigated, hexane gave the highest yield (Table 4.2).

Table 4.2: Effect of different viscosity of solvents on photodimerization of isoprene (15 wt%, and 0.1 mol% 1,1-dinaphthylmethanone). Samples were irradiated for 24 h.

Solvents	Viscosity (cP at 20-25°C)	Relative integration of dimers signal (%)
Hexane	0.3	60
Cyclohexane	1.0	48
Tetradecane	2.3	41
Hexadecane	3.4	43

4.5 Conclusions

In this work we were able to get more understanding on how the methyl substitution patterns in different conjugated dienes and the different structures affect their photosensitized dimerization. We identified electronic factors, steric effects and concentrations of excited states – due to longer lifetimes – as an ensemble of variables that defines the efficiency of photodimerization of the conjugated diene.

The outstanding reactivity of 1,3-cyclohexadiene should encourage further development of photosynthetic routes to produce 1,3-cyclohexadiene directly from CO₂, water and sunlight. For now, we conclude that isoprene is still the most suitable substrate in the combined photobiological-photochemical route to produce jet fuels, as overall it has advantages in both steps – possible to be produced by cyanobacteria, ideal volatility, liquid at room temperature and most reactive among the small linear conjugated dienes. Our optimization of

the photosensitized dimerization under dilute conditions will be useful for further development of the large-scale realization of our combined photobiological-photochemical solution.

After getting deeper knowledge on the photosensitized dimerization of small conjugated dienes, in the next chapter we explore this photochemical route applied to larger substrates.

5 Light-Driven (Cross-)Dimerization of Terpenes as a Route to Renewable C₁₅ – C₃₀ Crudes for Fuel and Lubricant Oil Applications (Paper III)

There are several larger compounds available from renewable sources which also contain a conjugated diene unit in it. This chapter describes the use of some of these compounds (*i.e.* monoterpenes and sesquiterpenes) as substrates in the photodimerization sensitized by 1,1-dinaphthylmethanone – the photosensitizer introduced in Chapter 3. In this chapter, the starting materials are larger hydrocarbons, so the dimerization products can have applications other than the ones covered by the isoprene dimers. As reactivity differences are identified among the different substrates, a cross-photodimerization approach was developed to make a better use of the less reactive compounds. Some key physical properties of the hydrogenated crudes were measured and they indicate that these crudes can serve as surrogates to high energy density fuels and lubricant oils.

5.1 Introduction

As discussed in the previous chapters, the photosensitized dimerization of isoprene can be run successfully under sunlight irradiation and, followed by hydrogenation, it affords a mixture suitable as jet fuel surrogate. Yet, the C₁₀ compounds that are obtained cannot replace some other products from fossil origin (*e.g.* diesel-like fuels and lubricant oils). In this light, it was required to find further renewable substrates that provide crudes suitable to a more diverse range of products. In this chapter, the photosensitized dimerization of mono- and sesquiterpenes is discussed as an alternative route to diesel-like fuels and lubricant base oils (LBO). This work also addresses the cross-photodimerization of the substrates, including the cross-photodimerization with isoprene. The different approaches render a range of products from C₁₀ to C₃₀ hydrocarbons, with substrates that can be harvested from different renewable sources, including cyanobacteria (Fig. 5.1).

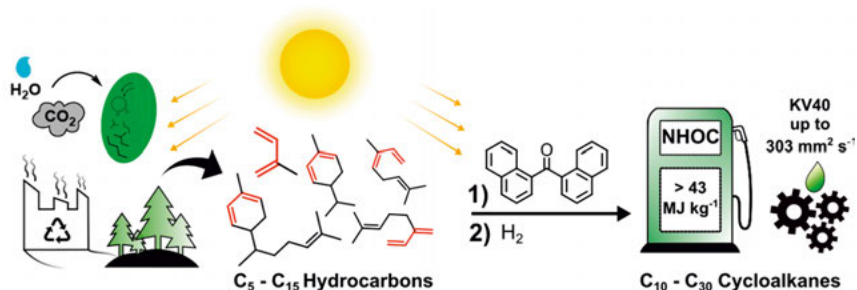


Fig. 5.1 The photosensitized dimerization of several conjugated dienes from different renewable sources (*i.e.* photosynthetic microorganisms, industrial waste and fast-growing trees and biomass), enabling a diversity of products: jet fuel, diesel-like fuels and lubricant oils.

5.2 Photodimerization of Monoterpenes

The optimized photosensitized dimerization reactions of α -phellandrene **5.1**, β -myrcene **5.2** and ocimene **5.3** (Fig 5.2) were performed using 1,1-dinaphthylmethanone **3.4** as the photosensitizer, under irradiation at 365 nm and using the high-surface-area coiled setup introduced in Chapter 3 (see Fig. 3.3A). These compounds were chosen based on their potential and existing renewable sources, discussed in Chapter 2.

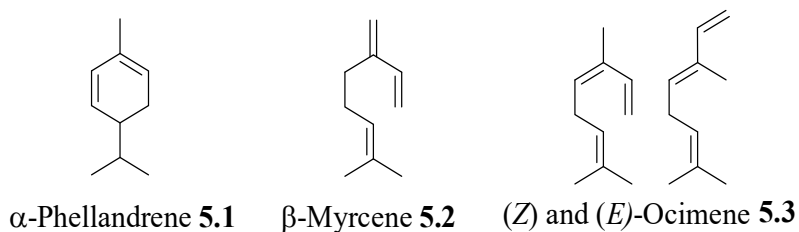


Fig. 5.2 Structure of the monoterpenes studied in this work.

The yields of dimerization under optimized conditions are reported in Table 5.1, along with the reaction conditions and the triplet energies calculated at the (U)M06-2X/6-311+G(d,p) level with thermal free energy corrections at 298 K. The triplet energies were calculated to assure the suitability of the monoterpenes to the photosensitized dimerization, *i.e.* to check if their triplet energies were lower than the triplet energy of the photosensitizer **3.4** (55.5 kcal mol⁻¹).¹²⁰ Compared to the photosensitized dimerization of isoprene, one can see the much higher efficiency of the photosensitized dimerization of α -phellandrene **5.1** – as similar but even more reactive than 1,3-cyclohexadiene (see Chapter 4). Indeed, the dimerization of **5.1** is also more efficient than the reactions of the other aliphatic monoterpenes, requiring only 12 hours to reach

a conversion higher than 90 wt%. The main reason for the outstanding result is the endocyclic nature of the conjugated diene in **5.1**, which halts the twisting of that moiety and grants a longer life-time to the triplet excited state.¹³¹ We also performed the photosensitized dimerization of **5.1** in a larger scale (262 g), in which a FEP tubing with larger internal diameter (6.35 mm) were coiled around a larger template (2 L jacketed beaker, Ø:130 mm; height: 280 mm). The reaction time required in that case was longer (24 h), which is a result of the poorer light penetration in wider FEP tubes.

Table 5.1 Photosensitized dimerization of monoterpenes with photosensitizer **3.4**. Optimized conditions (high-surface-area setup, 365 nm).

	α-Phellandrene	Myrcene	Ocimene
$E(T_1)$, kcal mol⁻¹	49.6	52.1	47.5 (<i>Z</i>) 47.4 (<i>E</i>)
Reaction time, h	12	48	48
Photosensitizer, mol%	0.2	0.5	0.5
Yield, wt%	96.1; (99) ^a	59.4	16.5

^a In parenthesis: reaction run at 262 g scale, using a FEP tubing with larger internal diameter (6.35 mm) and a larger template (2 L jacketed beaker, Ø:130 mm; height: 280 mm). The yield of 99 % was achieved after 24 h.

Remarkably, the high reactivity of **5.1** is also realized under simulated sunlight irradiation, reaching up to 90.8 wt% yield of dimers after 12 h (1 sun equivalent, AM 1.5 G, 0.2 mol% of **3.4**) and a considerable yield is reached under natural sunlight irradiation (46.6 wt%, exposed to daylight for 18 h, Uppsala, Sweden 59°51'09.5"N 17°39'19.9"E, approx. 30 m above sea level, in September, 2020). In the experiments with simulated and natural sunlight, the flat spiral setup was used (Fig. 3.3B). These two experiments highlight the feasibility of these reactions to be carried out under sunlight. The lower conversion when sunlight irradiation is used could be related to the lower light intensity under such conditions. Knowing that the light intensity plays an important role on photoreactions, we investigated the effects of different light intensities on the conversions of **5.1** (Fig. 5.3A). Furthermore, we found a linear correlation of the light intensity and the pseudo rate constant, (Fig. 5.3B) with a conversion dependency of 1.19 mmol per h mW⁻¹ cm².

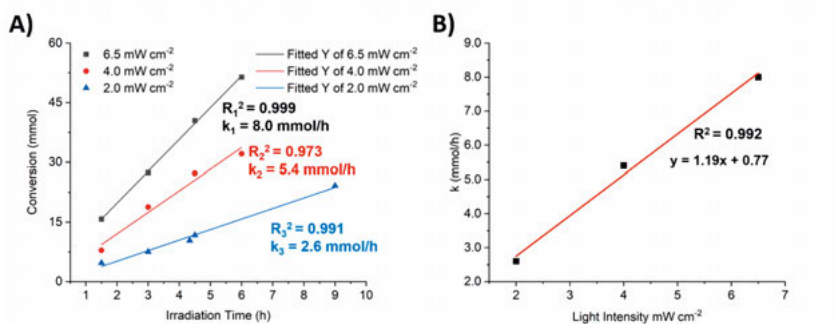


Fig. 5.3 Experiments with varying light intensities. **A)** Conversion of **5.1** into dimers *versus* irradiation time, under irradiation at 365 nm in different intensities, 0.2 mol% of 1,1-dinaphthylmethanone. **B)** Correlation between the light intensity and the conversion rate constant in the dimerization of α -phellandrene.

The mixtures of dimers produced in each reaction are products of [2+2], [4+2] and [4+4] cycloadditions. Consequently, and based on ¹H NMR data of the crude mixtures, the likely structures of the dimers of α -phellandrene, myrcene and ocimene are displayed in Fig. 5.4. Similar to the isoprene dimers discussed in Chapter 3, the dimers of monoterpenes are cycloalkenes and, therefore, their hydrogenation should provide high energy density cycloalkanes.⁹ Additionally, [4+2] cycloadducts of myrcene have been reported to be suitable for diesel-fuel blends.²⁷

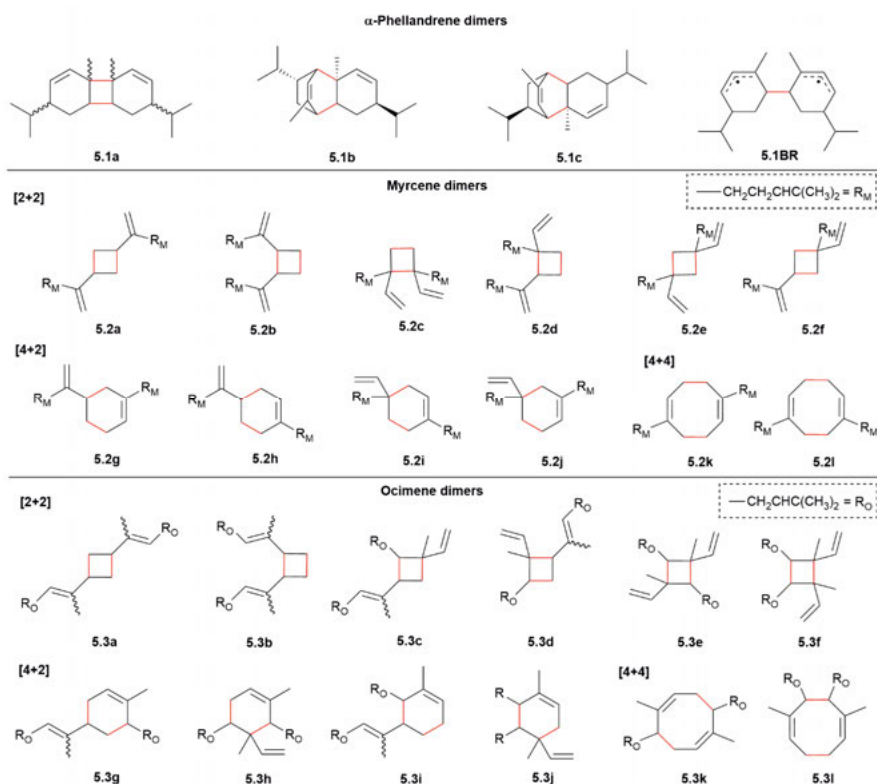


Fig. 5.4 Structures of [2+2], [4+2] and [4+4] cycloadducts of α -phellandrene, myrcene and ocimene produced on the photosensitized dimerization. Bonds in red are the bonds formed in the photodimerization.

In order to predict the suitability of the dimers of monoterpenes as diesel-like fuel surrogates, the heats of combustion for some hydrogenated dimers were calculated following the method developed by Pahima *et al* (Table 5.2).⁵⁹ The calculated enthalpies of combustion for the various hydrogenated dimers are in between 42.3 and 43.3 MJ kg⁻¹, with the [2+2] and [4+4] dimers having the highest enthalpies of combustion (Table 5.2, entries 3, 4 and 8). Since they were in a suitable value range to high energy density fuels,⁹ we measured the experimental heats of combustion and further fuel properties: density, viscosity and cold properties such as pour point (see section 5.5).

Table 5.2 Heats of combustion computed at the M06-2X/6-31+G(d,p) level. The Self-Consistent Reaction Field Solvent method (SCRf) was used to model the solvent toluene, using the Solvation Model Based on Density (SMD).

Entry	Hydrogenated dimer	Heat of combustion (MJ kg ⁻¹)
1	5.1a-H ₂	42.46

2	5.1c-H₂	42.30
3	5.2a-H₂ (cis)	43.29
4	5.2a-H₂ (trans)	43.32
5	5.2g-H₂	43.02
6	5.2k-H₂	43.19
7	5.3h-H₂	43.10
8	5.3k-H₂	43.23

5.3 Myrcene and Ocimene Reactivities

Following the observed differences in reactivities towards the photodimerization, we investigated the possible reasons for the lower reactivities of myrcene and ocimene. As revealed by the optimization of geometries at the T₁ state, the triplet state biradicals of myrcene and ocimene are twisted. In comparison to α -phellandrene, myrcene and ocimene have more motion-freedom for not being restricted by a cyclic structure. This motion-freedom allows the access to deactivation pathways more easily, which reduces their triplet state lifetimes. As discussed in Chapter 4, small cyclic conjugated dienes (C₅ and C₆) have triplet lifetimes on the μ s order, while acyclic dienes are on the ns order.¹³¹ Consequently, it reduces their reactivity towards dimerization. Another factor in the case of myrcene is that it can undergo a photosensitized internal cyclization,⁸⁰ in which the diene moiety adds to the isolated double bond to form 5,5-dimethyl-1-vinylbicyclo[2.1.1]hexane **5.4** (Fig. 5.5).



5,5-dimethyl-1-vinylbicyclo[2.1.1]hexane **5.4**

Fig. 5.5 Product formed in the internal cyclization of myrcene.

We reasoned that the compound **5.4** halts further dimerization as it cannot be sensitized by **3.4** because the former, as an olefin, has a triplet energy that is much higher than the triplet energy of the photosensitizer **3.4**. One supporting evidence to our conclusions was obtained by carrying out the epoxidation of the isolated double bond in myrcene **5.2** and further attempting to dimerize the epoxide, photosensitized by **3.4** (Fig 5.6). The conversion into dimers was substantially higher than the one for myrcene **5.2** under the same reaction conditions (80.6 wt% *versus* 59.4 wt%). Therefore, compared to α -phellandrene, the lower yields for dimers of myrcene is highly influenced by its shorter triplet life-time and by the byproduct **5.4** that traps the reactant.

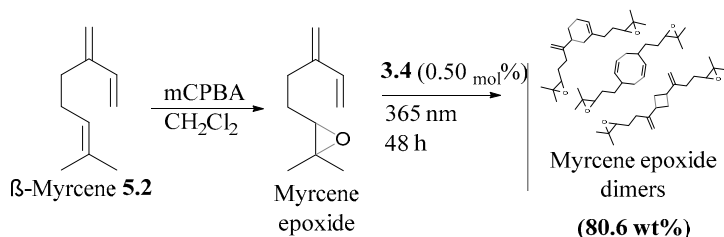


Fig. 5.6 Epoxidation of myrcene followed by photosensitized dimerization of myrcene epoxide. Note: the depicted structures for the productsd are not all the dimers formed in the reaction.

Regarding the low efficiency in the dimerization of ocimene **5.3** compared to myrcene **5.2**, a possible reason related to the differences in reactivity is the alkyl radical of their most stable triplet biradical structures (Fig. 5.7), as similar to the cases of isoprene and 1,3-pentadiene discussed in Chapter 4. In myrcene, the twisted triplet state is composed of one alkyl radical and one allyl radical, and the alkyl radical always reside at a terminal carbon. On the other hand, ocimene has one of its possible triplet biradical structures with the alkyl radical at an internal carbon (structure **5.3'**). Structure **5.3'** has a stabilizing methyl group bonded to the edge of the allyl moiety, unlike structure **5.3''** and, as a result, structure **5.3'** is more stable by 3 kcal mol⁻¹. Compared to the most stable biradical structure of myrcene (**5.2'**) the alkyl radical in structure **5.3'** is less reactive, and therefore the lower reactivity observed for ocimene is reasonable.

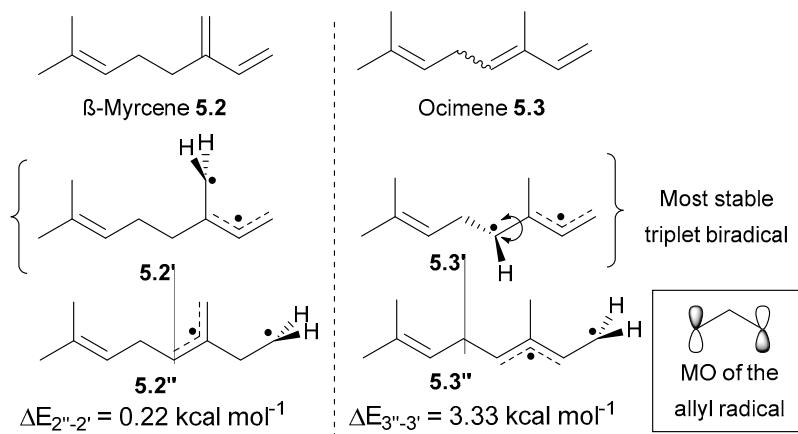


Fig. 5.7 Structures of triplet biradicals of myrcene and ocimene and their energy differences (calculated at the (U)M06-2X/6-311+G(d,p) level).

The different reactivities could also have been affected by differences in the rates of quenching of the photosensitizer triplet energy. The emission spectrum (phosphorescence) of the photosensitizer 1,1-dinaphthylmethanone was

recorded at 77 K and it shows maximum intensity at the 560 nm band (Fig. 5.8A). We monitored the intensity of this band in a series of measurements with increasing amounts of the three monoterpenes (quenchers), using cyclohexane as the solvent.

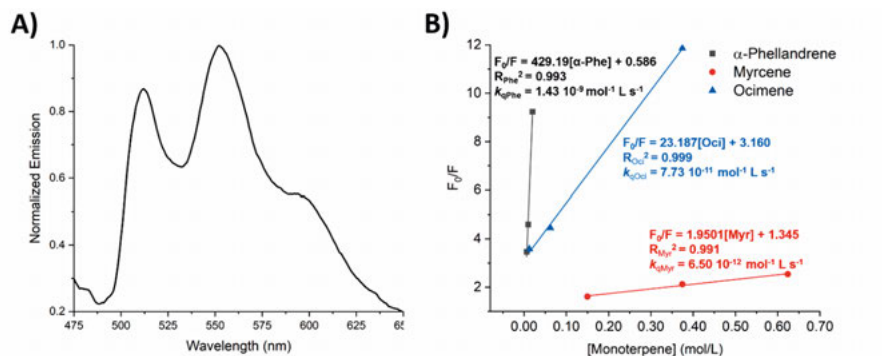


Fig. 5.8 A) Emission spectrum of 1,1-dinaphthylmethanone in cyclohexane, 25 μM , excitation at 338 nm. B) Stern-Volmer plot for the quenching of 1,1-dinaphthylmethanone by the three monoterpenes (α -phellandrene, myrcene and ocimene). The origins of the axes were set to non-zero for better visualization.

We then plotted the Stern-Volmer plots for each of the monoterpenes (Fig. 5.8B). Using 300 ns as the triplet lifetime τ of 1,1-dinaphthylmethanone, the Stern-Volmer plots for these quenching experiments allow us to determine the quenching rate constant k_q for the different monoterpenes (Fig. 5.8B). Ocimene has the second highest k_q , followed by myrcene, while the k_q of α -phellandrene is hundred times higher than that of ocimene. Even though these results support the higher efficiency of the dimerization of α -phellandrene, the conclusions should be taken with care because we use neat conditions of the monoterpene in the reactions, *i.e.* high amounts of the quencher, the energy transfer – quench of the photosensitizer - becomes very favorable in all cases.

5.4 Cross-Photodimerization and Beyond C_{20} Crudes

Following the understanding of the lower reactivities of myrcene and ocimene, we hypothesized that the observed higher reactivity of α -phellandrene could be useful to enhance the conversion of the other monoterpenes through a cross-photodimerization. Thus, different ratios of **5.1** mixed with **5.2** and **5.3** were tested in the presence of 0.25 mol% of the photosensitizer **3.4**. In both cases, improvements of the conversion of the monoterpenes were observed (Fig. 5.9). When mixing α -phellandrene with ocimene in the ratio of 2:1, 76.6 wt% of ocimene was observed to be converted into dimers and cross-dimers.

The (cross)-photodimerization of myrcene was even further enhanced, reaching conversions higher than 90 wt% after 24 h.

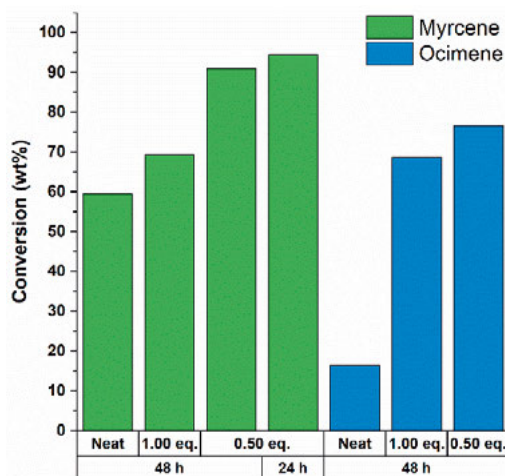


Fig. 5.9 Improvements on the conversion to dimers of ocimene and myrcene in the cross-photodimerization with α -phellandrene (0.25 mol% of **3.4**). The labels 1.0 eq. and 0.5 eq. describe the amount of monoterpene used as starting material related to α -phellandrene (mol). Reaction times are also indicated on the x axis.

Once the cross-dimerization between monoterpenes was found to be a valuable way to improve the conversions of less reactive monoterpenes, we applied the same approach to obtain products in the range of C_{15} hydrocarbons. A 1:1 mixture of isoprene **5.5** and α -phellandrene **5.1** was irradiated under 365 nm light (0.25 mol% of **3.4**). After 48 h, the reaction produced mainly C_{15} cross-dimers, followed by C_{10} and C_{20} dimers of isoprene and α -phellandrene, respectively (Fig. 5.10).

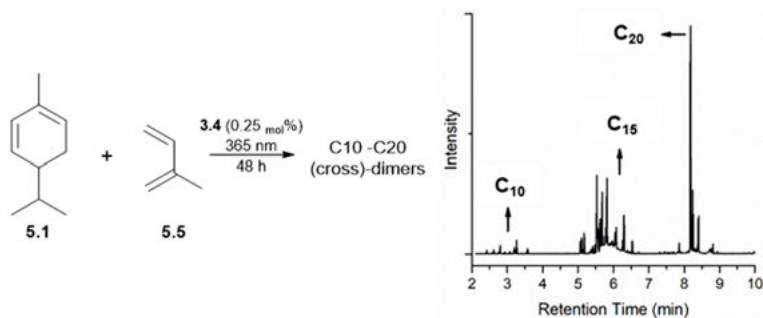


Fig. 5.10 GCMS trace of cross-dimerization between α -phellandrene and isoprene (1:1), where C₁₀ – C₂₀ hydrocarbons can be observed.

Subsequently, we were able to (cross-)dimerize the sesquiterpenes α -zingiberene **5.6** and β -sesquiphellandrene **5.7** present in the C₁₅ fraction of ginger oil sample (Fig. 5.11). The sesquiterpene α -zingiberene **5.6** is particularly interesting because of its endocyclic conjugated diene moiety, which has been shown to be a highly reactive feature in α -phellandrene **5.1** and 1,3-cyclohexadiene. Indeed, nearly full conversion of **5.6** was observed. Considering the initial amount of conjugated C₁₅-dienes in the ginger oil sample, the yield of dimers was of 61 wt%. Since sesquiterpenes are C₁₅ compounds, the obtained C₃₀ dimers are within the range of compounds that are suitable to lubricant oil applications. Therefore, we were able to expand the photosensitized dimerization approach to routes producing C₁₀ - C₃₀ crudes of hydrocarbons.

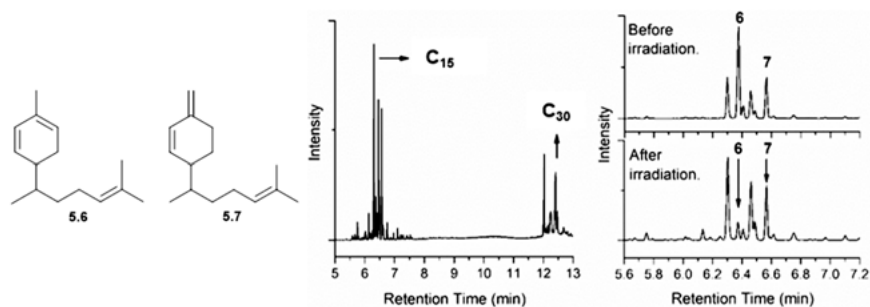


Fig. 5.11 GCMS trace of the ginger oil sample mixed with photosensitizer **3.4** (0.5 mol%) after irradiation under 365 nm, showing C₃₀ dimers. Inset: chromatogram for the region of C₁₅, before and after irradiation showing that **5.6** peak is very reduced after irradiation.

5.5 Physical Properties of Selected (Cross)Photodimers

The high computed heats of combustion (Table 5.2) and the visual increase in viscosity of some of the (cross)photodimers hints to the likely suitability of these crudes as fuels and lubricant oils. Thus, we selected four C₁₅ - C₃₀ (cross)-dimers to be hydrogenated (PtO₂, 0.15 wt%; H₂, 6 bar) and have further physical properties measured. The hydrogenated samples were identified as **HAPID**, **HAPD**, **HMD** and **HGOD** (hydrogenated α -phellandrene and isoprene cross-dimers; hydrogenated α -phellandrene dimers; hydrogenated myrcene dimers; and hydrogenated ginger oil dimers; respectively). Following the hydrogenation, some key properties were measured and compared to the properties of existing diesel-like fuels and lubricant base oils (Table 5.3).

Table 5.3 Selected properties measured for hydrogenated (cross)dimers and reference products for comparison.

Diesel fuels						
Property	HAPD C ₂₀ H ₃₆	HMD C ₂₀ H ₄₀	HAPID C ₂₀ H ₃₆ C ₁₅ H ₂₈	Diesel D-2 ¹³⁴	Bio-diesel ¹³⁴	
Density at 25 °C, g/mL	0.931	0.861	0.904	0.850	0.880	
Volumetric NHOC, MJ/L at 25 °C	40.13	37.65	39.15	35.97	32.94	
KV40, mm ² /s	41.1	12.7	6.45	1.3 – 4.1	4.0 – 6.0	
Pour point, °C	-21	< -45	< -45	-35 to -15	-5 to 10	
Lubricant and base oils						
Property	HAPD C ₂₀ H ₃₆	HMD C ₂₀ H ₄₀	HGOD C ₃₀ H ₅₆	C₃₀ PAO mix-ture ¹¹	LBO API Group II 6 ¹³⁵	LBO from estolides ¹³⁶
KV40, mm ² /s	41.1	12.7	303	15.23	41.5	102 to 519
KV100, mm ² /s	4.16	2.89	14.7	3.63	6.4	-
Pour point, °C	-21	< -45	-15	-72	-12	-15 to -6

NHOC = Net Heat of Combustion; KV40 = Kinematic Viscosity at 40 °C; KV100 = Kinematic Viscosity at 100 °C; LBO = Lubricant Base Oil.

As expected, the cycloalkanes in our products render high heats of combustion, higher than the ones of commercial diesel (Diesel D-2) and biodiesel,¹³⁴ and the pour points were also adequate. However, the **HAPD** and **HMD** have too high kinematic viscosities, which makes them unsuitable as a drop-in surrogate to diesel-like fuels. On the other hand, the use of viscosity improvers or blend formulations are alternatives to tune the viscosities into required values. In the case of **HAPID**, the kinematic viscosity at 40 °C is much closer to the one for Diesel D-2 and biodiesel, therefore the **HAPID** approaches a drop-in surrogate for diesel-like fuels.

The high viscosities of **HAPD** and **HMD** make them suitable for lubricant base oil applications.^{11,135} The product with highest kinematic viscosity, **HGOD**, also fits into the class of lubricant base oils, with viscosities comparable to those of LBO derived from estolides.¹³⁶ Yet, how much the viscosity changes with temperature (*i.e.* the viscosity indexes) of **HAPD**, **HMD** and **HGOD**, need improvements, and again, viscosity additives might provide the tuning required.

5.6 Conclusions

The photosensitized dimerization of terpenes could also be carried out under simulated and natural sunlight. In this work, we made use of the endocyclic nature of the conjugated diene moiety in α -phellandrene as a key feature to provide photosensitized dimerization and cross-dimerization reactions that are very efficient. The high reactivity of α -phellandrene enabled a better conversion of other less reactive compounds into C_{20} hydrocarbons, *via* the cross-photodimerization. Such approach applied to α -phellandrene and isoprene has allowed us to produce C_{15} crudes. Moreover, the photosensitized dimerization protocol could be extended up to C_{30} hydrocarbon production.

We therefore reached a point in which we can produce C_{10} , C_{15} , C_{20} and C_{30} hydrocarbons from substrates of renewable sources, and with the main energy source for the reactions being sunlight. Therefore, the light-driven route here reported is certainly an alternative to the synthesis of non-fossil fuels and lubricant oils.

The sunlight-driven photosensitized dimerization route has been shown to be useful to produce a diverse range of products. Yet, only conjugated dienes are suitable as substrates. Despite being a large class of compounds, it does not include other important building blocks that can be photosynthetically produced by cyanobacteria, such as the small hydrocarbons ethylene and isobutene.

6 Remote Electrostatic Repulsion Triggered by Excited State Antiaromaticity Relief as the Origin of the Photoacidity in an Organic Dye (Paper IV)

Despite that we successfully have demonstrated the triplet photosensitized dimerization route as an alternative to transform small hydrocarbons into fuels, there is still a need of alternative photochemical routes to oligomerize small photobiologically produced hydrocarbons other than the conjugated dienes. Photoacids that are activated under visible light irradiation represent such a potential catalyst to oligomerize small alkenes, *e.g.*, isobutene and ethylene, which can be produced photosynthetically. In this chapter, an initial step is taken in that direction by introducing a new type of superphotoacid. The new photoacid is formed by one dibenzotropylium cation unit and one anilinium cation unit, and the computational assessment of its properties reveals a strong photoacidity under visible light irradiation. A new type of photoacidity mechanism was found as the driving force to the enhanced acidic character in the excited state, which opens up a field for future development and design of photoacids.

6.1 Introduction

Photoacids are compounds that become more acidic upon electronic excitation,⁸⁴ and they find applications in light-controlled processes that range from modulation of the pH of the medium,^{92,137,138} initiation of polymerization reactions^{139,140} and organic synthesis.^{141–143}

The strength of the photoacid, *i.e.* how low is its pK_a^{hv} , can affect the suitable applications of a photoacid, so it is important to be able to tune it. For example, pyrene-based photoacids such as hydroxy- and aminopyrenes show pK_a^{hv} values that range from 1.0 to -12.9.^{91,144–146} The lifetime of the photoacid is another important feature when applying photoacids to organic synthesis. Das *et al.* have developed photoacids with higher intersystem crossing rates, which yielded to a longer lifetime of the photoacid and facilitated the bimolecular protonation reaction of silylenol ethers.¹⁴⁷

Here, we hypothesize that a very strong photoacid could be used to promote a light induced oligomerization of alkenes. Therefore, we designed the new photoacid 5-[4-(dimethylammonio)-2,6-dimethylphenyl]-5H-dibenzo[a,d][7]annulen-5-ylum bis(tetrafluoroborate) **HDMAPAN-(BF₄)₂** and its conjugate base (Fig. 6.1) and computationally assessed its photoacidity using the Born-Haber thermodynamic cycle (*see* Chapter 2). After finding a strong photoacidic character, we computationally investigated the possible cause of the photoacidity of **HDMAPAN-(BF₄)₂**.

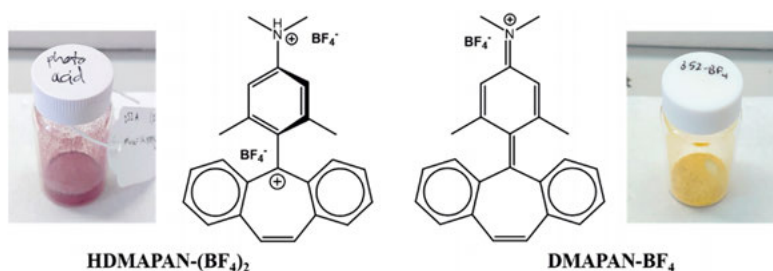


Fig. 6.1 Structure of the photoacid **HDMAPAN-(BF₄)₂** and its conjugate base, **DMAPAN-BF₄**, as well as their respective isolated solid samples.

There are three major mechanistic interpretations of the origins of photoacidity in different organic compounds, and they are usually presented as combining factors.¹⁴⁸ First, photoacidity is commonly explained by a reorganization of charge distributions in the nearby regions of the proton donating group upon excitation.^{149,150} Another interpretation describes the influence of the easiness of delocalizing the negative charge of the conjugate base as a driving force to the photoacidity.¹⁵¹ Finally, the concept of excited state antiaromaticity (ESAA) relief has also been used.^{63,151} The rules of aromaticity in the excited state were derived by Baird in 1972.¹⁰⁷ They are the reversal of Hückel's rule in the S_0 state, *i.e.* systems with $4n+2$ π -electrons are antiaromatic in their lowest $\pi\pi^*$ triplet and singlet excited states.^{108,152} More recently, the values of nucleus-independent chemical shifts (NICS) – a (anti)aromaticity index – were correlated to the ΔpK_a values of naphthalene derivatives.¹⁵³

Our investigation of the origins of the photoacidity in **HDMAPAN-(BF₄)₂** could not find support in the existing mechanistic interpretations. Unusual to other photoacids, the photoexcitation in **HDMAPAN-(BF₄)₂** is localized to a fragment remote to the unit containing the photoacidic proton (respectively, dibenzotropylium and anilinium units), and the units do not interact electronically as they are oriented orthogonally to each other. Therefore, we postulated a new mechanism that functions through space as an electrostatically repulsive interaction develops between the two units upon excitation. Our computational data support this hypothesis and indicate that the charge redistribution occurs as a consequence of ESAA relief.

6.2 The Ground State of HDMAPAN-(BF₄)₂ and its Conjugate Base

Initially, we determine the crystal structures of **HDMAPAN-(BF₄)₂** and its conjugate base **DMAPAN-BF₄** (Fig. 6.2). They are markedly different in their conformations. While **HDMAPAN-(BF₄)₂** has a twisted structure, with the anilinium fragment orthogonal to the dibenzotropylium fragment, the conjugate base has its fragments facing the same direction, in a butterfly-like conformation.

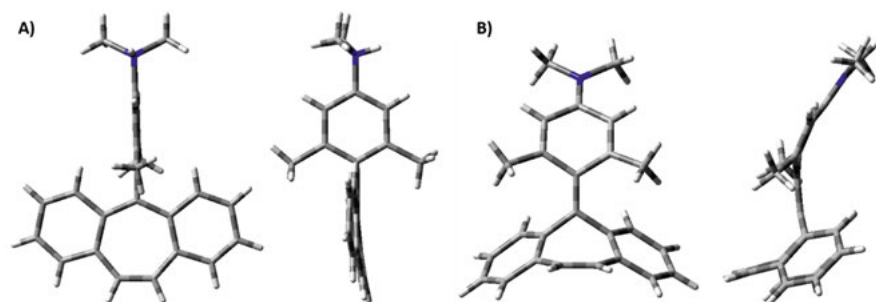


Fig. 6.2 A) Crystal structure of **HDMAPAN-(BF₄)₂** and B) **DMAPAN-BF₄**. Nitrogen atoms are represented in blue. The counterions BF₄⁻ were omitted.

The analysis of the ¹H and ¹³C NMR spectroscopic data in acetonitrile, together with comparisons of computed NMR spectra of structures optimized at the CAM-B3LYP/6-311+G(d,p) level, indicated that the conformers in solution are similar to the crystal structures. Thereby, the computed twisted conformer **tw-HDMAPAN-(BF₄)₂** and the computed butterfly conformer **btf-DMAPAN-BF₄** are the representative structures of the photoacid and conjugate base in solution. We utilized these two structures as the input to the energies in the Born-Haber thermodynamic cycle. The Gibbs free energies of solvation were obtained using the Gibbs free energy of the gas phase geometry and the total energy of a single point calculation in solvent phase (SMD) using the gas phase geometry. From this data we determined the $pK_a = 3.0$. Additionally, we performed an experimental determination of the pK_a by measuring the UV-Vis absorption spectra of aqueous solutions of **DMAPAN-BF₄** with different pH values, ranging from 1.57 to 8.46 (Fig. 6.3).

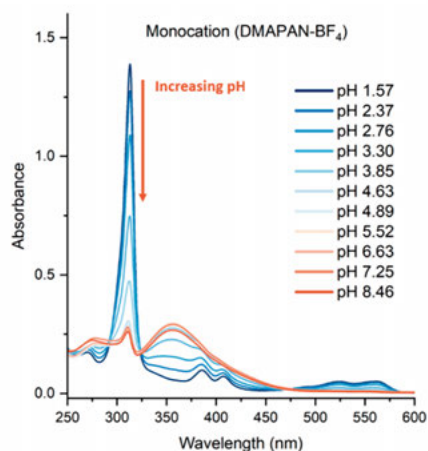


Fig. 6.3 UV-Vis spectra of **DMAPAN-BF₄** in aqueous solutions at different pH.

Plotting the absorbance measured at 313 nm against the pH gave rise to a curve that could be fitted to a sigmoidal curve (Boltzmann, Fig. 6.4). From the point of inflection, the $pK_a = 3.14$, confirming the value we estimated computationally.

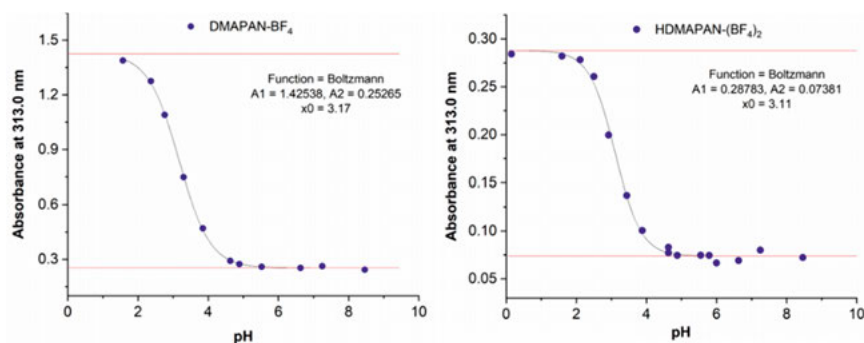


Fig. 6.4 Sigmoidal curve fitting for the experiment with **DMAPAN-BF₄** (left) and for the experiment with **HDMAPAN-(BF₄)₂** (right).

6.3 The Excited State and Photoacidity of HDMAPAN-(BF₄)₂

Further inspection of the absorption spectra of **HDMAPAN-(BF₄)₂** and **DMAPAN-BF₄** in Fig. 6.3 (blue and orange, respectively), gives information about the energies of the S₀ → S₁ transition in each of these compounds. Considering that the transition energy for the conjugate base (band at 356 nm, 3.48 eV) is higher than the transition energy for the photoacid (band at 568 nm, 2.18 eV), according to the definitions in the Förster thermodynamic cycle (Fig. 2.6) a decrease in the *pK_a* upon excitation should not be observed, and therefore, no photoacidic character.

The Förster thermodynamic cycle considers the twisted conformer of **HDMAPAN-(BF₄)₂** and the butterfly conformer of **DMAPAN-BF₄**. However, a rapidly conformational change of **HDMAPAN-(BF₄)₂** in the excited state is hindered due to the presence of the methyl groups in the position 3 and 5 of the anilinium ring. In addition, the experimental emission spectrum of **HDMAPAN-(BF₄)₂** shows a small Stokes shift (0.03 eV, Fig. 6.5), indicating negligible changes in the excited state of the photoacid.

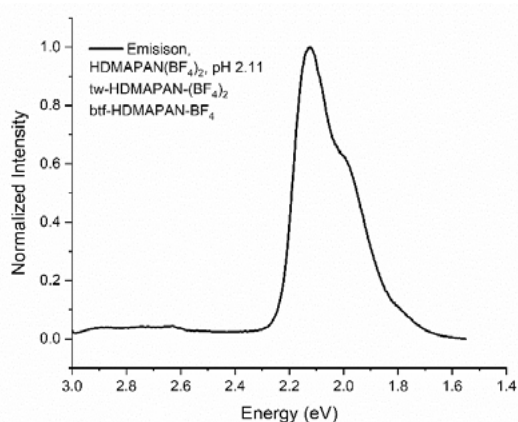


Fig. 6.5 Experimental emission spectrum **HDMAPAN-(BF₄)₂**. The excitation was at 407 nm.

The computed energies of the different conformers of **HDMAPAN-(BF₄)₂** and **DMAPAN-BF₄** in the S₁ state reveal a preference for the twisted conformer in both cases. Therefore, we computationally assessed the *pK_a^{hv}* of the photoacid using the Born-Haber thermodynamic cycle and the twisted conformers of the photoacid and the conjugate base. In this assessment, we found the *pK_a^{hv}* = -12.3, which represents a jump of 15.3 units from the experimental *pK_a*.

Table 1 Relative energies of twisted and butterfly conformers of **HDMAPAN-(BF₄)₂** and **DMAPAN-BF₄** in the S₁ states. CAM-B3LYP/6-311+G(d,p) level, (SMD, water).

	State	ΔG_{tw-btf} (kcal mol ⁻¹)
HDMAPAN-(BF₄)₂	S ₁	-11.4
DMAPAN-BF₄	S ₁	-25.9

6.4 Probing the Origins of the Photoacidity in HDMAPAN-(BF₄)₂

A first puzzling fact about the first singlet excited state of **HDMAPAN-(BF₄)₂** and its photoacidity is that the S₀ → S₁ is a pure HOMO → LUMO transition, and these molecular orbitals are located in the dibenzotropylium fragment (Fig. 6.6A). The changes in bond distances in the S₀ state and S₁ state are in accordance to the population of the LUMO, and they are mostly localized in the dibenzotropylium unit (Fig. 6.6B-C).

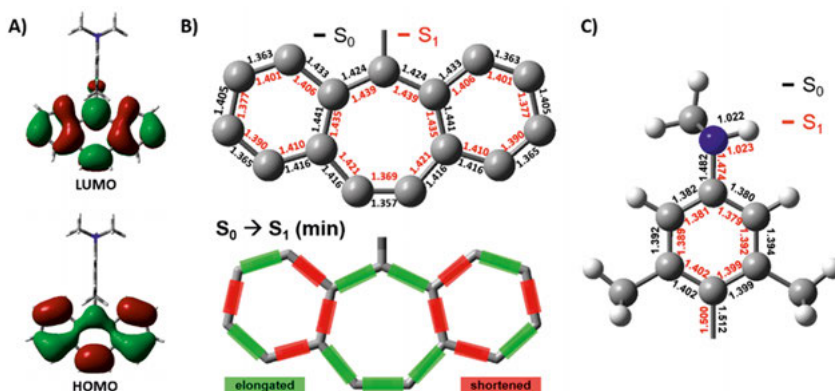


Fig. 6.6 A) Frontier molecular orbitals of **tw-HDMAPAN-(BF₄)₂**. B) Bond lengths in the dibenzotropylium unit and C) anilinium unit in their S₀ and S₁ states. Bond lengths in black and red are reported in Ångström. Note: one methyl group (bonded to the N atom) was removed from the anilinium for better visualization on the figure. Calculated at CAM-B3LYP/6-311+G(d,p) level, solvent = water.

To understand how the HOMO → LUMO transition in the dibenzotropylium unit could be affecting the acidity of the proton in the anilinium unit, we computed the electrostatic potential (ESP) maps of the **tw-HDMAPAN-(BF₄)₂** in different electronic states (Fig. 6.7). The ESP maps show a charge redistribution in the dibenzotropylium unit that places slightly more positive character

on the “top” (region closest to the anilinium ring) of the flanking 6-member rings.

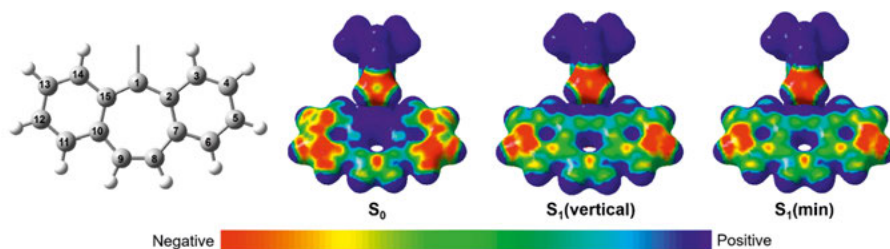


Fig. 6.7 Electrostatic potential maps of **tw-HDMPAN-(BF₄)₂** in different electronic states. Blue indicate more positively charged regions, and red is more negatively charged regions. Calculated at CAM-B3LYP/6-311+G(d,p) level, solvent = water.

The redistribution of charges upon excitation can be seen as a closer approach of positive charges in the dibenzotropylium towards the anilinium ring, and thus, closer to the acidic proton. In this view, the repulsive electrostatic interaction between the acidic proton and the dibenzotropylium unit would be strengthened upon excitation, leading to an increased acidity (photoacidity). We further tested this hypothesis through two approaches.

First, we placed rigid insulating spacers (bicyclo[1.1.1]pentane groups) between the dibenzotropylium and the anilinium units and calculated their pK_a values in the ground and excited states, as done before for the **tw-HDMPAN-(BF₄)₂**. Interestingly, the ΔpK_a values are gradually reduced as the number of spacers increases (Fig. 6.8), supporting our hypothesis.

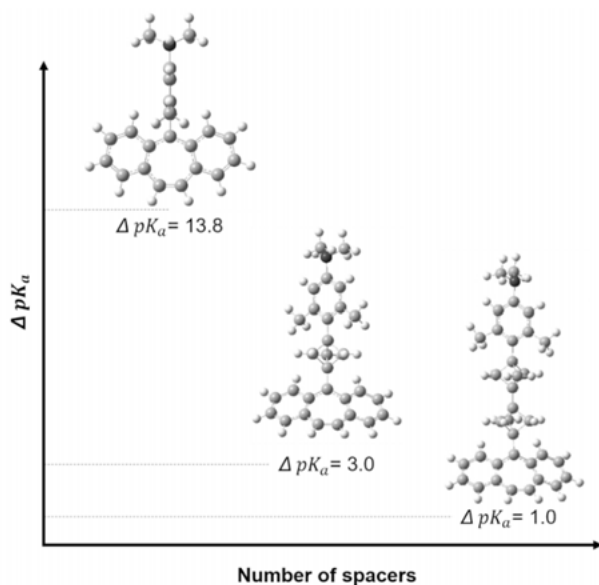


Fig. 6.8 Structures of **tw-HDMPAN-(BF₄)₂** and two derivatives containing the spacer bicyclo[1.1.1]pentane, showing how the ΔpK_a is affected by the distance between the anilinium and the dibenzotropylium units. Here, $\Delta pK_a = pK_a - pK_a^{hv}$. Calculated at CAM-B3LYP/6-311+G(d,p) level.

Next, we used constrained DFT calculations to compute the energies of a system containing one *N,N*,3,5-tetramethylanilinium cation with an approaching positive point charge 0.5 at different distances. The results indicate a rise in energy as the point charge gets closer to the anilinium cation (Fig. 6.9), once again supporting our hypothesis for the origins of the photoacidity in the **tw-HDMPAN-(BF₄)₂**. An opposite trend in the energy of the system is found when using *N,N*,3,5-tetramethylaniline (neutral molecule, Fig. 6.9).

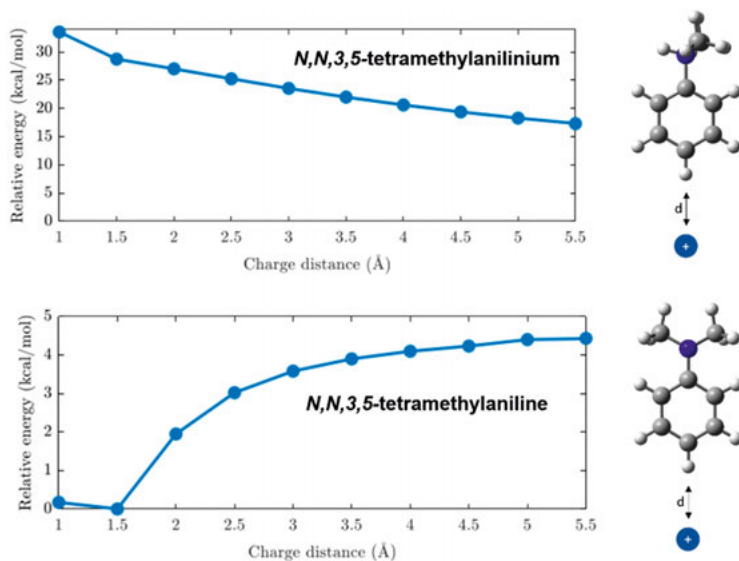


Fig. 6.9 The effects of an approaching positive charge of 0.5 on the relative energies of the *N,N,3,5*-tetramethylanilinium (top) and *N,N,3,5*-tetramethylaniline (bottom).

Finally, as several authors have earlier identified the ESAA relief as the driving force to different photochemical and photophysical phenomena, including photoacidity, we investigated the aromatic character of **tw-HDMAPAN-(BF₄)₂** and the conjugate base in its different electronic states. We computed the values of multicenter index (MCI)¹⁵⁴ for all the rings in the two species (Fig. 6.10). The observed decrease of MCI values in the 7-member ring in the dibenzotropylium unit upon excitation to the S₁ state indicates a loss of aromaticity. On the other hand, the changes in the MCI values of the anilinium unit in the **tw-HDMAPAN-(BF₄)₂** are negligible. It is then rightful to say that the excited state antiaromaticity of the **tw-HDMAPAN-(BF₄)₂** triggers a redistribution of charges in the dibenzotropylium unit, which escalate to a larger electrostatic repulsion between that unit and the acidic proton, giving rise to a photoacidic character.

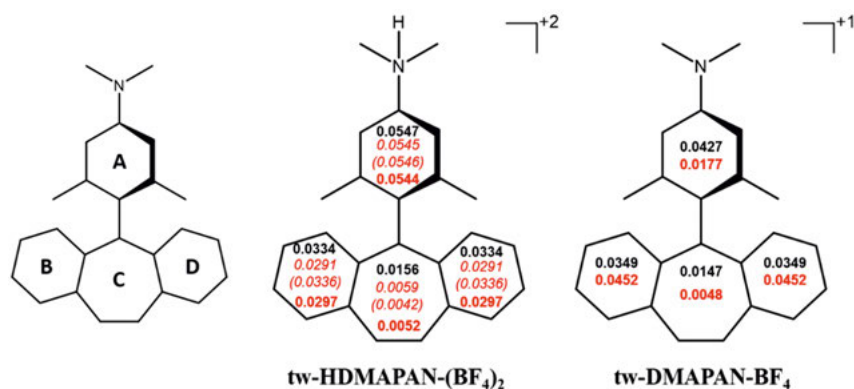


Fig. 6.10 MCI values of **tw-HDMPAN-(BF₄)₂** and **tw-DMPAN-BF₄** in different electronic states: S₀ (in black and bold), S₀ → S₁ (vertical excitation, in red and italic) and S₁ (optimized, in red and bold). MCI values for **tw-HDMPAN-(BF₄)₂** in the first T₁ state were also computed (vertical excitation, in parenthesis, red and italic). Calculated at CAM-B3LYP/6-311+G(d,p) level, solvent = water.

6.5 Conclusions

We have designed and characterized a new photoacid that exhibits a very low pK_a^{hv} , in the range of superphotoacids. Most important, the photoacid operates through a new mechanism of photoacidity, and we gave sufficient computational data to support it: the localized electronic excitation triggers a charge redistribution, placing a positive charge character closer to the unit containing the acidic proton. These two units therefore interact electrostatically and the photoacidity is a result of this destabilizing interaction.

Despite not yet realizing the photoacid catalyzed oligomerization of small alkenes, the new photoacid **HDMPAN-(BF₄)₂** here described can be a potential candidate for such application or a gate opener to a new class of photoacids that can be useful as the catalyst in the oligomerization.

7 Conclusions and Outlook

Hydrocarbons are the ideal compounds to be used as aviation fuels and lubricant oils, so their replacement by other technologies for these specific applications are far in time, if ever possible. Their present production and use represent, however, a major part of the GHG emissions and have negative impacts on the climate change. Therefore, ways of making hydrocarbon fuels and lubricant oils is a demand to mitigate the environmental impacts of the transport sector.

We have developed new routes to bio-jet fuels and lubricant oils that rely on the use of sunlight as the main energy source. In order to counterbalance the CO₂ emitted in the combustion of hydrocarbon fuels, we have combined the photodimerization of hydrocarbons with their production from metabolically engineered cyanobacteria and other renewable sources.

The results from the LCA in our work to produce jet fuel *via* bio-isoprene (Paper I) confirm the reduction of the climate impact of our solution when compared to fossil-based jet fuel (our process amounts to 0.7 tonne CO₂ eq./tonne fuel, 80 % lower than the conventional jet fuel). We showed that a well-known organic photochemical reaction – the photosensitized dimerization of conjugated dienes – could be successfully applied in the production of renewable jet fuel. The design of new reaction setups, providing higher surface area exposed to light, together with the use of a more efficient photosensitizer (1,1-dinaphthylmethanone), provided a conversion into dimers >90 % in 44 h (365 nm light), using low amounts of the photosensitizer. These results represent a large improvement on the optimization when compared to the results from the 1960s, where the reaction was run for 5 days and using 5 % of benzophenone as the photosensitizer. Moreover, the obtained mixture of C₁₀ dimers are suitable as jet fuel after hydrogenation with only a mild thermal conversion required between the isomers in order to have an adequate flash point. The final products meet all the key property requirements of a jet fuel.

The photosensitized dimerization as a route to jet fuels was further studied in paper II, where we were able to unravel the varying reactivities of different small conjugated dienes and conclude that isoprene is the ideal substrate in the photobiological step (due to the low boiling point that favors the escape from the cells and the existing possibility to be photosynthetically produced), as well as ideal in the photochemical step, showing the highest efficiency in the dimerization when compared to other small acyclic dienes.

The works in papers I and II require further study of the ways to scale up the production of bio-isoprene by cyanobacteria and the shortening of reaction times in the dimerization step. From a sustainability point of view, it is also required to find alternative sources for the nutrients utilized by cyanobacteria, as they were the main sources of the climate change impact in the LCA. In addition, the design of photosensitizers with higher absorption in the visible light would also benefit the more optimal use of sunlight.

In paper III we were able to show that the photosensitized dimerization is not limited to be used to produce jet fuels, but it can also be a route to lubricant oils and diesel-like fuels. The key aspect in this diversity of products was the use of larger substrates (mono- and sesquiterpenes) and the combination of more reactive substrates with less reactive substrates (cross-dimerization). Further understanding of the different reactivities was provided by the quenching experiments, DFT calculations and the correlation of light intensity and the conversion rates. Additional work required is related to the scalability of the process (similar to previously discussed for papers I and II) and the adjustments that are needed in the viscosities of the crudes obtained for lubricant oils. Altogether, the first three papers contribute to place the sunlight-driven photosensitized dimerization of conjugated dienes as an important route to enable a sustainable production of hydrocarbons used in the transport sector.

In the last paper (paper IV), a new photoacid was studied with the aim to be used as a catalyst in the oligomerization of alkenes. The strong computed photoacidity ($pK_a^{hv} = -12$) was shown to originate from a new mechanism that involves the rearrangement of charge upon excitation in a remote unit, and the electrostatic repulsion of that unit and the acidic proton. The rearrangement of charge is a result of excited state antiaromaticity alleviation which that moiety exhibits upon excitation. Therefore, unlike the first three papers that contribute to a known photochemical reaction, paper IV can be seen as a door opener for a new class of photoacids and their use in oligomerization reactions of alkenes. Yet, our experimental attempts in the reaction itself have not been successful. The future of such route might rely in photoacids that have a longer excited state lifetime, ideally triplet state photoacids.

Together, the work in this thesis contributes to the development of a field that has great importance in the present context of climate change: renewable energy. Furthermore, this thesis contributes to a deeper understanding of photosensitized dimerization of conjugated dienes and the origins of the photoacidity phenomenon.

Acknowledgements

Research and education are certainly not done on an individual basis. I would like to mention a few people to whom I am very thankful for making this thesis possible.

I first would like to highly thank my main supervisor *Assoc. Prof. Henrik Ottosson* for his guidance and support since we first met during my exchange studies in Uppsala and throughout my PhD studies. I am also thankful to my co-supervisor *Dr. Per Wiklund* for our great fuel-related discussions and for his industrial perspective, which has certainly shed light on the directions of our projects. I thank *Dr. Anup Rana* for his more practical guidance in the lab and valuable suggestions to my work.

I am thankful for working in collaboration with the Microbial Chemistry groups at Uppsala University: *Assoc. Prof. Pia Lindberg*, *Assoc. Prof. Karin Stensjö*, *Prof. Peter Lindblad*, *Dr. João S. Rodrigues* and *Dr. Henna Mustila*. I also acknowledge our collaborators at SLU who performed the LCA, *Assoc. Prof. Cecilia Sundberg* and *Dr. Dalia M. M. Yacout*, and *Mathias Berglund* at RISE in Borås, who was responsible for the determination of the fuel properties reported in this thesis. *Dr. William Siljebo* and *Dr. Tomas Gustafsson* at RISE in Örnköldsvik are also acknowledged for their contributions in the scaling up of the combined photobiological-photochemical production of jet fuel.

It was a pleasure to work with present and past members of the Ottosson Group. I hereby would like to acknowledge *Dr. Raffaello Papadakis*, *Dr. Kjell Jorner*, *Dr. Rabia Ayub*, *Dr. Ouissam El Bakouri*, *Dr. Josene Maria Toldo*, *Dr. Tomas Slanina*, *Prof. Joshua Smith*, *Dr. Wangchuk Rabten*, *Nathalie Proos Vedin*, *Hugo Arrou-Vignod*, *Dr. Jiajie Yan*, *Dr. Preethanuj Preethalayam*, *Dr. Sindhujaa Vajravel* and *Dr. Juan Carlos Roldao*. You all have contributed to my studies by sharing knowledge in computational and experimental chemistry, and microbial chemistry, as well as by sharing good moments of fika, lunch and excited state adventures.

I give an extra acknowledgement to those who proofread my thesis and contributed with valuable feedback: *Dr. Per Wiklund*, *Dr. Preethanuj*

Preethalayam, Dr. Sindhuja Vajravel and Nathalie Proos Vedin. I also acknowledge *Malin Svensson, Iris Cruz Santana and Nathalie Proos Vedin* for helping me with the Populärvetenskaplig Sammanfattning.

I also would like to thank all the present and past members of the Synthetic Molecular Chemistry program for the moments shared at the workplace and the fun activities we have done. I especially acknowledge the senior members *Sascha Ott, Anders Thapper, Andreas Orthaber, Eszter Borbas and Stefano Crespi*. I also thank all the nice colleagues I met in the other programs in the Chemistry department, from House 7, House 2 and BMC.

I thank *Assoc. Prof. Vinh Nguyen* from University of New South Wales for his supervision during my exchange in Sydney, *Domenic Pace* for the collaboration in Paper IV, and all the members of Nguyen's group for being very welcoming and providing a great experience in the lab. In connection, I deeply thank the Liljewalch foundation for funding my exchange in Sydney and my trip to the GreenIUPAC conference in 2022.

Finally, I must acknowledge several people that have not been scientifically involved with this thesis, but have surely made it possible indirectly: my parents *Rute Rodrigues Cid Gomes* and *Antonio Reginaldo Gomes*, I am extremely grateful for your love and the education you provided me; my sisters, *Larissa* and *Leticia* for being my first best friends; my nephew, *Lucas*, and my niece, *Lilian*, who I could only meet a few times, but all of those times were full of joy.

My friends at the other side of the Atlantic Ocean: *Aline, Tamires, Rodrigo, Sandra, Samanta, Tayla, Antonio, Silma, Desiree, Talita, Melissa, Larissa, Julia, Carmen, Emilio, Bia, Bruno, Kersul, Fabi, Felipe, Chalegra, Mari* and *Jé*. Thank you all so much for always welcome me in my visits to Brazil, meet me for trips and for remind me of what *saudade* means.

My dear friends in Uppsala, I would not have made it without you: *Iris, Malin, Son, Johanna, Maja, Eira, Theo, Cornelia, Danne, Gabi* and *Spandana*; and last, but not least, I thank my *sambo Daniel* for all his support. Thank you all for being there every time I needed during these years and for making my stay in Uppsala wonderful.

Populärvetenskaplig Sammanfattning

Råolja är huvudkällan till ett stort antal produkter som används i vårt dagliga liv, såsom olika plaster, lösningsmedel, färg och bränslen. Även om det har varit mycket användbart för samhällets framväxt under de senaste århundradena, leder utvinningen och raffineringen av råolja samt användningen av dess derivat – till exempel bränslen – till att föroreningar släpps ut i atmosfären. Växthusgaser, så som koldioxid, är exempel på dessa och bidrar till klimatförändringarna på vår planet. Dessutom är råolja en resurs som inte kan ersättas på kort tid, därför behövs ett substitut inom en snar framtid i och med dess begränsade natur och på grund av de skadliga effekter som dess hantering och användning har på miljön. Med andra ord, inte bara källan bör bytas ut utan även den industriella processen måste bli mer hållbar.

En av de viktigaste fossilbaserade produkterna som behöver bytas ut är bränslen. Dessa är kemiska föreningar som kallas kolväten och deras förbränning i bilar och flygplan producerar koldioxid. Alternativa bränslen är vätgas, vars förbränning endast producerar vatten, och el – som i elbilar. Problemet är att dessa två alternativ inte kan tillgodose behovet av flygbränslen – särskilt för långa flygningar – eller andra bränslen med hög energidensitet (diesel). För dessa typer av bränslen är kolväten ideala föreningar. Som ett alternativ finns vissa biotekniskt modifierade mikroorganismer (cyanobakterier) som drivs av solljus och som kan producera små kolväten från vatten och koldioxid, vilket skulle kunna ge upphov till en netto koldioxidneutral process, men dessa små föreningar återfinns i gasform och är inte tillräckligt stora för att användas som flygbränsle eller diesel. Fler kemiska omvandlingar krävs för att omvandla dem till sådana produkter. Ett mer hållbart sätt att göra det på är att använda ljus från solen, vilket är en av de renaste och mest rikliga energikällorna som finns tillgängliga. På så sätt kan man tänka sig en kombinerad fotobiologisk-fotokemisk metod som använder solljus i båda stegen (Fig. 1).

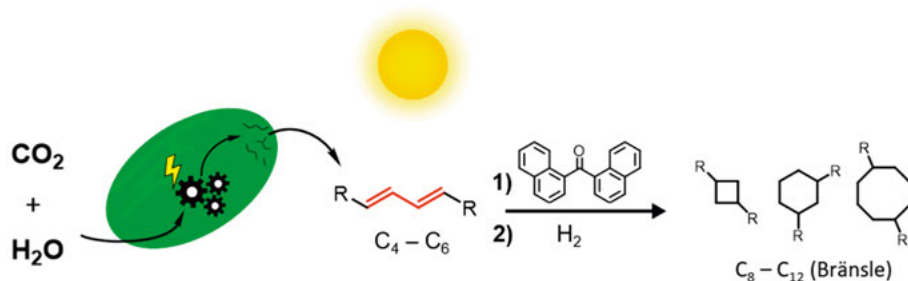


Fig. 1 Representation av det kombinerade fotobiologiska-fotokemiska tillvägagångssättet för att producera bränslen med solljus och substrat från biotekniskt modifierade cyanobakterier. Denna avhandling fokuserar på det andra steget – den fotokemiska sammankopplingsreaktionen av biosubstraten.

Användningen av ljus för att främja reaktioner är ett område som kallas fotokemi. I denna avhandling beskrivs två sätt att använda solljus till att främja omvandlingen av små kolväten till råvara som kan användas som bränsle och smörjoljor. Båda tillvägagångssätten använder en förening som är ansvarig för att absorbera ljuset och sedan använda den energin för att främja reaktionen hos de små kolvätena. I den första metoden kallas denna förening för en fotosensibilisator (PS) och energin från det absorberade ljuset överförs till det mindre kolvätet via kollision. Därefter kan det mindre kolvätet som fick energin (dvs föreningen har exciterats) reagera med ett annat kolväte och bilda större föreningar (Fig. 2).

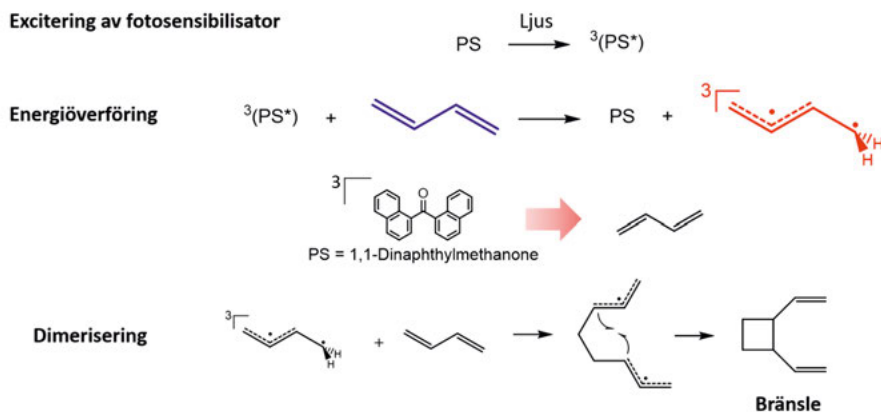


Fig. 2 Dimerisering av små kolväten (konjugerade diener) främjas av en fotosensibilisator (PS). Den bildade produkten kan användas som bränsle efter hydrogenering. Den illustrerade produkten är ett exempel bland flera möjliga isomerer.

I den andra metoden föreslår vi att en förening som blir surare när den absorberar ljus (en fotosyra) också kan främja reaktioner hos de små kolvätena

genom att överföra ett laddat väte till ett kolväte, vilket initierar en kedjereaktion (Fig. 3). En förening eller ett tillstånd som är mer surt ger en situation där dissociationen av en förening i en negativ och positiv (väte) del blir lättare. En fördel är att surheten hos fotosyran upphör när ljuskällan tas bort, vilket gör att ljuset kan användas för att styra när reaktionen ska avslutas eller hur långa oligomererna ska bli.

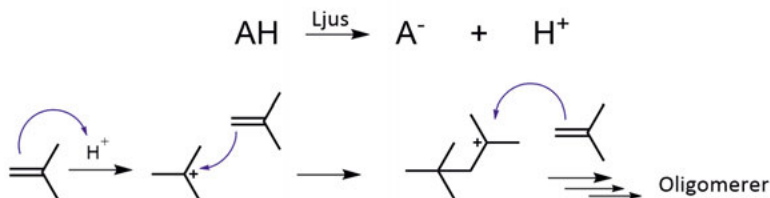


Fig. 3 Oligomerisering av alkener som främjas av (foto)syror. I figuren motsvarar AH fotosyran.

Tillvägagångssätt likt dessa är mer hållbara, eftersom de kombinerar den renare källan av små kolväten som kommer från mikroorganismer samt användningen av solljus för att främja ytterligare reaktioner för att producera bränslen och smörjoljor. Denna avhandling ger en djupare förståelse för sådana reaktioner och beskriver tillämpningen av detta kombinerade tillvägagångssätt, vilket bidrar till ytterligare utveckling för att mildra klimatförändringarnas effekter. Teknikmognadsnivån i vårt kombinerade tillvägagångssätt är dock i ett tidigt skede (runt 2 på en skala från 1 till 9), där ytterligare utveckling och skalbarhet krävs för att få teknologin till en kommersiell nivå. De främsta begränsningarna är de i nuläget låga mängderna av små kolväten som cyanobakterier kan producera, den stora mängden näringsämnen som skulle krävas av cyanobakterierna i en storskalig produktion samt den något långa tid som krävs i fotodimeriseringssteget (som för närvarande är mellan 12-48 timmar). I det avseendet kan vidareutveckling av reaktionsuppsättningen möjliggöra kortare reaktionstider, och ytterligare framtagning av nya absorberande föreningar (fotosyra eller fotosensibilisator) kan också ge en bredare användning av solljusspektrumet.

Popular Science Summary

Crude oil is the main source of several products used in our daily lives, such as plastics, solvents, paints and fuels. Though very useful for the progress of societies in the past centuries, the extraction and refining of crude oil and the use of its derivatives – for example fuels – release pollutants into the atmosphere. Some of these pollutants are the so-called greenhouse gasses, which include carbon dioxide and contribute to the effects of climate change in our planet. Furthermore, crude oil is a source that cannot be replaced by new technologies in a short time, therefore alternatives are needed in the near future due to its finite nature and because of the damaging effects that its handling and use have on the environment. In other words, not only the source should be replaced, but also the industrial process has to be more sustainable.

Fuels are one of the main fossil-based products that are required to be replaced. They are normally compounds called hydrocarbons and their combustion in cars and airplanes produces carbon dioxide. Existing alternatives are hydrogen gas, which only produces water upon combustion, and electricity – as in electric cars. The problem is that these two options cannot address the need of aviation fuels – especially for long flights – or other high energy density fuels (diesel). For those types of fuels, hydrocarbons are the ideal compounds. Alternatively, some bioengineered microorganisms (cyanobacteria) are powered by sunlight and can produce small hydrocarbons from water and carbon dioxide, which could yield a net carbon neutral process, however, these small compounds are gaseous and not large enough to be used as aviation fuel or diesel. More chemical conversions are required to transform them into such products. A more sustainable way to do it is by using light provided by the sun, which is one of the cleanest and most abundant energy sources available to us. In that way, a combined photobiological-photochemical approach that uses sunlight in both steps can be envisioned (Fig. 1).

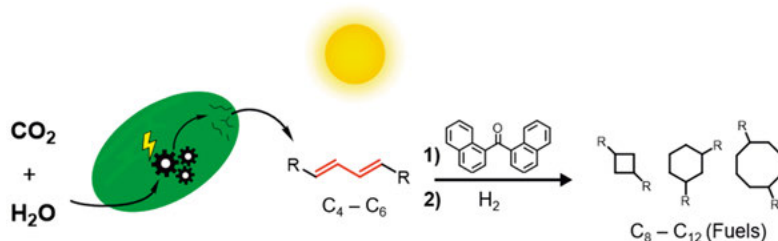


Fig. 1 Representation of the combined photobiological-photochemical approach to produce fuels using sunlight and substrates sourced from bioengineered cyanobacteria. This thesis focusses on the second step – the photochemical elongation of the bio-substrates.

The use of light to promote reactions is a field called photochemistry. In this thesis, two routes are described to use sunlight to promote the conversion of small hydrocarbons into crudes that can be used as fuels and lubricant oils. Both routes utilize a compound that is responsible for absorbing the light and then utilizing that energy to promote the reaction of the small hydrocarbons. In the first route, that compound is called a photosensitizer (PS) and the energy of the light absorbed is transferred to the small hydrocarbon *via* collision. Later the small hydrocarbon that received that energy (*i.e.* the compound that is excited) can react with another small hydrocarbon, forming larger compounds (Fig. 2).

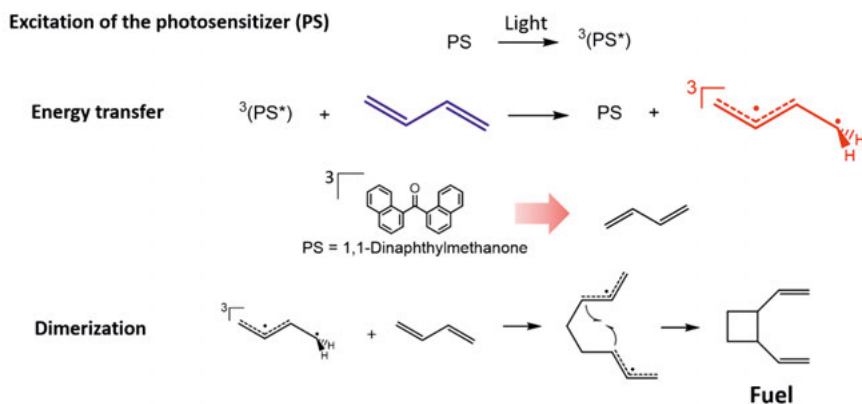


Fig. 2 Dimerization of small hydrocarbons (conjugated dienes) promoted by a photosensitizer (PS). The product formed can be used as fuel after hydrogenation. The product shown is one example of several possible isomers.

In the second route we propose that a compound that becomes more acidic when it absorbs light (a photoacid) can also promote the reaction of the small hydrocarbons by transferring one charged hydrogen to one hydrocarbon, initiating a chain reaction (Fig. 3). A more acidic compound or state is a

condition in which the dissociation of a compound into one negative and positive (hydrogen) units is easier. One benefit is that the photoacidity vanishes when the light is turned off, which can offer light-control of the reaction termination and the length of the oligomers.

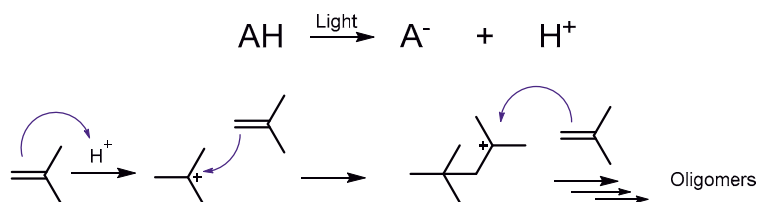


Fig. 3 Oligomerization of alkenes promoted by (photo)acids. In the figure, AH represents the photoacid.

Such routes are more sustainable, because they combine the cleaner source of small hydrocarbons coming from microorganisms and the use of sunlight to promote the further reactions in order to produce fuels and lubricant oils. This thesis provides a deeper understanding of such reactions and describes the application of this combined approach, contributing to further development in the mitigation of the climate change impacts. However, the technology readiness level of our combined approach is at an early stage (around 2 on a scale from 1 to 9), in which further development and scalability is required to bring the technology to a commercial level. The main bottlenecks are the presently low amounts of small hydrocarbons that cyanobacteria can produce, the large amount of nutrients that would be required by the cyanobacteria in a large-scale production and the somewhat long duration required in the photodimerization step (which at the present is in between 12 - 48 h). In that regard, further engineering of reaction setups could enable shorter reaction times, and the further development of new absorbing species (photoacid or photosensitizer) may also provide a broader use of the sunlight spectrum.

References

- 1 J. Barnes, *Levels of Life*, Vintage Books, London, 2013.
- 2 S. Arrhenius, XXXI. On the influence of carbonic acid in the air upon the temperature of the ground, *The London, Edinburgh, and Dublin Philosophical Magazine and Journal of Science*, 1896, **41**, 237–276.
- 3 J. Tyndall, On the Absorption and Radiation of Heat by Gases and Vapours and on the Physical Connection of Radiation, Absorption, and Conduction, *Philosophical Magazine ser.*, 1861, **4**, 273–285.
- 4 International Energy Agency, <https://www.iea.org/data-and-statistics/>, (accessed 11 December 2020).
- 5 International Renewable Energy Agency, *IRENA (2019), Global Energy Transformation: A Roadmap to 2050*, 2019.
- 6 L. Caspeta, N. A. A. Buijs and J. Nielsen, The role of biofuels in the future energy supply, *Energy Environ Sci*, 2013, **6**, 1077–1082.
- 7 International Renewable Energy Agency Abu Dhabi., *ADVANCED Biofuels : What holds them back?*, IRENA, 2019.
- 8 International Energy Agency, *The Future of Hydrogen*, 2019.
- 9 J. A. Muldoon and B. G. Harvey, Bio-Based Cycloalkanes: The Missing Link to High-Performance Sustainable Jet Fuels, *ChemSusChem*, 2020, **13**, 5777–5807.
- 10 S. Chu and A. Majumdar, Opportunities and challenges for a sustainable energy future, *Nature*, 2012, **488**, 294–303.
- 11 S. Shylesh, A. A. Gokhale, C. R. Ho and A. T. Bell, Novel Strategies for the Production of Fuels, Lubricants, and Chemicals from Biomass, *Acc Chem Res*, 2017, **50**, 2589–2597.
- 12 J. D. Woodroffe and B. G. Harvey, High-Performance, Biobased, Jet Fuel Blends Containing Hydrogenated Monoterpenes and Synthetic Paraffinic Kerosenes, *Energy and Fuels*, 2020, **34**, 5929–5937.
- 13 K. Dutta, A. Daverey and J. G. Lin, Evolution retrospective for alternative fuels: First to fourth generation, *Renew Energy*, 2014, **69**, 114–122.
- 14 M. Xie, W. Wang, W. Zhang, L. Chen and X. Lu, Versatility of hydrocarbon production in cyanobacteria, *Appl Microbiol Biotechnol*, 2017, **101**, 905–919.
- 15 N. Betterle and A. Melis, Photosynthetic generation of heterologous terpenoids in cyanobacteria, *Biotechnol Bioeng*, 2019, **116**, 2041–2051.
- 16 B. Pattanaik and P. Lindberg, Terpenoids and their biosynthesis in cyanobacteria, *Life*, 2015, **5**, 269–293.
- 17 P. J. L. B. Williams and L. M. L. Laurens, Microalgae as biodiesel & biomass feedstocks: Review & analysis of the biochemistry, energetics & economics, *Energy Environ Sci*, 2010, **3**, 554.
- 18 R. Miao, H. Xie, X. Liu, P. Lindberg and P. Lindblad, Current processes and future challenges of photoautotrophic production of acetyl-CoA-derived solar fuels and chemicals in cyanobacteria, *Curr Opin Chem Biol*, 2020, **59**, 69–76.

- 19 J. S. Rodrigues and P. Lindberg, Engineering Cyanobacteria as Host Organisms for Production of Terpenes and Terpenoids, *Cyanobacteria Biotechnology*, 2021, 267–300.
- 20 J. S. Rodrigues and P. Lindberg, Metabolic engineering of *Synechocystis* sp. PCC 6803 for improved bisabolene production, *Metab Eng Commun*, 2021, **12**, DOI:10.1016/j.mec.2020.e00159.
- 21 M. Sakai, T. Ogawa, M. Matsuoka and H. Fukuda, *Photosynthetic Conversion of Carbon Dioxide to Ethylene by the Recombinant Cyanobacterium, Synechococcus* sp. PCC 7942, *Which Harbors a Gene for the Ethylene-Forming Enzyme of Pseudomonas syringae*, 1997, vol. 84.
- 22 H. Mustila, A. Kugler and K. Stensjö, Isobutene production in *Synechocystis* sp. PCC 6803 by introducing α -ketoisocaproate dioxygenase from *Rattus norvegicus*, *Metab Eng Commun*, 2021, e00163.
- 23 P. Lindberg, S. Park and A. Melis, Engineering a platform for photosynthetic isoprene production in cyanobacteria, using *Synechocystis* as the model organism, *Metab Eng*, 2010, **12**, 70–79.
- 24 J.-D. Woodroffe and B. G. Harvey, Thermal cyclodimerization of isoprene for the production of high-performance sustainable aviation fuel, *Energy Advances*, 2022, **1**, 338–343.
- 25 D. M. Morris, R. L. Quintana and B. G. Harvey, High-Performance Jet Fuels Derived from Bio-Based Alkenes by Iron-Catalyzed [2+2] Cycloaddition, *ChemSusChem*, 2019, **12**, 1646–1652.
- 26 K. E. Rosenkoetter, C. R. Kennedy, P. J. Chirik and B. G. Harvey, [4 + 4]-cycloaddition of isoprene for the production of high-performance bio-based jet fuel, *Green Chemistry*, 2019, **21**, 5616–5623.
- 27 O. Staples, J. H. Leal, P. A. Cherry, C. S. Mcenally, L. D. Pfefferle, T. A. Semelsberger, A. D. Sutton and C. M. Moore, *Camphorane as a renewable diesel blendstock produced by cyclodimerization of myrcene*, .
- 28 C. P. Nicholas, Applications of light olefin oligomerization to the production of fuels and chemicals, *Appl Catal A Gen*, 2017, **543**, 82–97.
- 29 J. D. Woodroffe and B. G. Harvey, A Simple Process for the Dimerization and Cross-Coupling of Isoprene and Myrcene to High-Performance Jet and Diesel Blendstocks, *Energy and Fuels*, 2022, **36**, 2630–2638.
- 30 J. Keasling, H. Garcia Martin, T. Soon Lee, A. Mukhopadhyay, S. W. Singer and E. Sundstrom, Microbial production of advanced biofuels, *Nat Rev Microbiol*, 2021, **19**, 701-715.
- 31 J. Ungerer, L. Tao, M. Davis, M. Ghirardi, P. C. Maness and J. Yu, Sustained photosynthetic conversion of CO₂ to ethylene in recombinant cyanobacterium *Synechocystis* 6803, *Energy Environ Sci*, 2012, **5**, 8998–9006.
- 32 J. W. K. Oliver, I. M. P. Machado, H. Yoneda and S. Atsumi, Cyanobacterial conversion of carbon dioxide to 2,3-butanediol, *Proc Natl Acad Sci U S A*, 2013, **110**, 1249–1254.
- 33 D. Sun, Y. Li, C. Yang, Y. Su, Y. Yamada and S. Sato, *Fuel Processing Technology*, 2020, 197.
- 34 C. Angelici, B. M. Weckhuysen and P. C. A. Bruijninx, *ChemSusChem*, 2013, **6**, 1595–1614.
- 35 C. Durall, P. Lindberg, J. Yu and P. Lindblad, Increased ethylene production by overexpressing phosphoenolpyruvate carboxylase in the cyanobacterium *Synechocystis* PCC 6803, *Biotechnol Biofuels*, 2020, **13**, 16.
- 36 S. Vajravel, S. Sirin, S. Kosourov and Y. Allahverdiyeva, Towards sustainable ethylene production with cyanobacterial artificial biofilms, *Green Chemistry*, 2020, **22**, 6404–6414.

- 37 X. Gao, F. Gao, D. Liu, H. Zhang, X. Nie and C. Yang, Engineering the methylerythritol phosphate pathway in cyanobacteria for photosynthetic isoprene production from CO₂, *Energy Environ Sci*, 2016, **9**, 1400–1411.
- 38 R. Sun, M. Zheng, X. Li, J. Pang, A. Wang, X. Wang and T. Zhang, Production of renewable 1,3-pentadiene from xylitol via formic acid-mediated deoxydehydration and palladium-catalyzed deoxygenation reactions, *Green Chemistry*, 2017, **19**, 638–642.
- 39 S. Liu, Y. Qi, R. Feng, L. Cui, Q. Dai and C. Bai, Multifunctional Ce/ZrSi Catalyst Synergistically Converting 1,4-Pentanediol Derived from Levulinic Acids to Renewable Pentadiene, *ACS Sustain Chem Eng*, 2021, **9** 8341–8346.
- 40 J. A. Mmongoyo, Q. A. Mgani, S. J. M. Mdachi, P. J. Pogorzelec and D. J. Cole-Hamilton, Synthesis of a kairomone and other chemicals from cardanol, a renewable resource, *European Journal of Lipid Science and Technology*, 2012, **114**, 1183–1192.
- 41 H. Mutlu, R. Hofsäß, R. E. Montenegro and M. A. R. Meier, Self-metathesis of fatty acid methyl esters: Full conversion by choosing the appropriate plant oil, *RSC Adv*, 2013, **3**, 4927–4934.
- 42 P. N. T. van Velzent and W. van der Harts, The Isomerization of 1,4mCyclohexadiene Ions to the 1,3=Cyclohexadiene Structure as Studied by Photodissociation, *Organic Mass Spectrometry*, 1984, **19**, 190–192.
- 43 Y. Hu, N. Li, G. Li, A. Wang, Y. Cong, X. Wang and T. Zhang, Solid Acid-Catalyzed Dehydration of Pinacol Derivatives in Ionic Liquid: Simple and Efficient Access to Branched 1,3-Dienes, *ACS Catal*, 2017, **7**, 2576–2582.
- 44 T. W. Lyons, D. Guironnet, M. Findlater and M. Brookhart, Synthesis of p-xylene from ethylene, *J Am Chem Soc*, 2012, **134**, 15708–15711.
- 45 E. Sjöstrom, *Wood chemistry: fundamentals and applications*, Academic Press, Second., 1993.
- 46 G. Frank, Photosensitised reactions of α -pinene, *Journal of the Chemical Society B: Physical Organic*, 1968, 130–132.
- 47 R. L. Burwell, The Mechanism of the Pyrolyses of Pinenes, *J Am Chem Soc*, 1951, **73**, 4461–4462.
- 48 J. J. W. Coppen, *Eucalyptus: The Genus Eucalyptus (Medicinal and Aromatic Plants - Industrial Profiles)*, 2002.
- 49 K. H. C. Baser, M. Kürkçüoğlu, B. Demirçakmak, N. Uülker and S. H. Beis, Composition of the essential oil of schinus molle l. Grown in Turkey, *Journal of Essential Oil Research*, 1997, **9**, 693–696.
- 50 N. R. Baral, O. Kavvada, D. Mendez-Perez, A. Mukhopadhyay, T. S. Lee, B. A. Simmons and C. D. Scown, Techno-economic analysis and life-cycle greenhouse gas mitigation cost of five routes to bio-jet fuel blendstocks, *Energy Environ Sci*, 2019, **12**, 807–824.
- 51 E. M. Kim, J. H. Eom, Y. Um, Y. Kim and H. M. Woo, Microbial synthesis of myrcene by metabolically engineered *Escherichia coli*, *J Agric Food Chem*, 2015, **63**, 4606–4612.
- 52 P. P. Peralta-Yahya, M. Ouellet, R. Chan, A. Mukhopadhyay, J. D. Keasling and T. S. Lee, Identification and microbial production of a terpene-based advanced biofuel, *Nat Commun*, 2011, **2**, 483.
- 53 F. K. Davies, V. H. Work, A. S. Beliaev and M. C. Posewitz, Engineering limonene and bisabolene production in wild type and a glycogen-deficient mutant of *Synechococcus* sp. PCC 7002, *Front Bioeng Biotechnol*, 2014, **2**, 21.
- 54 C. Formighieri and A. Melis, Regulation of β -phellandrene synthase gene expression, recombinant protein accumulation, and monoterpene hydrocarbons production in *Synechocystis* transformants, *Planta*, 2014, **240**, 309–324.

- 55 C. Formighieri and A. Melis, Sustainable heterologous production of terpene hydrocarbons in cyanobacteria, *Photosynth Res*, 2016, **130**, 123–135.
- 56 U.S. Patent No. 7,846,222, 2010.
- 57 H. A. Meylemans, R. L. Quintana and B. G. Harvey, Efficient conversion of pure and mixed terpene feedstocks to high density fuels, *Fuel*, 2012, **97**, 560–568.
- 58 B. G. Harvey, M. E. Wright and R. L. Quintana, High-density renewable fuels based on the selective dimerization of pinenes, *Energy and Fuels*, 2010, **24**, 267–273.
- 59 E. Pahima, S. Hoz, M. Ben-Tzion and D. T. Major, Computational design of biofuels from terpenes and terpenoids, *Sustain Energy Fuels*, 2019, **3**, 457–466.
- 60 N. J. Turro, V. Ramamurthy and J. C. Scaiano, *Principles of molecular photochemistry: an introduction*, University science books, 2009.
- 61 T. Shinmyozu, R. Nogita, M. Akita and C. Lim, in *CRC Handbook of Organic Photochemistry and Photobiology*, eds. W. M. Horspool and F. Lenci, CRC Press LLC, Boca Raton, FL, 2 nd., 2004, pp. 1–21.
- 62 G. S. Hammond, J. Saltiel, A. A. Lamola, N. J. Turro, J. S. Bradshaw, D. O. Cowan, R. C. Counsell, V. Vogt and C. Dalton, Mechanisms of Photochemical Reactions in Solution. XXII.1 Photochemical cis-trans Isomerization, *J Am Chem Soc*, 1964, **86**, 3197–3217.
- 63 M. Rosenberg, C. Dahlstrand, K. Kilså and H. Ottosson, Excited state Aromaticity and Antiaromaticity: Opportunities for Photophysical and photochemical rationalizations, *Chem Rev*, 2014, **114**, 5379–5425.
- 64 K. I. Öberg, Photochemistry and Astrochemistry: Photochemical Pathways to Interstellar Complex Organic Molecules, *Chem Rev*, 2016, **116**, 9631–9663.
- 65 P. Klán and J. Wirz, *Photochemistry of organic compounds: from concepts to practice*, John Wiley & Sons, 2009.
- 66 J. W. Raymond and W. T. Simpson, Experimental and Theoretical Study of Sigma-Bond Electronic Transitions in Alkanes, *J Chem Phys*, 1967, **47**, 430–448.
- 67 S. K. Rajagopal, K. Nagaraj, S. Deb, V. Bhat, D. Sasikumar, E. Sebastian and M. Hariharan, Extending the scope of the carbonyl facilitated triplet excited state towards visible light excitation, *Physical Chemistry Chemical Physics*, 2018, **20**, 19120–19128.
- 68 D. Sasikumar, A. T. John, J. Sunny and M. Hariharan, Access to the triplet excited states of organic chromophores, *Chem Soc Rev*, 2020, **49**, 6122–6140.
- 69 E. V. Anslyn and D. A. Dougherty, *Modern physical organic chemistry*, University science books, 2006.
- 70 L. D. Elliott, S. Kayal, M. W. George and K. Booker-Milburn, Rational design of triplet sensitizers for the transfer of excited state photochemistry from UV to visible, *J Am Chem Soc*, 2020, **142**, 14947–14956.
- 71 M. A. El-Sayed, Spin—orbit coupling and the radiationless processes in nitrogen heterocyclics, *J Chem Phys*, 1963, **38**, 2834–2838.
- 72 M. A. El-Sayed, The Triplet State: Its Radiative and Nonradiative Properties, *Acc Chem Res*, 1968, **1**, 8–16.
- 73 T. Förster, Fluoreszenz Organischer Verbindungen (Vandenhoeck and Ruprecht, Göttingen, 1951), *G. Nienhuis and C. Th. J. Alkemade, Physica C*, 1976, **81**, 181.
- 74 D. L. Dexter, A theory of sensitized luminescence in solids, *J Chem Phys*, 1953, **21**, 836–850.
- 75 R. S.-H. Liu, California Institute of Technology, 1965.

- 76 W. L. Dilling, Photochemical cycloaddition reactions of nonaromatic conjugated hydrocarbon dienes and polyenes, *Chem Rev*, 1969, **69**, 845–877.
- 77 J. E. Baldwin and J. P. Nelson, Cycloadditions. VI. Photosensitized Dimerization of α -Phellandrene, *Journal of Organic Chemistry*, 1966, **31**, 336–338.
- 78 G. S. Hammond, N. J. Turro and R. S. H. Liu, Mechanisms of photochemical reactions in solution. XVI. 1 Photosensitized dimerization of conjugated dienes, *J Org Chem*, 1963, **28**, 3297–3303.
- 79 R. S. H. Liu, N. J. Turro and G. S. Hammond, Mechanisms of Photochemical Reactions in Solution. XXXI. Activation and Deactivation of Conjugated Dienes by Energy Transfer, *J Am Chem Soc*, 1965, **87**, 3406–3412.
- 80 R. S. H. Liu and G. S. Hammond, Photosensitized Internal Addition of Dienes to Olefins, *J Am Chem Soc*, 1967, **89**, 4936–4944.
- 81 H. J. Kuhn, S. E. Braslavsky and R. Schmidt, Chemical actinometry (IUPAC technical report), *Pure and Applied Chemistry*, 2004, **76**, 2105–2146.
- 82 C. G. Hatchard and C. A. Parker, A new sensitive chemical actinometer-II. Potassium ferrioxalate as a standard chemical actinometer, *Proc R Soc Lond A Math Phys Sci*, 1956, **235**, 518–536.
- 83 D. Hernández-Guerra, A. Hlavačková, C. Pramthaisong, I. Vespoli, R. Pohl, T. Slanina and U. Jahn, Photochemical C–H Amination of Ethers and Geminal Difunctionalization Reactions in One Pot, *Angewandte Chemie - International Edition*, 2019, **58**, 12440–12445.
- 84 W. Domcke and A. L. Sobolewski, *Science*, 2003, 302, 1693–1694.
- 85 A. Weller, Zur kinetik der fluoreszenzumschwangung, *Zeitschrift für physikalische Chemie*, 1958, **15**, 438–453.
- 86 Th. Förster, Fluoreszenzspektrum und Wasserstoffionen-konzentration, *Naturwissenschaften*, 1949, **36**, 186–187.
- 87 T. Förster, Die pH-Abhängigkeit der Fluoreszenz von Naphthalinderivaten, *Zeitschrift für Elektrochemie und angewandte physikalische Chemie*, 1950, **54**, 531–535.
- 88 A. Weller, Quantitative untersuchungen der fluoreszenzumschwangung bei naphtholen, *Zeitschrift für Elektrochemie, Berichte der Bunsengesellschaft für physikalische Chemie*, 1952, **56**, 662–668.
- 89 O. Falklöf and B. Durbeej, Distinguishing between keto-enol and acid-base forms of firefly oxyluciferin through calculation of excited-state equilibrium constants, *J Comput Chem*, 2014, **35**, 2184–2194.
- 90 L. M. Tolbert and J. E. Haubrich, *Photoexcited Proton Transfer from Enhanced Photoacids*, 1994, vol. 116.
- 91 D. Maus, A. Grandjean and G. Jung, Toward Magic Photoacids: Proton Transfer in Concentrated Sulfuric Acid, *Journal of Physical Chemistry A*, 2018, **122**, 9025–9030.
- 92 L. Wimberger, J. Andréasson and J. E. Beves, Basic-to-acidic reversible pH switching with a merocyanine photoacid, *Chemical Communications*, , DOI:10.1039/d2cc00805j.
- 93 D. Jacquemine, E. A. Perpète, I. Ciofini and C. Adamo, Fast and reliable theoretical determination of pKa* for photoacids, *Journal of Physical Chemistry A*, 2008, **112**, 794–796.
- 94 C. J. Cramer, *Essentials of computational chemistry: theories and models*, John Wiley & Sons, 2013.
- 95 F. Jensen, *Introduction to computational chemistry*, John wiley & sons, 2017.
- 96 C. Adamo and D. Jacquemin, The calculations of excited-state properties with Time-Dependent Density Functional Theory, *Chem Soc Rev*, 2013, **42**, 845–856.

- 97 R. B. Hermann, Theory of hydrophobic bonding. II. Correlation of hydrocarbon solubility in water with solvent cavity surface area, *J Phys Chem*, 1972, **76**, 2754–2759.
- 98 B. Lee and F. M. Richards, The interpretation of protein structures: estimation of static accessibility, *J Mol Biol*, 1971, **55**, 379-IN4.
- 99 D. A. Liotard, G. D. Hawkins, G. C. Lynch, C. J. Cramer and D. G. Truhlar, Improved methods for semiempirical solvation models, *J Comput Chem*, 1995, **16**, 422–440.
- 100 A. v. Marenich, C. J. Cramer and D. G. Truhlar, Universal solvation model based on solute electron density and on a continuum model of the solvent defined by the bulk dielectric constant and atomic surface tensions, *Journal of Physical Chemistry B*, 2009, **113**, 6378–6396.
- 101 E. Cancès, B. Mennucci and J. Tomasi, A new integral equation formalism for the polarizable continuum model: Theoretical background and applications to isotropic and anisotropic dielectrics, *J Chem Phys*, 1997, **107**, 3032–3041.
- 102 B. Mennucci and J. Tomasi, Continuum solvation models: A new approach to the problem of solute’s charge distribution and cavity boundaries, *J Chem Phys*, 1997, **106**, 5151–5158.
- 103 B. Mennucci, E. Cancès and J. Tomasi, Evaluation of solvent effects in isotropic and anisotropic dielectrics and in ionic solutions with a unified integral equation method: theoretical bases, computational implementation, and numerical applications, *J Phys Chem B*, 1997, **101**, 10506–10517.
- 104 J. Tomasi, B. Mennucci and E. Cancès, The IEF version of the PCM solvation method: an overview of a new method addressed to study molecular solutes at the QM ab initio level, *Journal of Molecular Structure: THEOCHEM*, 1999, **464**, 211–226.
- 105 M. J. Frisch, G. W. Trucks, H. B. Schlegel, G. E. Scuseria, M. A. Robb, J. R. Cheeseman, G. Scalmani, V. Barone, G. A. Petersson, H. Nakatsuji, X. Li, M. Caricato, A. V. Marenich, J. Bloino, B. G. Janesko, R. Gomperts, B. Mennucci, H. P. Hratchian, J. V. Ortiz, A. F. Izmaylov, J. L. Sonnenberg, D. Williams-Young, F. Ding, F. Lipparini, F. Egidi, J. Goings, B. Peng, A. Petrone, T. Henderson, D. Ranasinghe, V. G. Zakrzewski, J. Gao, N. Rega, G. Zheng, W. Liang, M. Hada, M. Ehara, K. Toyota, R. Fukuda, J. Hasegawa, M. Ishida, T. Nakajima, Y. Honda, O. Kitao, H. Nakai, T. Vreven, K. Throssell, Montgomery Jr, J. E. Peralta, F. Ogliaro, M. J. Bearpark, J. J. Heyd, E. N. Brothers, K. N. Kudin, V. N. Staroverov, T. A. Keith, R. Kobayashi, J. Normand, K. Raghavachari, A. P. Rendell, J. C. Burant, S. S. Iyengar, J. Tomasi, M. Cossi, J. M. Millam, M. Klene, C. Adamo, R. Cammi, J. W. Ochterski, R. L. Martin, K. Morokuma, O. Farkas, J. B. Foresman and D. J. Fox, Gaussian 16, *Gaussian 16, Inc., Wallingford CT*.
- 106 Y. Houari, D. Jacquemin and A. D. Laurent, Methodological keys for accurate simulations, *Physical Chemistry Chemical Physics*, 2013, **15**, 11875–11882.
- 107 N. Colin Baird, *The Molecular Orbital Theory of Organic Chemistry*, McGraw-Hill, 1971, vol. 93.
- 108 H. Ottosson, Exciting excited-state aromaticity, *Nat Chem*, 2012, **4**, 969–971.
- 109 J. C. Soc and C. Commun, *Evidence for the Generation of Aromatic Cationic Systems in the Excited State. Photochemical Solvolysis of Fluoren-9-01*, 1985.
- 110 R. Papadakis, H. Li, J. Bergman, A. Lundstedt, K. Jorner, R. Ayub, S. Haldar, B. O. Jahn, A. Denisova, B. Zietz, R. Lindh, B. Sanyal, H. Grennberg, K. Leifer and H. Ottosson, Metal-free photochemical silylations and transfer hydrogenations of benzenoid hydrocarbons and graphene, *Nat Commun*, 2016, **7**, 1-10.
- 111 R. Papadakis and H. Ottosson, *Chem Soc Rev*, 2015, **44**, 6472–6493.

- 112 M. Hada, S. Saito, S. Tanaka, R. Sato, M. Yoshimura, K. Mouri, K. Matsuo, S. Yamaguchi, M. Hara, Y. Hayashi, F. Röhrlich, R. Herges, Y. Shigeta, K. Onda and R. J. D. Miller, Structural Monitoring of the Onset of Excited-State Aromaticity in a Liquid Crystal Phase, *J Am Chem Soc*, 2017, **139**, 15792–15800.
- 113 Z. Zhao, X. Zheng, L. Du, Y. Xiong, W. He, X. Gao, C. Li, Y. Liu, B. Xu, J. Zhang, F. Song, Y. Yu, X. Zhao, Y. Cai, X. He, R. T. K. Kwok, J. W. Y. Lam, X. Huang, D. Lee Phillips, H. Wang and B. Z. Tang, Non-aromatic annulene-based aggregation-induced emission system via aromaticity reversal process, *Nat Commun*, 2019, **10**, 1–10.
- 114 L. J. Karas, C. H. Wu and J. I. Wu, Barrier-Lowering Effects of Baird Antiaromaticity in Photoinduced Proton-Coupled Electron Transfer (PCET) Reactions, *J Am Chem Soc*, 2021, **143**, 17970–17974.
- 115 R. K. Mohamed, S. Mondal, K. Jorner, T. F. Delgado, V. v. Lobodin, H. Ottosson and I. v. Alabugin, The Missing C1-C5 Cycloaromatization Reaction: Triplet State Antiaromaticity Relief and Self-Terminating Photorelease of Formaldehyde for Synthesis of Fulvenes from Enynes, *J Am Chem Soc*, 2015, **137**, 15441–15450.
- 116 P. Bultinck, R. Poncè and S. van Damme, Multicenter bond indices as a new measure of aromaticity in polycyclic aromatic hydrocarbons, *J Phys Org Chem*, 2005, **18**, 706–718.
- 117 F. Feixas, J. Vandenbussche, P. Bultinck, E. Matito and M. Solà, Electron delocalization and aromaticity in low-lying excited states of archetypal organic compounds, *Physical Chemistry Chemical Physics*, 2011, **13**, 20690–20703.
- 118 E. Matito, M. Duran and M. Sola, The aromatic fluctuation index (FLU): A new aromaticity index based on electron delocalization, *J Chem Phys*, 2005, **122**, 014109.
- 119 E. Jongedijk, K. Cankar, M. Buchhaupt, J. Schrader, H. Bouwmeester and J. Beekwilder, Biotechnological production of limonene in microorganisms, *Appl Microbiol Biotechnol*, 2016, **100**, 2927–2938.
- 120 S. V. Jovanovic, D. G. Morris, C. N. Pliva and J. C. Scaiano, Laser flash photolysis of dinaphthyl ketones, *J Photochem Photobiol A Chem*, 1997, **107**, 153–158.
- 121 S. L. Murov, Ph.D. Thesis, Univ. Chicago, Chicago, IL, 1967.
- 122 J. P. Fouassier, D. J. Lounnot, F. Wieder and J. Faure, Laser investigation of some oxazole and oxadiazole derivatives, *Journal of Photochemistry*, 1977, **7**, 17–28.
- 123 K. Meier and H. Zweifel, Thioxanthone ester derivatives: efficient triplet sensitizers for photopolymer applications, *Journal of Photochemistry*, 1986, **35**, 353–366.
- 124 A. C. Cope and E. M. Hardy, The Introduction of Substituted Vinyl Groups. V. A Rearrangement Involving the Migration of an Allyl Group in a Three-Carbon System, *J Am Chem Soc*, 1940, **62**, 441–444.
- 125 International Energy Agency (IEA), *Energy Policies of IEA Countries: Sweden 2019 Review*, 2019.
- 126 Swedish Energy Agency, *Energy in Sweden 2022 – An overview*, 2022.
- 127 S. Canizales, M. Sliwszcinka, A. Russo, S. Bentvelzen, H. Temmink, A. M. Verschoor, R. H. Wijffels and M. Janssen, Cyanobacterial growth and cyanophycin production with urea and ammonium as nitrogen source, *J Appl Phycol*, 2021, **33**, 3565–3577.

- 128 T. Beyl, T. M. Louw and R. W. M. Pott, Cyanobacterial growth in minimally amended anaerobic digestion effluent and flue-gas, *Microorganisms*, 2019, **7**, 428.
- 129 K. P. Papadopoulos, C. N. Economou, A. G. Tekerlekopoulou and D. v. Vayenas, Two-step treatment of brewery wastewater using electrocoagulation and cyanobacteria-based cultivation, *J Environ Manage*, 2020, **265**, 110543.
- 130 K. Sandros and , Hans L. J. Bäckström, Transfer of Triplet State Energy in Fluid Solutions, *Acta Chem Scand*, 1962, **16**, 958–968.
- 131 R. A. Caldwell and M. Singh, Lifetimes of Conjugated Diene Triplets, *J. Am. Chem. Soc.*, 1982, **104**, 12152–12172.
- 132 K. Nakabayashi, S. Toki and S. Takamuku, Triplet States of Cyclic Olefins and Dienes. On the Lifetimes and Chemical Reactivities Studied by Pulse Radiolysis, *Chem Lett*, 1986, **15**, 1889–1892.
- 133 X. Allonas, J. Lalevée and J. P. Fouassier, Influence of the S0 - T1 structural changes on the triplet-triplet sensitization of dienes, *Chem Phys*, 2003, **290**, 257–266.
- 134 F. Edition, Biodiesel Handling and Use Guide, *Natl. Renew. Energy Lab. Innov. Our Energy Futur.*
- 135 Å. K. Rudolphi, E. Kassfeldt and M. Torbacke, *Lubricants : Introduction to Properties and Performance*, John Wiley & Sons Ltd, 2014.
- 136 B. Saha and D. Vlachos, (Hemi) cellulosic Lubricant Base Oils via Catalytic Coupling and Deoxygenation Pathways, *Green Chemistry*, 2021, **23**, 4916-4930.
- 137 P. K. Patel, J. E. Arias, R. S. Gongora, F. E. Hernandez, A. Moncomble, S. Aloïse and K. Y. Chumbimuni-Torres, Visible light-triggered fluorescence and pH modulation using metastable-state photoacids and BODIPY, *Physical Chemistry Chemical Physics*, 2018, **20**, 26804–26808.
- 138 L. Wimberger, S. K. K. Prasad, M. D. Peeks, J. Andréasson, T. W. Schmidt and J. E. Beves, Large, Tunable, and Reversible pH Changes by Merocyanine Photoacids, *J Am Chem Soc*, 2021, **143**, 20758–20768.
- 139 C. Fu, J. Xu and C. Boyer, Photoacid-mediated ring opening polymerization driven by visible light, *Chemical Communications*, 2016, **52**, 7126–7129.
- 140 J. v Crivello and J. H. W. Lam, Photoinitiated cationic polymerization by triarylselenonium salts, *Journal of Polymer Science: Polymer Chemistry Edition*, 1979, **17**, 1047–1057.
- 141 B. Yang, K. Dong, X. S. Li, L. Z. Wu and Q. Liu, Photoacid-Enabled Synthesis of Indanes via Formal [3 + 2] Cycloaddition of Benzyl Alcohols with Olefins, *Org Lett*, 2022, **24**, 2040–2044.
- 142 J. Saway, Z. M. Salem and J. J. Badillo, *Synthesis (Germany)*, 2021, **53**, 489–497.
- 143 Z. M. Salem, J. Saway and J. J. Badillo, Photoacid-Catalyzed Friedel-Crafts Arylation of Carbonyls, *Org Lett*, 2019, **21**, 8528–8532.
- 144 J. F. Ireland and P. A. H. Wyatt, *Acid-Base Properties of Electronically Excited States of Organic Molecules*, .
- 145 A. Yamaguchi, M. Namekawa, T. Kamijo, T. Itoh and N. Teramae, Acid-base equilibria inside amine-functionalized mesoporous silica, *Anal Chem*, 2011, **83**, 2939–2946.
- 146 L. N. Silverman, D. B. Spry, S. G. Boxer and M. D. Fayer, Charge transfer in photoacids observed by stark spectroscopy, *Journal of Physical Chemistry A*, 2008, **112**, 10244–10249.

- 147 A. Das, T. Banerjee and K. Hanson, Protonation of silylenol ether via excited state proton transfer catalysis, *Chemical Communications*, 2016, **52**, 1350–1353.
- 148 S. Eckert, M. O. Winhart, C. Kleine, A. Banerjee, M. Ekimova, J. Ludwig, J. Harich, M. Fondell, R. Mitzner, E. Pines, N. Huse, P. Wernet, M. Odelius and E. T. J. Nibbering, Electronic Structure Changes of an Aromatic Amine Photoacid along the Förster Cycle, *Angewandte Chemie - International Edition*, 2022, DOI:10.1002/anie.202200709.
- 149 Y. F. Wang and Y. C. Cheng, Molecular electrostatic potential on the proton-donating atom as a theoretical descriptor of excited state acidity, *Physical Chemistry Chemical Physics*, 2018, **20**, 4351–4359.
- 150 S. G. Schulman, Correspondence of fluorescing states of naphthols and naphtholate anions and its effect on the calculation of pK_a* from spectral shifts, *Spectroscopy Letters*, 1973, **6**, 197–202.
- 151 N. Agmon, W. Rettig and C. Groth, Electronic determinants of photoacidity in cyanonaphthols, *J Am Chem Soc*, 2002, **124**, 1089–1096.
- 152 M. Solà, Aromaticity rules, *Nat Chem*, 2022, **14**, 585–590.
- 153 Z. Wen, L. J. Karas, C. H. Wu and J. I. C. Wu, How does excited-state anti-aromaticity affect the acidity strengths of photoacids?, *Chemical Communications*, 2020, **56**, 8380–8383.
- 154 P. Bultinck, M. Rafat, R. Ponec, B. van Gheluwe, R. Carbo-Dorca and P. Popelier, Electron delocalization and aromaticity in linear polyacenes: atoms in molecules multicenter delocalization index, *J Phys Chem A*, 2006, **110**, 7642–7648.

Acta Universitatis Upsaliensis

*Digital Comprehensive Summaries of Uppsala Dissertations
from the Faculty of Science and Technology 2227*

Editor: The Dean of the Faculty of Science and Technology

A doctoral dissertation from the Faculty of Science and Technology, Uppsala University, is usually a summary of a number of papers. A few copies of the complete dissertation are kept at major Swedish research libraries, while the summary alone is distributed internationally through the series Digital Comprehensive Summaries of Uppsala Dissertations from the Faculty of Science and Technology. (Prior to January, 2005, the series was published under the title “Comprehensive Summaries of Uppsala Dissertations from the Faculty of Science and Technology”.)

Distribution: publications.uu.se
urn:nbn:se:uu:diva-492631



ACTA
UNIVERSITATIS
UPSALIENSIS
UPPSALA
2023